An Assessment of Moisture Induced Damage in Asphalt Pavements

A Master's Thesis

Submitted to the Faculty of

Worcester Polytechnic Institute

In partial fulfillment of the requirements for the

Degree of Master of Science

by

Yar Zar Moe Htet

April, 2015

Approved by:

Professor Rajib B. Mallick, CEE

Professor Paul Mathisen, CEE

Professor Nima Rahbar, CEE

Abstract

Moisture-induced damage is one the major causes of deterioration of asphalt pavements and extensive research has been conducted on this topic. Theoretical and experimental results have led the researchers to believe that moisture-induced damages are caused mainly by the generation of pore water pressure in asphalt mixtures when traffic passes over a pavement. The Moisture Induced Sensitivity Tester (MIST) has been recently developed to simulate the phenomenon of repeated pore pressure generation and deterioration in the laboratory. The objective of this study was to evaluate moisture-induced damage in typical Maine Department of Transportation (DOT) asphalt mixes, with the use of MIST, pre and post testing, and analysis of data. The MIST was used to condition Hot Mix Asphalt (HMA) samples that were compacted from eight typical Maine DOT mixes, with different types of aggregates and asphalt binder. A modified Dynamic modulus test in Indirect Tensile Mode was used for the determination of damage. A layered elastic model, along with a fatigue-cracking criterion, was utilized to assess the total impact on the pavement lives. Monte Carlo analysis was conducted to determine the distribution of number of repetitions to failure of pavements that are subjected to moisture damage. The major conclusions are that most of the mixes are likely to experience a reduction in their life due to the effect of moisture and that the Micro-Deval and the fine aggregate absorption test results can be related to such damage. A composite factor, consisting of both of these test results, is recommended for regular use by the DOT to screen mixes with high moisture damage potential.

Acknowledgement

First and foremost I would like to express my deepest gratitude to my immediate advisor, Professor Rajib B. Mallick and co-advisor, Professor Paul Mathisen, for their support, guidance and patience throughout the course of this research project. I am extremely lucky to have had an opportunity to experience their broad knowledge. I would also like to give my thanks to Professor Nima Rahbar for supporting and believing in me until the completion of this research project.

I would also like to give my special thanks my mentor, Ryan Worsman, in guiding me and supporting me with my experimental procedures and career development. His invaluable advices have given me the confidence that I needed to complete my Master's study.

Finally, I would like to acknowledge Maine Department of Transportation for providing the necessary research materials to conduct this study.

Table of Contents

Table of Figures

Table of Tables

Background

Pavements are usually classified as either flexible (Hot Mix Asphalt, HMA) or rigid (Portland Cement Concrete (PCC). Both flexible pavement an rigid pavements are susceptible to environmental factors and traffic related damages. Environment condition, such as excessive moisture, can negatively impact the performance of pavement structures. Moisture induced damage is one of the most significant damages that can affect the performance of flexible or rigid pavements. The main focus of this thesis is on the simulation and analysis of effects of moisture on HMA that is used in flexible pavements. All pavements are generally designed for a specific design life. A particular design method called Mechanistic-Empirical Pavement Design Guide (MEPDG) was adopted by AASHTO in 2002[1]. The MEPDG method is based on a combination of mechanistic and empirical approaches.

Many studies have been conducted by Universities, State, and Federal agencies to understand the mechanics behind the effects, and the ways to solve the fundamental problems of moisture-induced damages. Results of several prominent studies were summarized at a national seminar held in San Diego, CA, that was held to discuss the alarming issues of moisture sensitivity of asphalt pavement [2]. In this seminar, the results of a survey (dated August 4, 2002) conducted by Colorado Department of Transportation were presented. The survey participants included 55 agencies who were interested in moisture sensitivity in asphalt pavement. These 55 agencies included 50 states department of transportation, 3 FHWA Federal Land offices, the District of Columbia and 1 Canadian province. The results of the survey showed that 87% of the agencies tested mixes for moisture sensitivity, and that 82% of the agencies used some sort of anti-strip treatment to make mixes more resistant to moisture-induced damages. The various testing methods to assess the mixes include tensile test (AASHTO T283, ASTM D4867, or similar), compressive test (AASHTO T115 or similar), a retained stability test and wheel-tracking tests and tensile test. However, there was in general discontent with the reliability of predictions from the different test methods, and researchers had indicated the importance of the development of a better test method for the identification of moisture damage potential.

The main mechanism behind moisture damage is adhesive and/or cohesive failure. Adhesive failure is the stripping/removal of aggregate from the binder and cohesive failure is the failure within the asphalt binder as a loss of cohesion. Overall moisture affects the integrity of the aggregate, asphalt binder or the bonds between the asphalt and the aggregate; this is called moisture sensitivity of the materials in pavement. The cause of the loss of adhesion could be traced back to the moisture in mixes, poor compactions, inadequately dried or dirty aggregate, poor drainage or poor aggregate or asphalt chemistry. Furthermore, the loss in adhesion between the aggregate and binder is accelerated by traffic and freeze-thaw cycles.

Raveling in the pavement occurs when the surface layer of the pavement is progressively weathered either by environmental conditions or the traffic abrasions. This phenomenon is also related to poor compactions, inferior aggregates, low binder content, high fine content, moisture damages and traffic loadings. These types of pavement failures and distresses are largely associated with a failure in adhesive bonds between aggregate and binder and they are usually visible on roadways. The loss of cohesiveness in the asphalt binder can result in the loss of stiffness of the structure (stiffness can be directly related to strength). The damage in the mixes due to both adhesive and cohesive failures, as a result of the effect of moisture, needs to be determined by suitable laboratory tests, such as those related to the determination of dynamic modulus or tensile strength. However, more importantly, a laboratory simulation or conditioning procedure must be utilized to simulate the conditions under which repeated pore water pressure is developed in pavement mixes, which leads to adhesive and/or cohesive failure. Finally, results of tests conducted on pre and post conditioned mixes need to be explained on the basis of test properties of the constituents of the mix (asphalt and aggregate) such that the end users can select or screen the specific materials through the adoption of proper specifications.

Objective

The objective of this research was to assess the damages in pavement structure through the use of simulative conditioning, stiffness and strength and analysis of the test data.

Literature Review

Laboratory Experiments and Studies of Moisture-Induced Damages

A research for a new method to study the effects of the moisture susceptibility of asphalt paving mixes in laboratory condition was conducted by Mallick et al.,2003 [6]. This research was specifically conducted to develop a rational procedure to evaluate the moisture susceptibility of asphalt mixes. The development of the procedure to study the moisture susceptibility is based on the theory that pore pressure generated in pavement when pavement air pockets are saturated with moisture is significantly greater than the pavement with unsaturated with air pockets. Furthermore the research of this procedure takes into account for hydraulic scouring, a process by which the pavement loses its adhesive properties between asphalt and its fine aggregates because of the repeated generation of stress in the pores caused by the moisture. The concept was developed to determine a better conditioning procedure compared to the existing Lottman procedure, AASHTO T283 (Resistance of Compacted Bituminous Mixture to Moisture Induced Damage)[2]. Similar conclusions were also reached by other researchers, Regimand (2015).

The Moisture Induced Sensitivity Tester (MIST) was developed on the basis of this concept. The first model of such equipment was developed and designed to condition the samples through repeated generation of pore pressure, at user selected temperature and number of cycles. In this experiment, two types of HMA mixes with similar gradation and asphalt content but different aggregate, and with known differences in moisture damage potential, were used to observe the effect of the moisture induced damages. These two different mixes were compacted at 6-8% air void (construction void) and tested for its tensile strength (under AASHTOT283 standards) with two different conditions (dry unconditioned and conditioned). Rutting under water was tested using the Asphalt Pavement Analyzer (APA) for each of the mix. The samples were then tested with the MIST. After the conditioning phase, the samples were kept at 25C water bath for 2 hours and tested for tensile strength.

The results from the preliminary tests indicated that the samples experienced moisture damages with conditioning parameter of 210 kPa at 5 Hz, 60C within an hour. These results from the preliminary tests were used in final tests with the new equipment. The results of tests conducted with 2000, 3000, 4000 and 6000 cycles at 60C and 40C showed that the strength of

the mixes decreased with increase in number of cycles. The retained tensile strength of the MIST conditioned and AASHTO T283 conditioned samples, and the known damage potential compared well. Some improvements in the test equipment were recommended, as a result of which two subsequent models were developed and evaluated, Mallick et al 2005 [18]. The MIST used in this study represents the most advanced, third generation equipment with automated sample conditioning and the availability of a wider selection of pressure, temperature and number of cycles, as well as dwell time after conditioning [13].

Indirect Tensile Test (IDT) (ASTM D6931) is a type testing method used in the determination of the strength of the HMA. IDT test is a destructive testing method and it has some limitations in determining the effect of moisture induced damages. IDT test cannot be used to determine effect of the moisture induced damages on the same sample (pre and post conditioning). Moisture induced damages are compared through the strength measured from unconditioned samples to strength measured from the conditioned samples from the same type of mixes. However, there are generally appreciable amount of variability in properties of HMA samples, because of the inherent nature of the construction materials (aggregates of different sizes and asphalt binder). Nevertheless, because of its simplicity, the Indirect Tensile Strength (ITS) remains the most widely utilized test for the evaluation of moisture damage potential in HMA.

Dynamic Modulus test, on the other hand, is considered as a non-destructive test if the strain values produced from the test are within elastic or recoverable range. Dynamic modulus of a particular sample can be measured both before and after moisture conditioning. This parameter is increasingly being used in the industry because the test provides a full characterization of mix over a broad range of temperatures and loading frequencies. Generally, dynamic modulus testing could be conducted in both compression and tensile mode. For tensile mode, the standard procedure is relatively more complicated. To avoid it, a relatively easier dynamic modulus test with thinner samples, and used in the indirect tensile mode, has been recently developed [10].

Ahmad et al., [4] investigated the effects of tropical climatic conditions on the HMA moisture-induced damages. The main goal of the study was to identify whether the use of Superpave mix design method is superior to that of Marshall mix design in tropical climatic countries. The experiment of the study involved comparing the results of moisture susceptibility

of the mixes using Superpave and Marshall mix design methods. The modified Lottman test (AASHTO T283) and Simple Performance Test (SPT) were performed on unconditioned and condition samples from different mix design methods. The conditioning of the sample was designed to reflect the tropical climatic conditions (freeze-thaw conditioning test procedure were omitted).

The results (Lottman test) of the study indicated that Superpave-designed mixtures retained higher tensile strength values than that of Marshall-design mixtures. The tensile strength ratio (TSR) decreased from unconditioned to conditioned sample; an indication of damage due to moisture. The ratio of dynamic modulus stiffness before and after moisture conditioning (ESR) and TSR were also in good agreement, with R^2 value of 0.70.

Studies of Flooded Pavement in Field Conditions and the Damages Associated with It

One of the major studies that were conducted to understand the effects of the flooded pavements was conducted by Gaspard et al, March 2007 [3]. The study was conducted in order to investigate the impact of flooding on the pavements and roadways due to Hurricane Katrina and Hurricane Rita in the New Orleans region. The study aimed to determine whether the contract modifications of several on-going construction projects that were flooded in the region are needed to accommodate the damage impact from the hurricanes. The authors hypothesized that the pavements that were submerged in water for over a prolonged period time can be structurally damaged. To some extent, damage was in fact found in asphalt pavement and concrete pavement with weak subgrades. In order to investigate the effects of the flooding and to estimate the cost of rehabilitation on the sections of pavements that were damaged, the Louisiana Transportation Research Center (LTRC) needed both "before and after" data from flooded pavements. The only project from which the pre-flooding pavement testing data was available was LA 46. Tests were conducted on 238 miles of state highways at 0.1 mile intervals. The tests included Falling Weight Deflectometer (FWD), Dynaflect, Dynamic Cone Penetrometer (DCP) testing and coring. There were three parameters that were utilized from the FWD data; the first sensor deflection (D1), effective structural number (SN_{eff}) and subgrade resilient modulus (M_r). The SN_{eff} was calculated using formulas from the 1993 AASHTO design guide [19]

($SN_{eff}=0.0045D^3\sqrt{E_p}$), deflections obtained from FWD testing, pavement layer thickness obtained from data using GPR and backed coring. SN_{eff} represents the effective structural strength of the existing pavement and base course. A two-way analysis of variance was performed on the entire data set. The statistical analysis was divided into 3 different analysis corresponding to the different types of pavement; HMA, Portland Cement Concrete (PCC) and composite. The dataset was also grouped into four different categories based on the flood duration, as Group 1, 2, 3 and 4 for data points that have been submerged for a week, two weeks, three weeks and non-flooded points, respectively

The results of the study indicated that thinner pavement section requires more structure than thicker sections for HMA pavement to protect against flooding since damage from flooding is greater in thinner pavement sections than thicker. For PCC pavement, thicker pavements have no significant loss of strength. The thinner PCC pavements had a structural loss of 0.43 inches of pavement and 0.47 inches of subgrades. The composite pavement however did not show the need for additional structure in the pavement layers. Only the subgrade lost its structural strength, losing its initial conditions and structural strength and the total loss was equivalent to a loss of 0.9 inches of asphalt concrete.

Helali et al., 2008, conducted a study to determine the impact of Hurricane Katrina and Hurricane Rita. The authors provided an assessment of pavements and roadways in Jefferson Parish, Louisiana after Hurricane Katrina and Rita [4]. In this report, the authors performed an assessment of pavement conditions based on both functional analysis and structural analysis. The existing PMS database consisted of historical roughness, distress, deflection and traffic data. This primarily served as benchmark data, and in the analysis it provided the scope of pre-disaster assessment. The post condition assessment of the pavements involved collecting the same type of data from the database, along with coring/boring of the submerged pavements. The pavement damage analysis involved pre-and-post roughness, distress and structural analyses. A statistical analysis was also conducted in this study to test the extent and significance of the damage.

The study was conducted by generating a system of data collection and analysis based on indices from 0 to 10 to differentiate the condition of the pavements - a system previously used in PMS. These indices include Ride Condition Index (RCI) for roughness, distress indexes (DI) for distress severities and surface distress index (SDI) for defects. These indices were weighed

differently to arrive at a Pavement Quality Index (PQI). The existence of as-built data also reduced the cost of obtaining data for the required back calculation analysis. After the data analysis, a damage assessment was conducted through functional analysis and structural analysis. The advantage of having a pavement management system is that it provides the study with up to date section condition and strength data for roads that are vulnerable to flooding. These two types of analysis were further broken down into network analysis, section level analysis, and roadway level analysis for each. These analyses were performed for both historical and post data.

The comparison between the flooded/non-flooded road section and historical and post analyses conditions indicated that the pavements that were submerged in the flood showed significant damages. For instance, the difference in SN_{eff} between flooded section and non-flooded section (control) after the analyses for the flexible pavement section was 1.0 SN units, which is equivalent to 2.3 inches of HMA material. The study also utilized results from a report based on the work conducted by LTRC in 2007, to compare the post flooding results with historical data of the pavements in the Parish.

The Center for Earthworks Engineering Research (CEER) at Iowa State University conducted a study on the impact of flooding of Western Iowa Missouri River in 2011 [5]. The flood event affected several counties in Iowa State including Woodbury, Monona, Harrison, Pottawattamie, Mills and Fremont. The result of the flood event included closures of several interchanges along Interstate 29 (I-29) and secondary roads in the above mention counties. These closures of road caused delay in travels and economic losses to the local business. It was reported that about $63.5 million would be needed to repair the transportation infrastructure and roadways. Some of the damages were observable, segment of the roadways were washed away, but more damages could be suspected in subgrade of the pavements.

CEER main goal was to assist county and city engineers by arranging and using rapid assessment technologies to evaluate the severity of the damages caused by the flood. Testing was conducted on bridge abutment backfills affected by flood, flooded and non-flooded secondary roadways and culverts. Since data for prior flooding were not available, the assessments of the damage due to flooding were made by comparing the measurement of flooded roadway and the measurements of the non-flooded roadway. Damage assessment procedures include Falling Weight Deflectometer Test (FWD), Dynamic Cone Penetrometer Test (DCP) and Ground

Penetration Radar Test (GPR) and hand auger soil borings. A total of 18.6 miles of roadway were investigated. The type of pavement and surface investigated in the study included gravel, chip seal surface over stabilized or unstabilized gravel base, PCC and HMA.

The type of damages associated with pavement roadway involved voids at shallow depth (< 6 in.) due to erosion of base material, voids at deeper depth (> 6 in.) due to erosion of subgrade, partial to complete erosion of PCC and HMA pavement and underlying base material, and erosion of granular shoulders. Bridges abutment damages involved erosion of bridge approach backfill material and erosion of embankment foreslopes. Damages associated with culverts involved erosion of culvert backfill, separation of culverts and water outflow blockage. Unpaved roadways experienced the worst damage since the structure integrity of these roadways was lesser in compare to the other constructions. Damages on unpaved roadways include erosion of gravel surface, rutting under traffic loading due to hauling of debris and full breach of roadway embankments. The estimated cost of repairing just on secondary roadways in western Iowa counties was about $12.6 million.

Methodology

The assessment of moisture induced damage was conducted using laboratory compacted samples materials from the Maine Department of Transportation (DOT). There were a total of 8 different mixes and each of the mixes has its own unique mix design. Table 1 lists the different pavement groups with Reference and Pin number. The plan of study involved compaction of the loose mixes using gyratory compactor, determination of Bulk Specific Gravity (BSG), porosity and air void, determination of Pre-MIST Dynamic Modulus (E*) in IDT mode, conducting Moisture Induced Sensitivity Test (MIST), determination of Post-MIST E* in IDT mode, a using quick drying method of the sample using Coredry, and determination of BSG, porosity and air void. Figure 1 presents a flow chart of the plan of study and the relevant AASHTO and ASTM standards.

Table 1: Tested Mixes Provided by Maine DOT

Reference No.	Town	Pin No.	Job-Mix-Formula
293530	Augusta	19932	PII- AU11-50B-95FTR-V2-64
287758	Durham (RTE 136)	20268	SHB-GO14-50D-95FTR-64WMA
276647	Parkman	19302	MAN-PH14-75D-12R-58
294065	Lebanon-Sanford	20272	CPI-LNH13-75D-95FTR-V1-64
289451	Auburn	20246	AAL-AB13-50D-95FT-V1-64WMA
287464	Rumford	20350	PII-PO14-75D-95FTR-64
288964	Presque Isle-Easton	19222.1	LAN-PI14-50B-95FTR-58
289218	Houlton	20423	SSI-H014-50B-95FTR-58

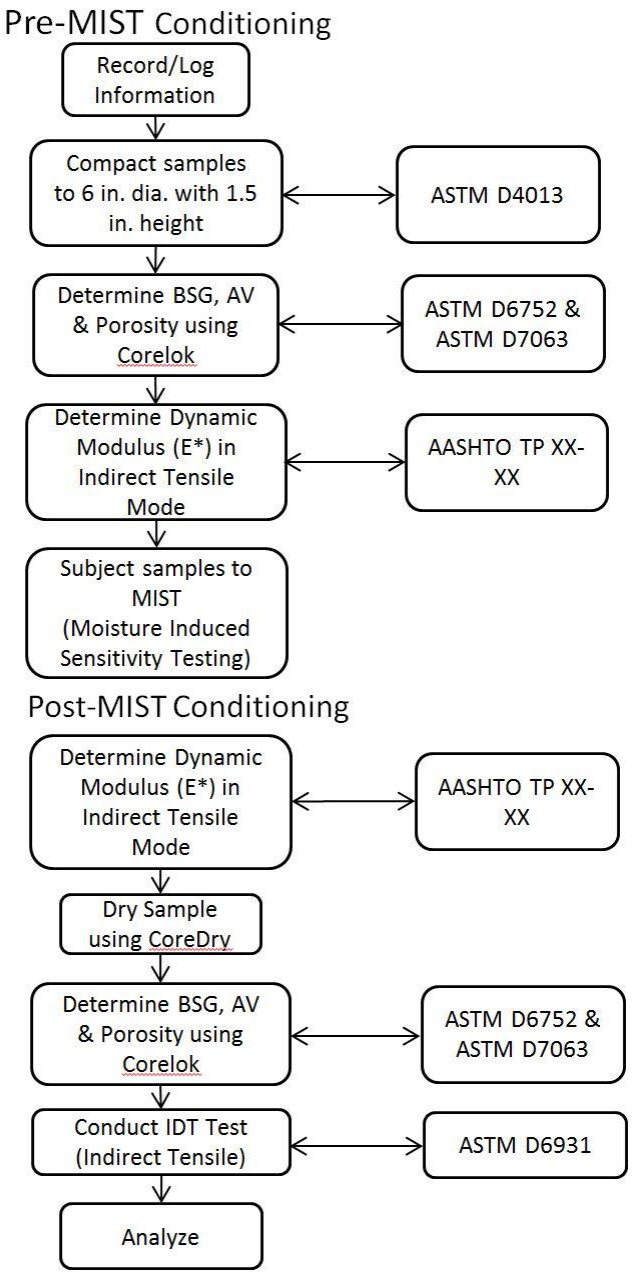

Figure 1 Plan of Study

The mixes provided by Maine DOT in this study were loose mix samples of the mixes that are typically used in various state road in Maine. The aggregate sources were unique to each mixes and the aggregate used in a particular mix did not come from a single source. Appendix D provides the maps of the aggregate source/quarry/plants. Four samples were made from each of the mixes. The samples were categorized and labeled according to the town where the pavement mixes were used (eg Augusta~Aug1,2.., Parkman~Park1,2.. etc.).

Compaction of Samples Using Gyratory Compactor

Figure 2a shows the premix condition of the as-obtained loose mixes in cardboard boxes. The loose mixes were compacted according to ASTM D4013-09-Standard Practice for Preparation of Test Specimens of Bituminous Mixtures by Means of Gyratory Shear Compactor [7]. The sequence of compaction is a factor. The loose mixes were reheated in oven at 150C for 4 hours, HMA. On the third hour, the loose mix was mixed in a mixing bowl for 2 minutes. The mix was placed in the oven for one more hour after mixing. Once the mix was in the oven for a total of 4 hours, it was compacted with the gyratory compactor, (Figure 2b). The target air void content was selected as 7%+/- 1 to be consistent with typical construction target air void content in the field. The theoretical maximum density (TMD) (obtained from Maine DOT) was utilized to select a specific amount of mix for a specific height for the compacted sample. All of the samples were compacted to a diameter of 6 in. (150 mm) and a height of 1.5in (38 mm). A total of 32 samples were compacted, 4 sample for each of the mixes.

a. Loose Mix provide by Maine DOT

b. Gyratory Compactor

c. Compacted Sample

Figure 2 Loose mix compacted using Gyratory Compactor

Determination of Bulk Specific Gravity, Porosity and Air Void using Corelok

The volumetric properties determined in this study include Bulk Specific Gravity, (ASTM D6752 & AASHTO T331), air void and Porosity (ASTM D7063). The Corelok equipment [15] was used in determination of these properties, since the determination of volumetric properties of coarse and open graded mixes usually result in unreliable and less accurate measurement when the traditional ASTM approaches (ASTM C29/29M) are utilized. The fundamental problem lies in the lack of control over the penetration and drainage of water in the sample. The use of Corelok machine mitigates this problem by sealing the sample with polymer bags in a vacuum chamber. By performing a single test all of the three volumetric properties can be determined. Table 2 and the following sections present the different formula utilized in the determination of these properties. Figure 3 shows the steps in the process.

Table 2 Corelok Data Collection Table for Volumetric Properties

Sample ID	A Bag Weight (g)	B Dry Sample Weight before Sealing (g)	C Sealed Sample Weight in Water (g)	D Dry Sample Weight After Water Submersion	E Ratio B/A	F Bag Apparent Gravity From Table	G Total Volume (A+D) - C	H (Volume of Bag) A/F	I (Volume of Sample) G - H	J Bulk Specific Gravity B/I

The BSG can be calculated using the formulas in the Table 2 presented above. The calculation of the porosity (ASTM D7063) in the GravitySuite software is based on the following underlying equations [8].

$$Bulk\ Specific\ Gravity = SG1 = \frac{A}{B - E - \frac{B - A}{F_T}}$$

$$apparent\ Specific\ Gravity = SG2 = \frac{A}{B - C - \frac{B - A}{F_{T1}}}$$

$$\%\ Porosity = \%\ Effective\ Air\ Voids = \frac{SG2 - SG1}{SG2} * 100$$

A	mass of dry specimen in air, g
B	mass of dry, sealed specimen, g
E	mass of sealed specimen underwater, g
Ft	apparent specific gravity of plastic sealing material
C	mass of unsealed specimen underwater, g
Ft1	apparent specific gravity of plastic sealing material at 25 +/- 1°C when sealed

Ft1 = 0.903 provided by the manufacture

A total of 32 different BSG, porosity and air void data were collected. After the experiment and data collection, the samples were left on the table counter to be dried with fans (air-dry). BSG and porosity data were also collected after completion of MIST, dynamic modulus in IDT for both pre and post MIST test.

Step-by-step procedure for determining BSG and porosity using Corelok

a. The specimen and "Corelok Bag" are weighed and recorded

b. The specimen is sealed inside "Corelok Bag" using Corelok machine which is set to program 2.

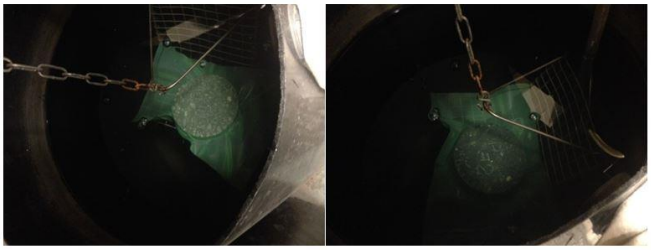

c. The sample is placed in the water bath equipped with scale which the sealed core is weighed and recorded. Once the stabilized weight of the seal specimen is recorded, the"Corelok Bag" is cut open under water and left under water for 4 minutes then the weight of the submerged specimen is recorded.

Figure 3 Step by step proedure for the use of Corelok equipment and determation of volumetric properties

Dynamic Modulus in IDT Mode (E)*

Dynamic Modulus, formally identify as$|E*|$ but also used interchangeably with complex modulus E*, is an absolute complex number that defines the relationship between stress and strain for a linear viscoelastic material. Dynamic modulus is often used in forensic studies and pavement rehabilitation design. Dynamic Modulus is calculated by taking the ratio of maximum (peak to peak) stress and recoverable (peak to peak) axial strain of a material subjected to a sinusoidal loading of axial compression testing. E* values are calculated over a range of temperature and frequencies of loading. Another parameter obtained by performing the dynamic modulus test is phase angle. Phase Angle is the lag between the peak stress and resulting peak strain. A master curve can be developed using this E* values and phase angle to describe the sensitivity of E* to temperature and frequency. A detailed procedure is described in AASHTO T342 [9].

Testing of E* accordingly to the standard of AASHTO T342 requires the sample size to be 4 inch (100 mm) in diameter by 6 inch (150 mm) in height. The test also has an extensive procedure with 30 combinations of temperature and frequency of loading. Kim et al. 2003 [10] has suggested a new form of testing method for E*, dynamic modulus in IDT mode. This new method is developed through adopting the testing nature of indirect tensile test, (IDT). One of the many arguments made by Kim et al. for adopting IDT configuration is that it is often impossible to obtain 6 inch tall sample from the field to meet the standards of AASHTO T342. A typical asphalt layer is only a few inches thick and coring is the most effective method to collect field samples. However, testing sample in IDT mode has several differences from the traditional dynamic modulus testing. Most importantly, the state of stress, which the sample experiences, is different. In traditional E* testing, the sample is subjected to uniaxial state stress but in modified E* test, the sample is subjected to biaxial state of stress. Figure 4 illustrates the schematic of IDT loading on a specimen and the state of biaxial stress developed in IDT mode. Another difference is the relationship between compaction direction and the direction in which the stress-strain analysis is performed. The compaction direction and the axial compression in the traditional E* test is the same but in the IDT test the considered stress-strain (tensile in nature) and compaction direction are perpendicular to one another. Kim et al. (2003, 10) addressed these differences by considering the fundamental properties of stress-strain relationship of IDT and the viscoelastic nature of the material, and developing a new set of equations [10]. The following equations address the difference in the analysis of the state of stress. With the accurate analytical solutions, the authors were able to validate the use dynamic modulus in IDT testing. It was also noted that the required testing time for E* in IDT is less than that required for the traditional E* testing. E* in IDT mode uses more frequencies and fewer temperature range of testing based on the time-temperature superposition principle [10].

Uniaxial State of Stress-Strain: $\sigma_y = E * \varepsilon_y \; or \; \varepsilon_y = \frac{\sigma_y}{E}$

Biaxial State of Stress-Strain: $\varepsilon_y = \frac{1}{E} * (\sigma_x - v\sigma_y)$

E = elastic modulus

σ_y = stress in y-direction

σ_x = stress in x-direction

v = Poisson's ratio

The equations for dynamic modulus in IDT mode equation are presented below. The coefficients for Poisson's ratio and dynamic modulus are dependent on the test machine apparatus. The setup and the software were developed accordingly to the guideline presented in AASHTO T342 and Kim et al 2003.

$$v = -\frac{\beta_1 U_0 - \gamma_1 V_0}{\beta_2 U_0 + \gamma_2 V_0}$$

$$|E^*| = 2 * \frac{P_0}{\pi a d} \frac{\beta_1 \gamma_2 - \beta_2 \gamma_1}{\gamma_2 V_0 - \beta_2 U_0}$$

U_0 = Horizontal Displacement obtain from the test

V_0 = Vertical Displacement obtain from the test

P_0 = Peak Load

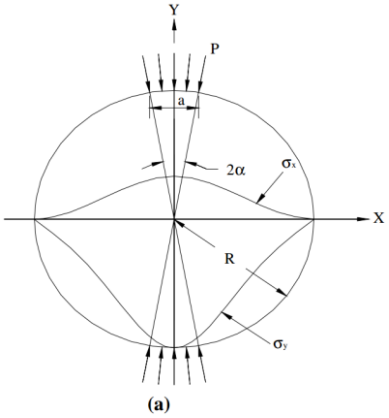

Figure 4 Schematic of IDT specimen subjected to strip load

Note: R = Radius of the specimen (m)

α = radial angle

l = gauge length in (m)

A MATLAB [14] code was developed to calculate the $\beta_1, \beta_2, \gamma_1$,and $\gamma_2$values. The boundary condition gauge length, l, is used as half of its value in the integration of β and γ values. The WPI Universal Testing Machine (UTM) machine setup has a gauge length of 2 inch and the loading strip width, a, of 0.75 inch. The coefficient values calculated using the code was compared against the values tabulated in Kim et al research (2003,10). Table 9 in Appendix A

presents the coefficient values for different gauge length using 0.75 inch loading strip width. The relevant equations are shown below.

$$\beta_1 = -\int_{-l}^{l} n(y)dy - \int_{-l}^{l} m(y)dy$$

$$\beta_2 = \int_{-l}^{l} n(y)dy - \int_{-l}^{l} m(y)dy$$

$$\gamma_1 = \int_{-l}^{l} f(x)dy - \int_{-l}^{l} g(x)dy$$

$$\gamma_2 = \int_{-l}^{l} f(x)dy + \int_{-l}^{l} g(x)dy$$

$$(y) = \frac{\left(\frac{1-y^2}{R^2}\right) * \sin(2\alpha)}{1 - \frac{2y^2}{R^2} * \cos 2\alpha + \frac{x}{R^4}^4}$$

$$\mathrm{n}(y) = tan^{-1}\left(\frac{1+y^2/R^2}{1-y^2/R^2} * \tan(\alpha)\right)$$

$$f(x) = \frac{\left(\frac{1-x^2}{R^2}\right) * \sin(2\alpha)}{1 + \frac{2x^2}{R^2} * \cos 2\alpha + \frac{x}{R^4}^4}$$

$$g(x) = tan^{-1}\left(\frac{1 - x^2/R^2}{1 + x^2/R^2} * \tan(\alpha)\right)$$

Testing Procedure for Dynamic Modulus in IDT

In this study, damages in HMA mixes were identified through changes in E*. The E* of the mixes were determined before and after MIST conditioning. The experiment used a different form of approach in the use of E* in IDT values and testing method. E* for different HMA mixes were tested at a single temperature value, 25°C and frequencies of 10 and 1 Hz.

After the determination of the BSG, porosity and air void of pre-MIST condition, E* of the eight different HMA mixes were tested. A total of 32 samples were tested for its E* value.

The tests were performed in an environmental chamber using a servo-hydraulic machine, also referred to as Universal Testing Machine (UTM) at WPI. Figure 7 shows the UTM and its components. The vertical and horizontal deformations in the samples were measured using linear variable displacement transducers (LVDT). The load and deformation data were collected with a National Instruments data acquisition system. The UTM software was developed using Lab View. The samples were instrumented with mounting studs for biaxial LVDTS. A total of 4 LVDTs were used to measure the deformations in each sample; two horizontal and 2 vertical. Figure 5 presents the process of the instrumentations of the mounting studs.

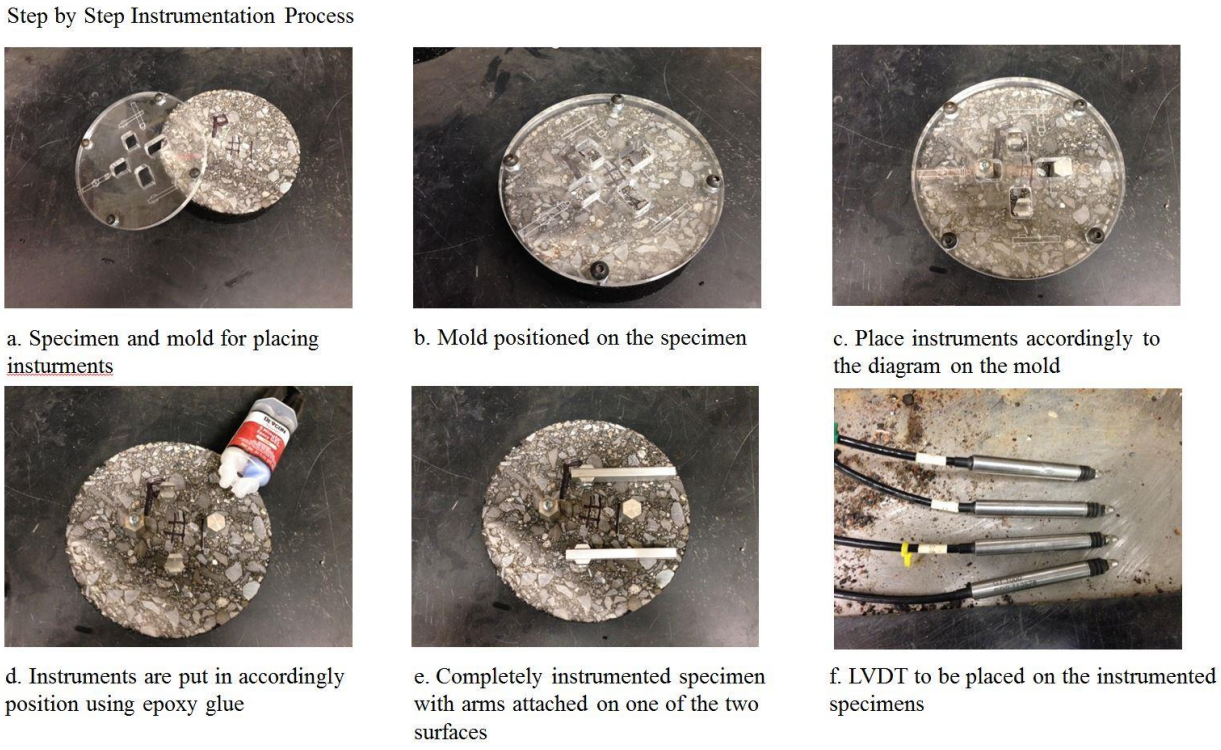

Figure 5 Step by step procedure for instrumentation of mount studs on samples

After instrumentation, the samples were left on the table counter to allow the epoxy to be cured (minimum of 2 days). Once the epoxy was cured, the sample was tested for E* in IDT mode. Figure 6 presents how the LVDTs were attached to a sample and the position of the sample in the equipment. The samples were tested from a higher to a lower loading of frequencies. The AASHTO TP-62 protocol was followed in applying the sinusoidal loads to the sample. To ensure that the test captures the linear viscoelastic behavior of the material, the loads were selected so that horizontal strain of the sample stayed within 50 -75 microstrain. The

number of data points to be collected was decided based on the objective of producing a smooth sinusoidal curve. In this experiment, a total of 60 periods of sinusoidal loading were applied to the sample at 10 Hz and 10 periods of sinusoidal loading were applied subjected at 1 Hz. The figures in Appendix B illustrate the typical graph from a test. An excel sheet was developed to plot the data generated from by the test and to determine whether the allowable strain was reached from the test.

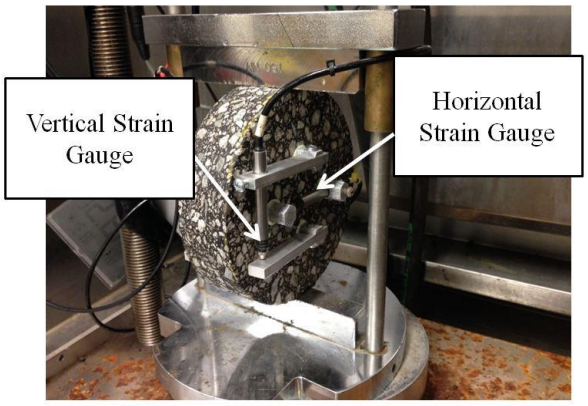

a. LVDT instrumentation for Normal Specimens (~constant thickness specimens where LVDT are attached on both the surfaces of the core)

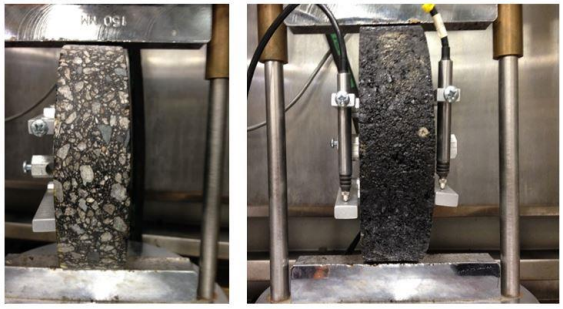

b. c.

Figure 6a. LVDT instrumentation for Crooked Specimens (varying thickness where LVDT are only attached to the surface most perpendicular to the wall of the cores) 6b. LVDT on both of the surfaces of the specimen

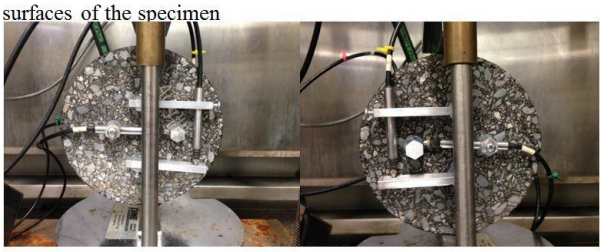

d. Normal Specimen with LVDT on both side of the surfaces

Figure 6 Placement and positioning of LVDT (sample that are crooked, usually field samples, and sample that are uniform, laboratory compacted samples)

The deformation values used for the calculation E* were taken from the last 5 periods of each test. Figures 72-74 in Appendix B illustrate the type of graph that can be generated using the data of the graph. A MATLAB code was developed to find peak to peak deformation since there was a large amount of data points; Appendix C contains this code. E* in IDT was tested for all 32 samples before and after the samples were conditioned in MIST. The change in the value (expressed as a percentage of the original) would indicate the degradation of the samples due to moisture induced damages.

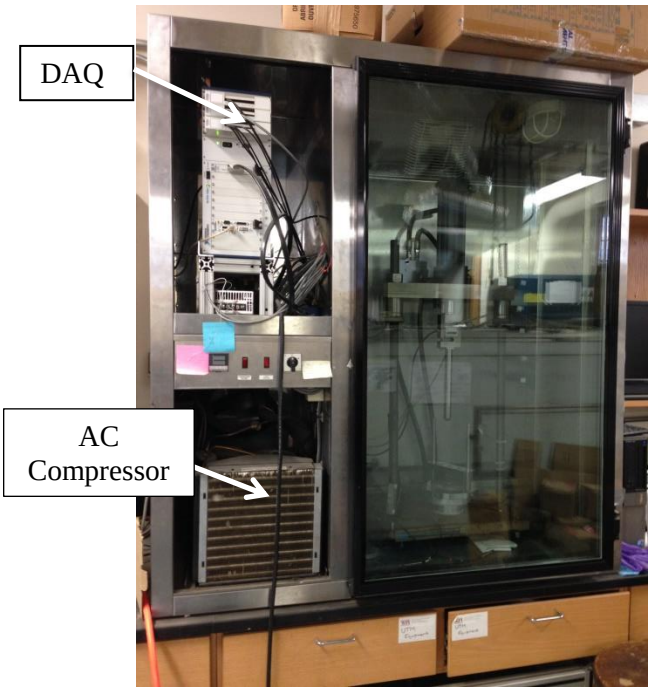

Figure 7 Universal Testing Machine, apparatus figure includes National Instrument Data Acquisition System, AC compressor for conditioning the environmental chamber

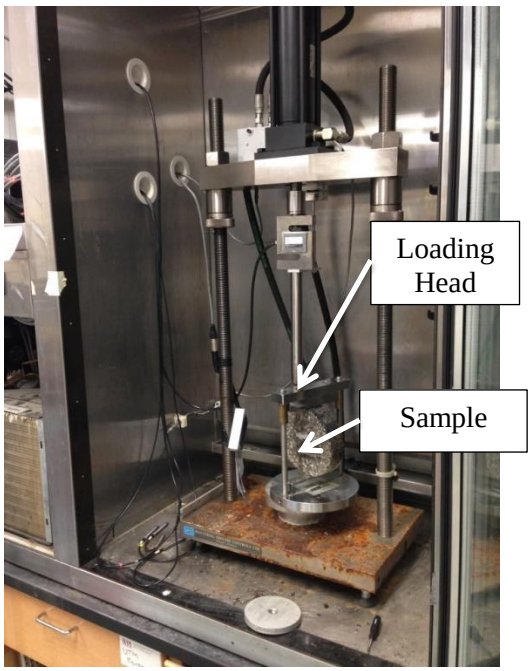

Figure 8 Sample placed in the environmental chamber in IDT mode

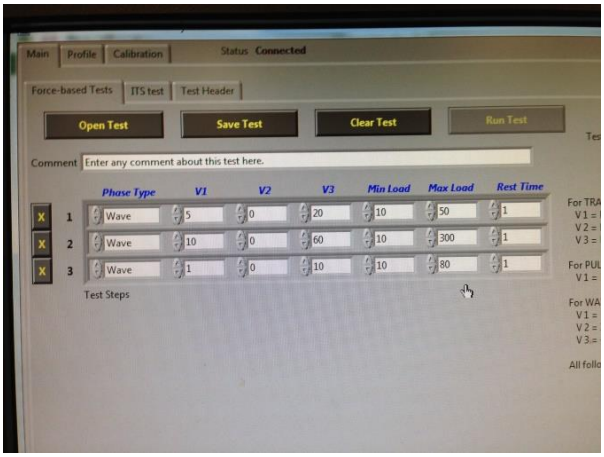

Figure 9 UTM software interface of input for sinousoidal load

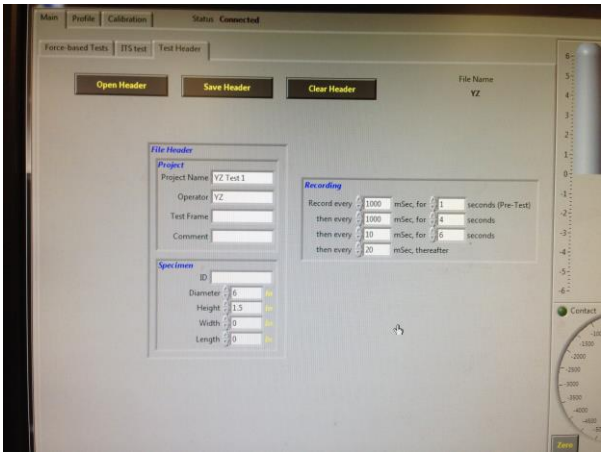

Figure 10 UTM software interface for number of data points to be collected

Moisture Induced Sensitivity Testing (MIST)

The MIST consists of an enclosed cylindrical chamber, which is filled with water once the sample is placed inside it. The chamber has a bladder that is used to create pressure inside the chamber with the use of air that is pumped into it. Since water is essentially an impressible fluid

all point of water experience the same pressure. When the bladder releases the air the chamber is depressurized. The bladder is located at the bottom of the chamber and separated from location of the sample in the chamber. Figure 11b shows the MIST chamber and the bladder location. The air is pumped in to the bladder through hydraulic motor and a piston. The amount of pressure created in the chamber is directly correlated to the amount air pumped into the bladder. The pressure in the chamber is monitored by a pressure gauge on the lid which in turn also controls the stroke length of the piston. To ensure the chamber is only filled with water before and during and the test, two valves, attached on top of the lid, release any entrapped air periodically. An additional water is replaced with the entrapped air though the valves. Figure 11b illustrates the lid with valves and pressure gauge attached to it. The process of air being pump into and released from the bladder is considered a cycle, and the number of cycles can be preset by the user.

The damage mechanism in the MIST conditioning process is hypothesized as follows. HMA mixes consist of both water accessible and water inaccessible voids, particularly inside the aggregates. The pressure created in the chamber forces the water to enter into the accessible voids of the HMA sample. As the number of cycle increases, the voids in the sample open up more and water continues to fill up the voids. The water moves around the inaccessible voids and these inaccessible voids tend to get compressed. The accessible void would get larger and open up as the cycle increases. A mix with good cohesive and adhesive properties would resist the intrusion of water and maintain the size of the voids, and hence would be less sensitive to pressurizing action of the water. It is further hypothesized, that this sensitivity would be captured by a change in E*. A mix that is less sensitive to moisture would probably show less change in E* because there is less effect on the density of the sample. On the other hand, mixes with poor cohesion and adhesive strength would demonstrate a higher change in E* because of either opening up of voids or due to closing of voids and resultant increase in density due to repeated pumping action. Note that unlike in the field, the sample is conditioned in the lab in a confined mold. The repeated action of water in unconfined condition in the field will not result in an increase in density and a resultant increase in E*. Therefore, under laboratory conditions, both increase and decrease in E* should be perceived as an indication of the moisture sensitivity of the mix.

The step by step MIST conditioning procedure is described in Figure 11. In this experiment, all 32 samples were conditioned at 30 psi, 25°C and with 10,000 cycles [5]. The samples were conditioned in MIST with the mounting studs attached to them since the post-MIST E* was needed to be tested after completion of MIST conditioning.

Step-by Step MIST conditioning procedure

a. MIST machine and its power button

b. The specimens are placed inside the chamber and water is added to the chamber once the specimens ready to be MIST conditioned. Then the chamber is sealed from the top.

c. The parameters for which the specimens will be conditioned at can be set under menu in the MIST machine. MIST conditioning parameters: Temperature (25°C), Cycles (10,000), Pressure (30 psi)

Figure 11 Step by step MIST procedure along with picture and description

Accelerated drying of sample using CoreDry

After performing the Post-MIST E* test, the samples needed to be tested for its new BSG, porosity and air void content since MIST conditioning may change these volumetric properties. However MIST conditioning results in forcing of the moisture to into the voids of the sample and therefore a long period of time would be required to dry the sample just by blowing drying with a fan. In order to accelerate the drying process, an industry approved drying system called CoreDry was used to dry the samples. CoreDry works by using a vacuum and thermoelectric cold trap to draw the water out from the pores of the sample and evaporating the

water by lowering the vapor pressure. This method of drying does not change the properties of the sample. Figure 12 illustrates the setup of the CoreDry machine.

Figure 12 CoreDry equipment

Figure 13 Picture of water discharing from the sample

Indirect Tensile Strength Test

After determining the post-MIST volumetric properties, the samples were tested for their strength. The goal of performing this test was to identify the relative strength of the mixes in post-MIST condition. Indirect tensile strength test was conducted according to ASTM D6931 [16]. Using universal testing machine, IDT strength test was conducted on three out of four samples from each of the mix group. The samples were tested at a loading rate of 2 in. (50 mm) per minute. The broken sample would be inspected to detect uncoated/stripped aggregates, if any. By breaking the samples, it can be determined whether the samples were well mixed or not.

Results & Data Analysis

Plan of Study

The primary goal of the data analysis of the results was to determine whether moisture-induced damages were present on the tested sample or not. The conditioning temperature of 25^{o}C was selected as this temperature expected in Spring or Fall. Figure 14 presents the flow chart of the plan of analysis.

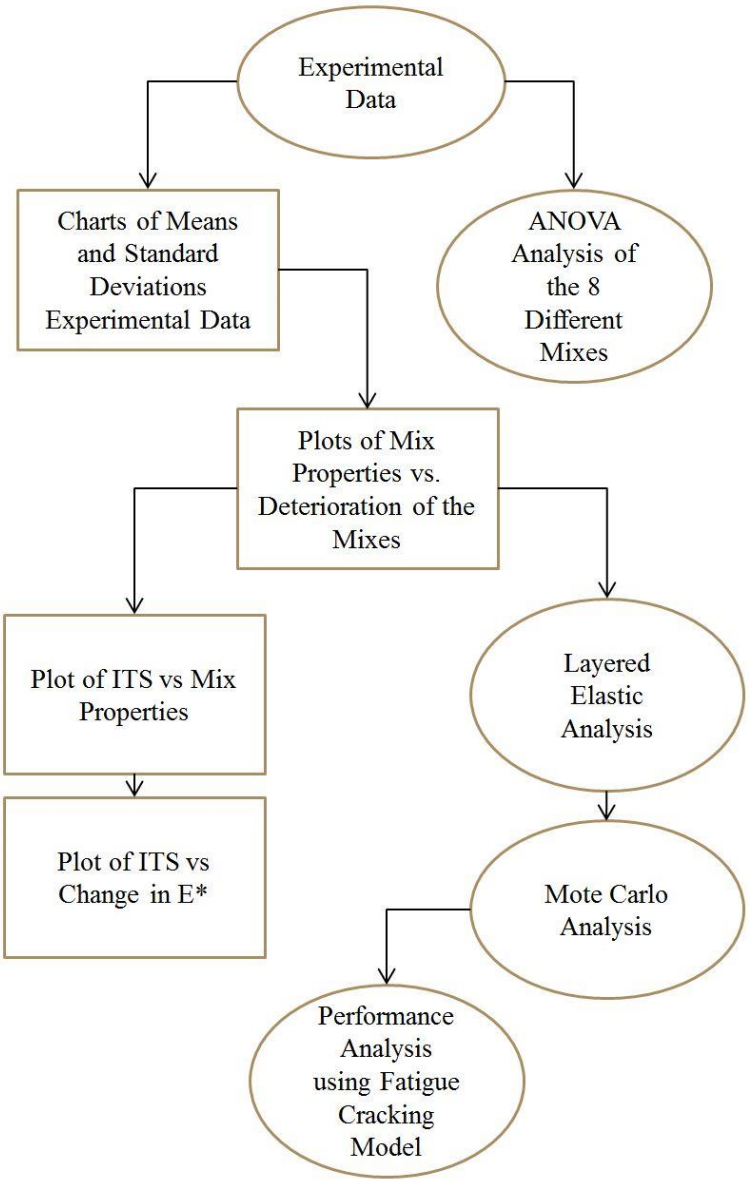

Figure 14 Plan of Analysis

Data Analysis of Mean and Standard Deviation of Different Results

Pre-MIST BSG, porosity and air void content were calculated from the collected data using the Corelok method. Table 3 in Appendix A illustrates different values of all 32 samples from 8 different mixes. All 32 samples for 8 different mixes were targeted to achieve 7+/-% air void content during compaction and all most all the samples were within the target air void content. The data were analyzed to determine the mean and standard deviation of each parameter for each mixes. Figure 15 provides the mean and standard deviation of air void content for the different mixes. One particular mix Durham (Dur) had a relatively low air voids, an average percent air void of 5.2. It was the only mix that did not achieve the targeted air void. This particular mix also had aggregates with a very high Micro-Deval number of 27%. It is suspected that the coarse aggregates in Dur mix were being crushed during the compaction, which caused a lowering of the air voids. Note that this aggregate fails the Maine DOT criteria for Micro-Deval test, which is set at a maximum of 18%. It is expected that the mix will experience similar breakdown of aggregates and resulting loss of voids during compaction in the field.

The percent porosity of the mixes was similar but less than compared to the air void content. This is justified because porosity essential means effective air voids, or air voids that area accessible to water. By knowing the percent porosity, one can determine the degree of interconnectivity of voids within a sample and this knowledge of interconnectivity can be correlated to permeability of the compacted sample. The mean and standard deviation of percent porosity of the different mixes are presented in Figure 16.

The mean and standard deviation of pre-MIST E* (10 and 1 Hz) are presented in Figure 17 and 18 and the mean and standard deviation of post-MIST E* (10 and 1 Hz) are presented in Figure 19 and 20. On average most of the mixes experienced decrease in E* except the Durham mix which showed as increased in E*. A high value of standard deviation of E* (in both pre-MIST and post-MIST) can be noticed in some mixes.

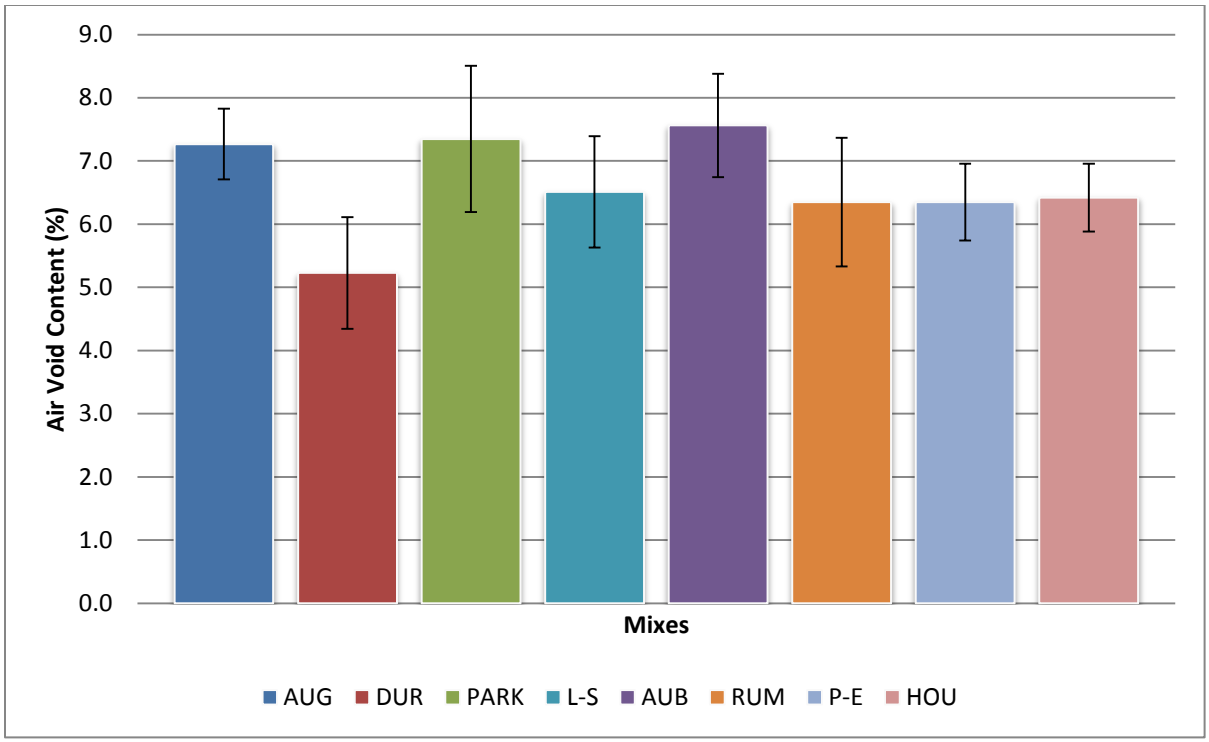

Figure 15 % Mean Pre-MIST Air Void Content

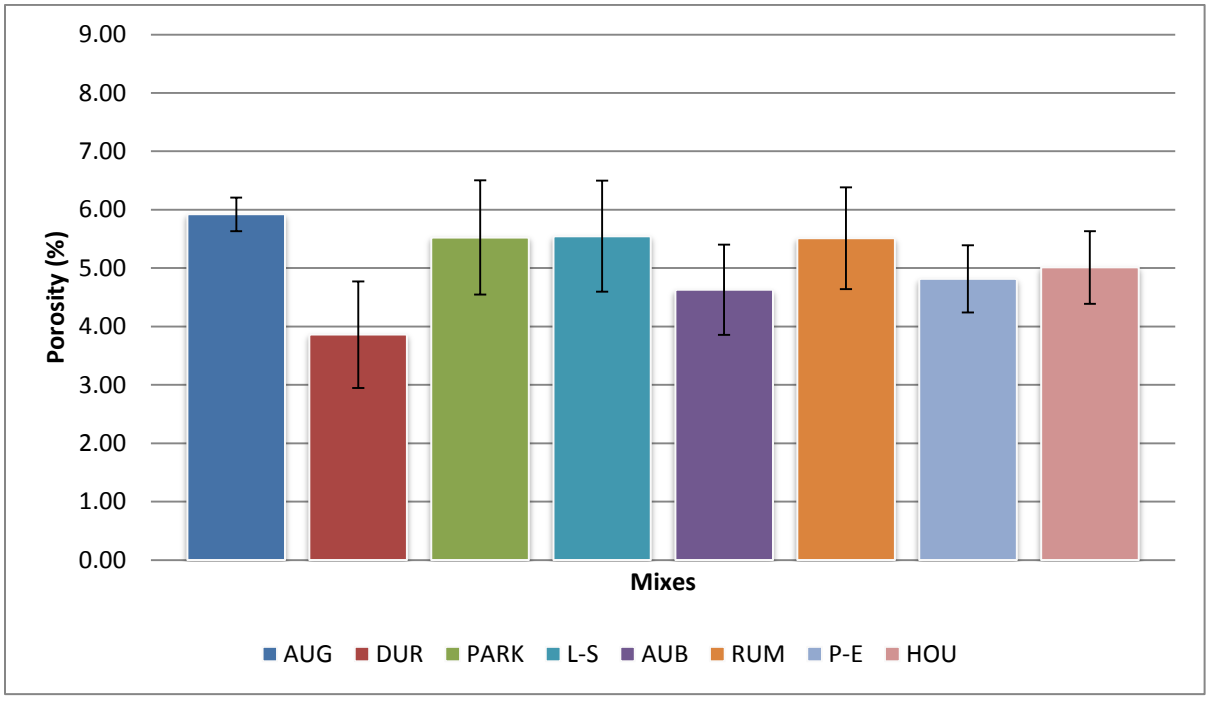

Figure 16 % Mean Pre-MIST Porosity

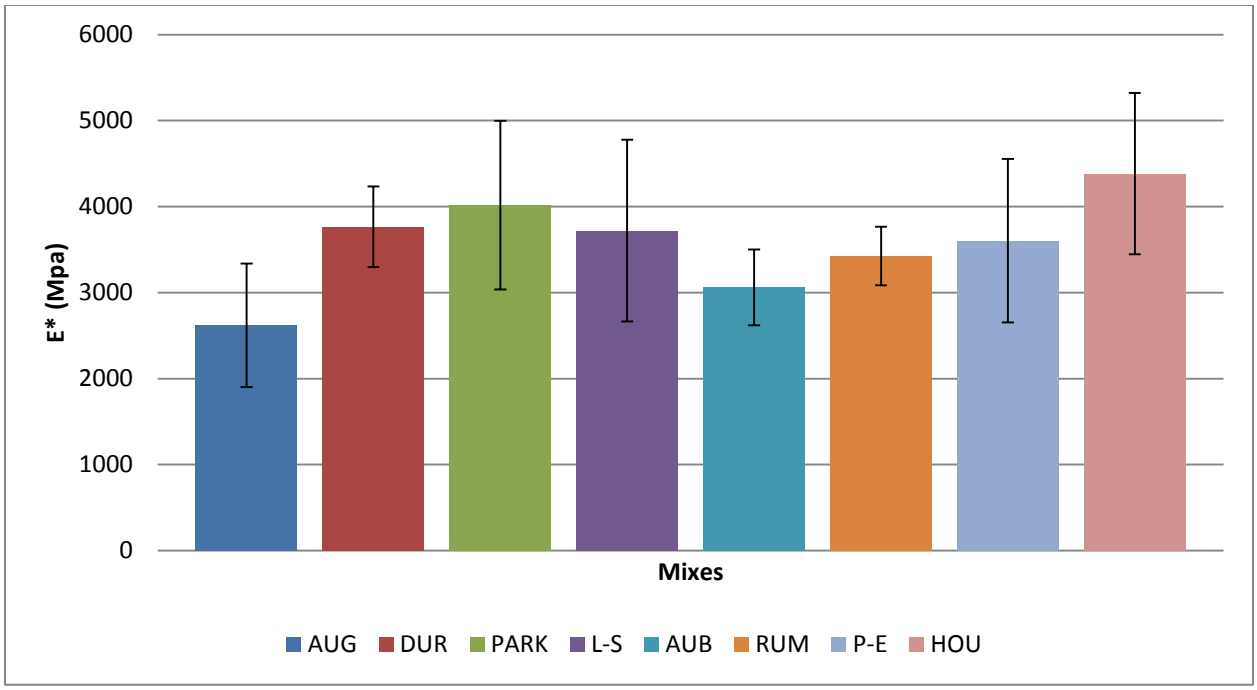

Figure 17 Pre Mist Mean 10 Hz Dynamic Modulus in IDT

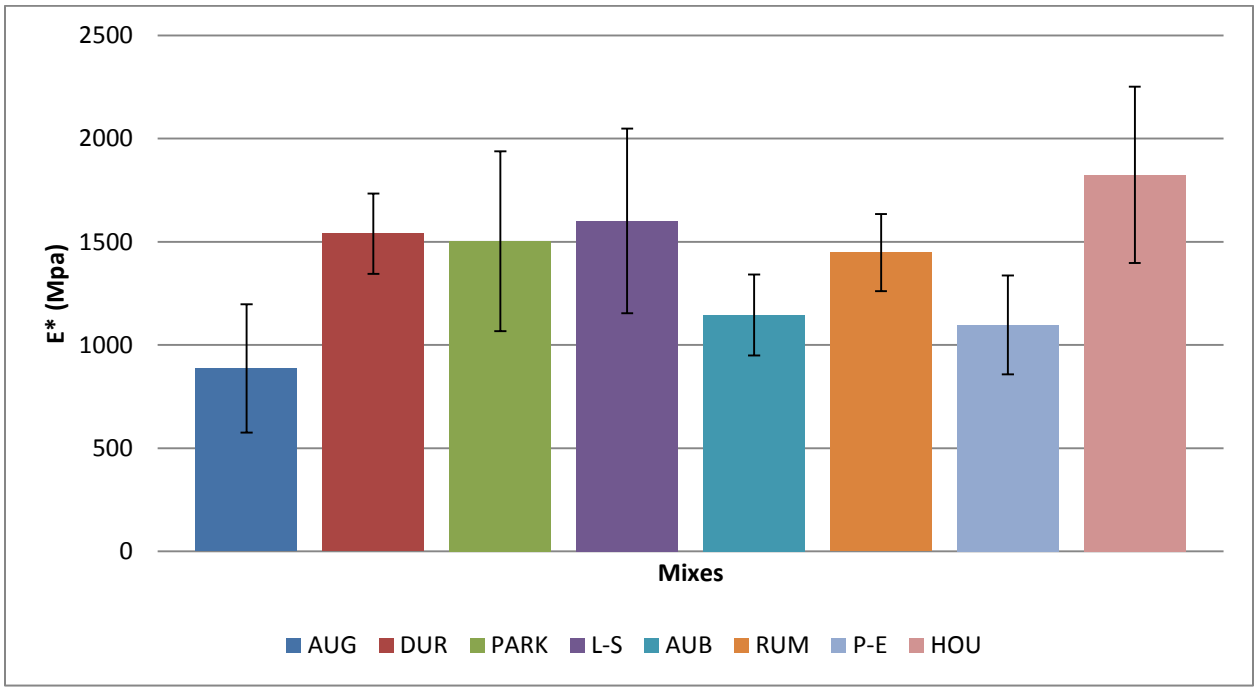

Figure 18 Pre Mist Mean 1 Hz Dynamic Modulus in IDT

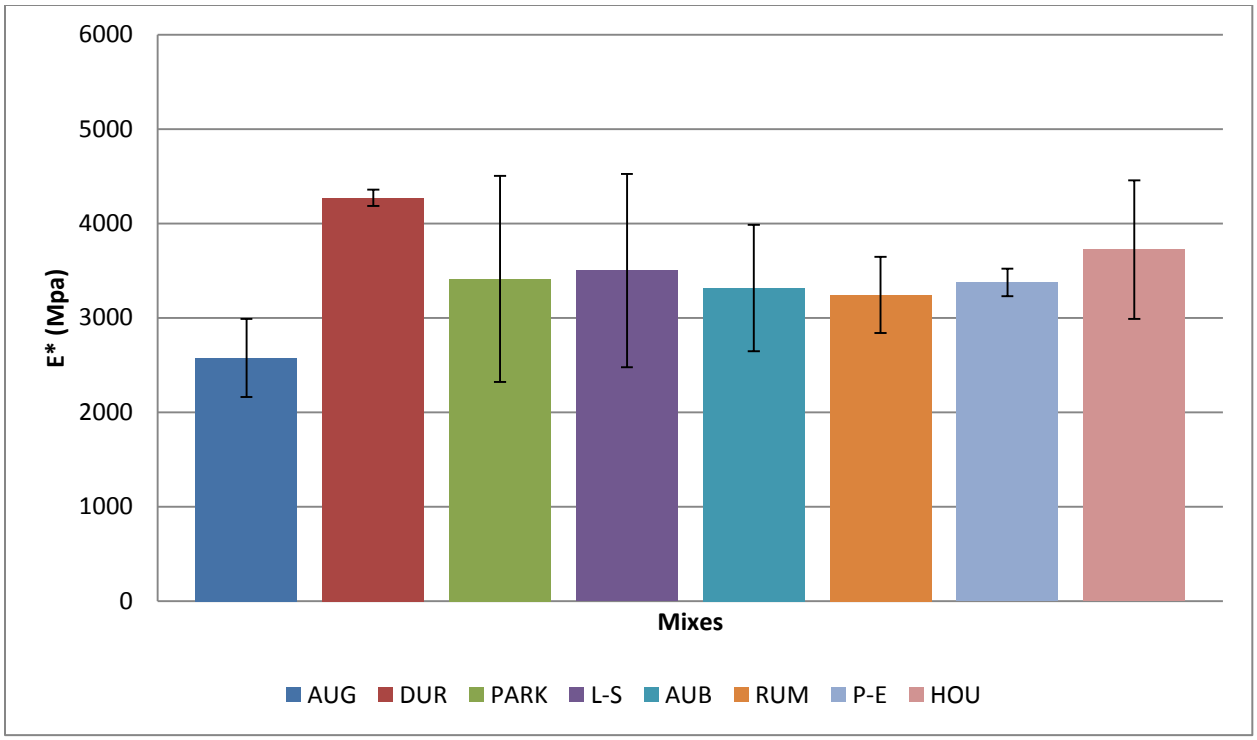

Figure 19 Post Mist Mean 10 Hz Dynamic Modulus in IDT

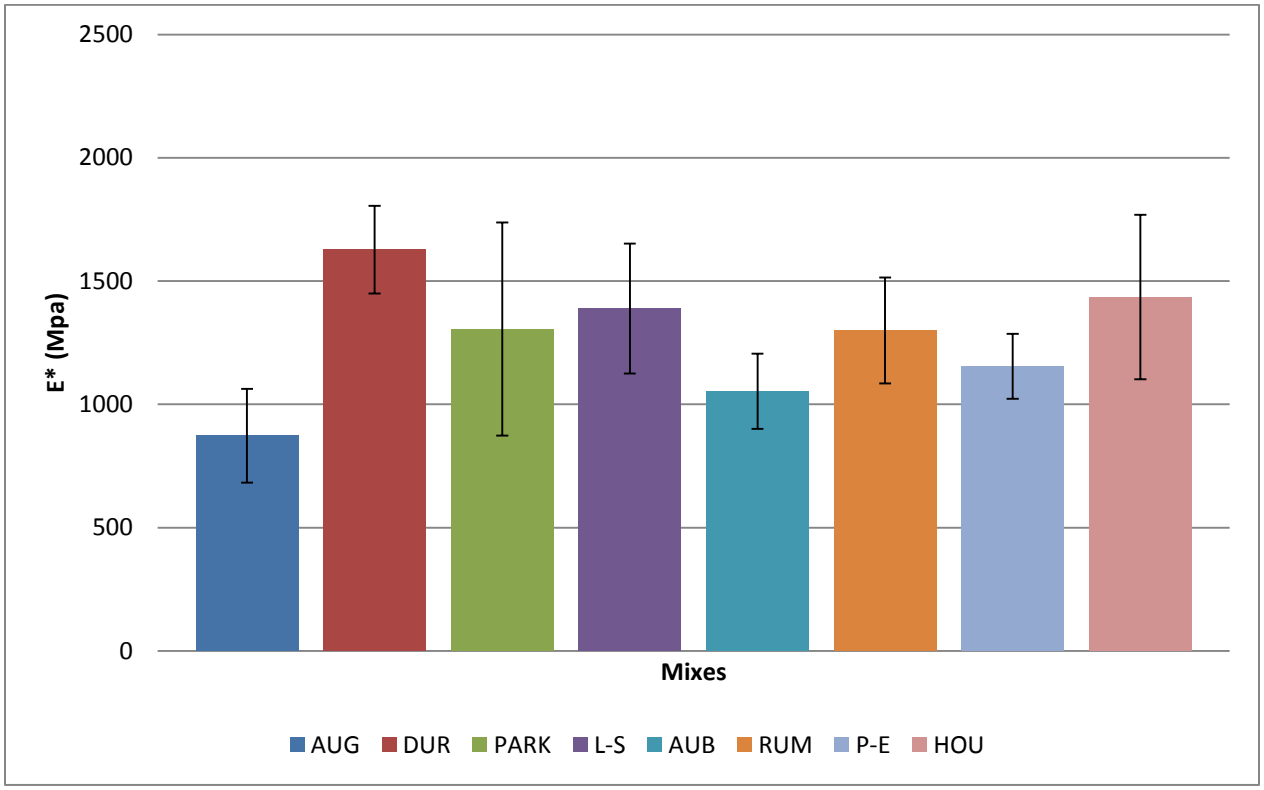

Figure 20 Post Mist Mean 1 Hz Dynamic Modulus in IDT

The change in E* values for different mixes are presented in Figure 22 through 37. As it can be interpreted from the graphs, percent change in E* (Post-Pre) are either negative or positive change. Some of the mixes exhibit only negative change in E* while others exhibit both positive and negative change in E*. The positive change in E* could be contributed to increase in the density of the sample. This behavior would not likely happen in field with unconfined condition as compared to a confined camber in the MIST. The confined condition in the sample forces the air voids in the sample to close up resulting in a compaction of the samples under water pressure during the MIST conditioning. Figure 21 illustrates a schematic of fine aggregates movement in the sample as pore water pressure is exerted on the inaccessible voids and coarse aggregate.

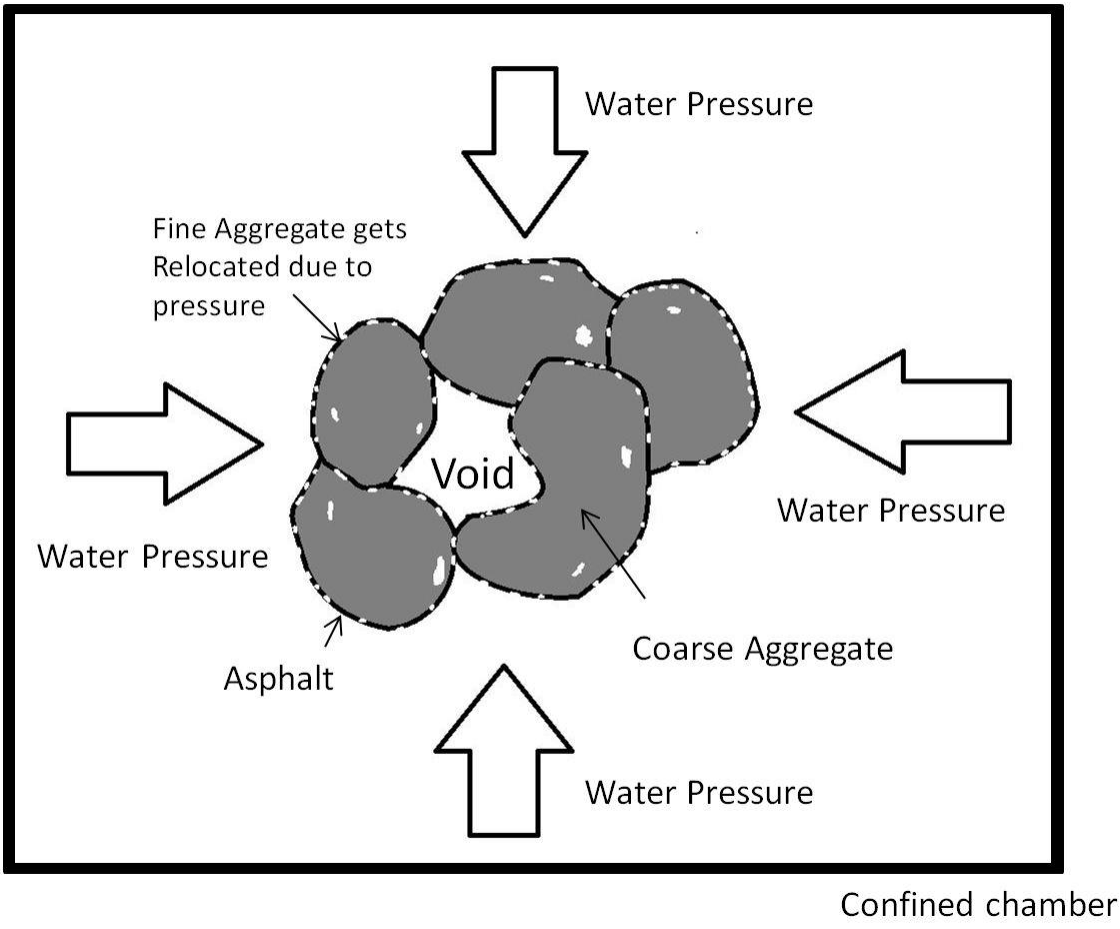

Figure 21 Schematic of pore water pressure on fine aggregate, asphalt, coarse aggregate and air void in a sample

A scatterplot between porosity and change in E* was graphed to determine whether there was any correlation between the two (Figure 38 and 39). Results from both 10 and 1 Hz loading frequencies showed no correlation.

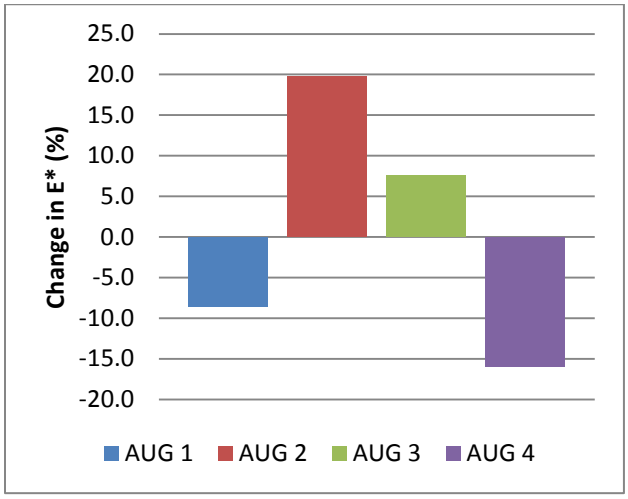

Figure 22 % Change in Pre-Mist E* 10 Hz

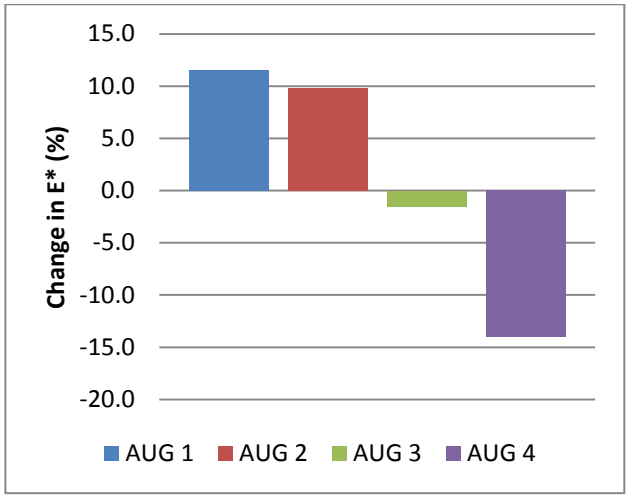

Figure 23 % Change in Pre-Mist E* 1 Hz

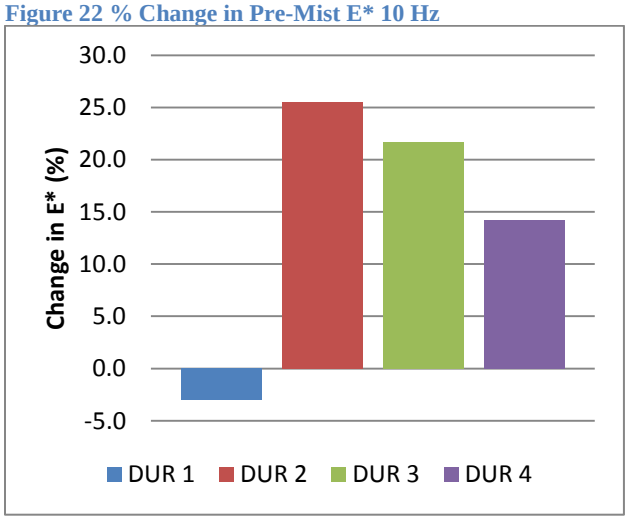

Figure 24 % Change in Pre-Mist E* 10 Hz

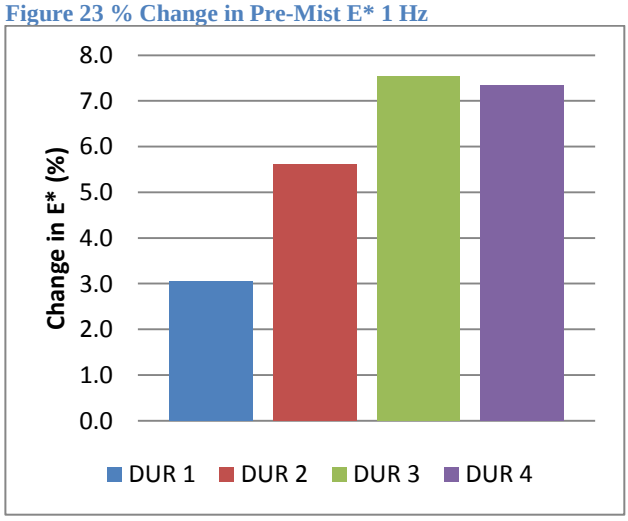

Figure 25 % Change in Pre-Mist E* 1 Hz

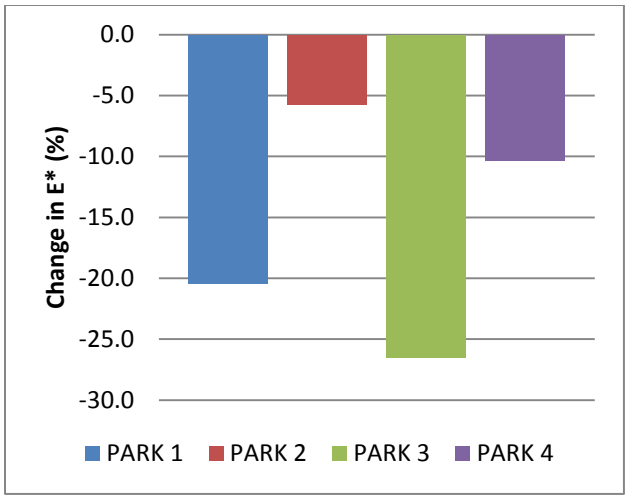

Figure 26 % Change in Pre-Mist E* 10 Hz

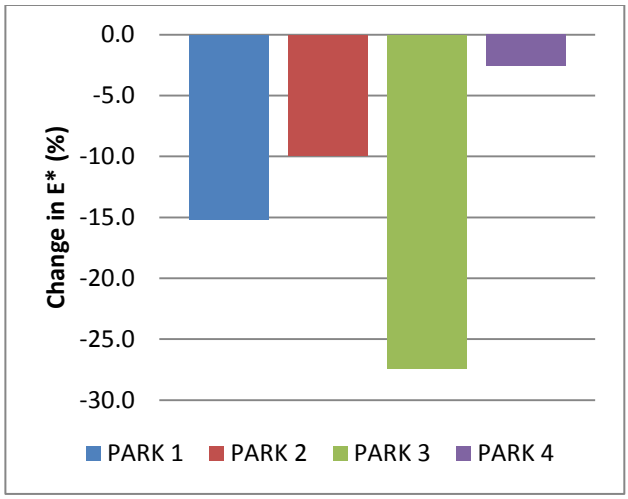

Figure 27 % Change in Pre-Mist E* 1 Hz

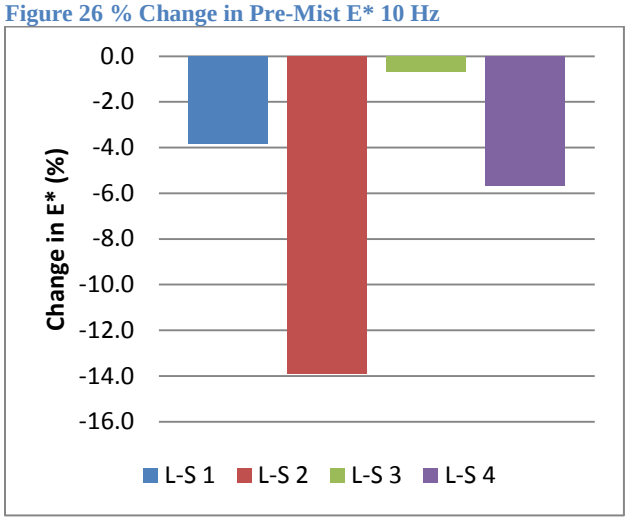

Figure 28 % Change in Pre-Mist E* 10 Hz

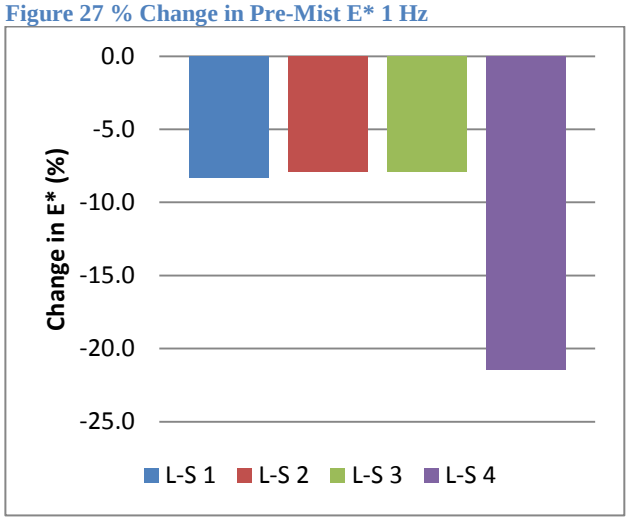

Figure 29 % Change in Pre-Mist E* 1 Hz

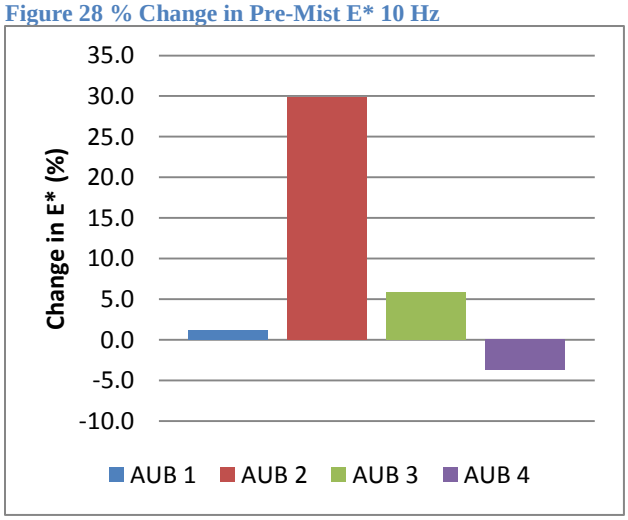

Figure 30 % Change in Pre-Mist E* 10 Hz

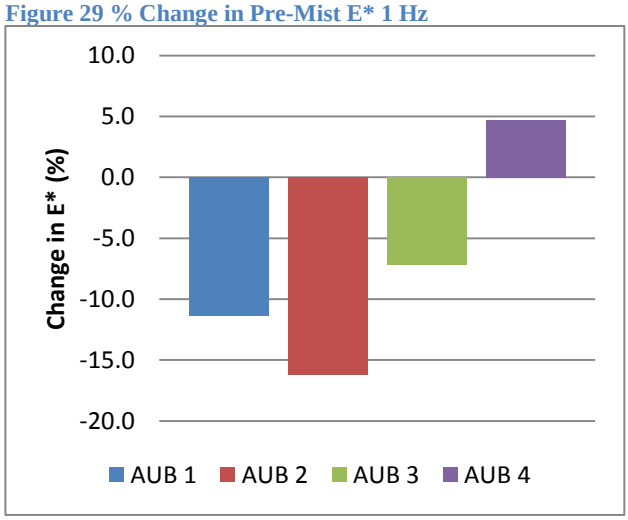

Figure 31 % Change in Pre-Mist E* 1 Hz

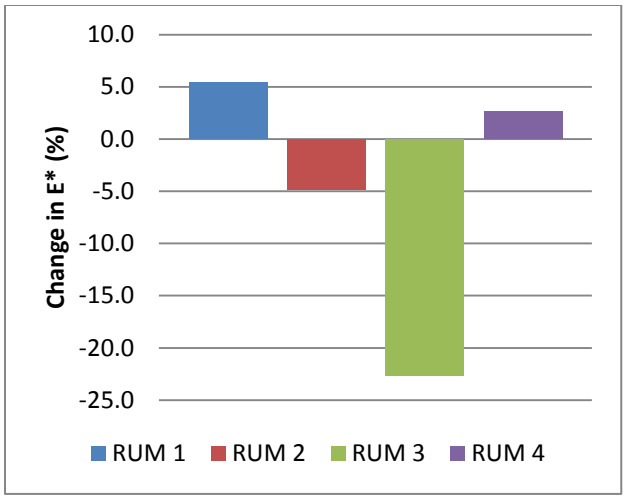

Figure 32 % Change in Pre-Mist E* 10 Hz

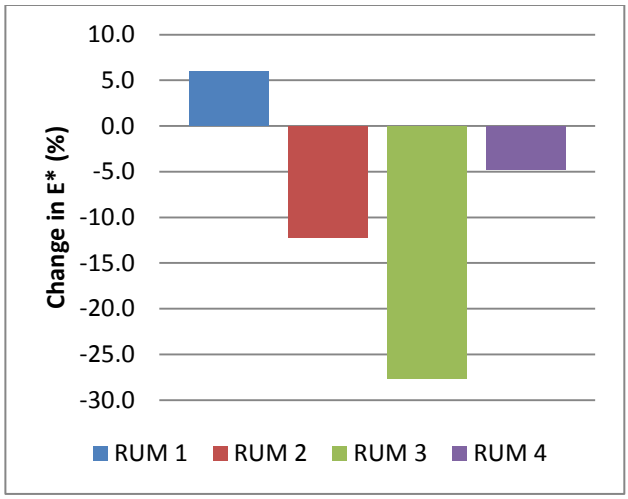

Figure 33 % Change in Pre-Mist E* 1 Hz

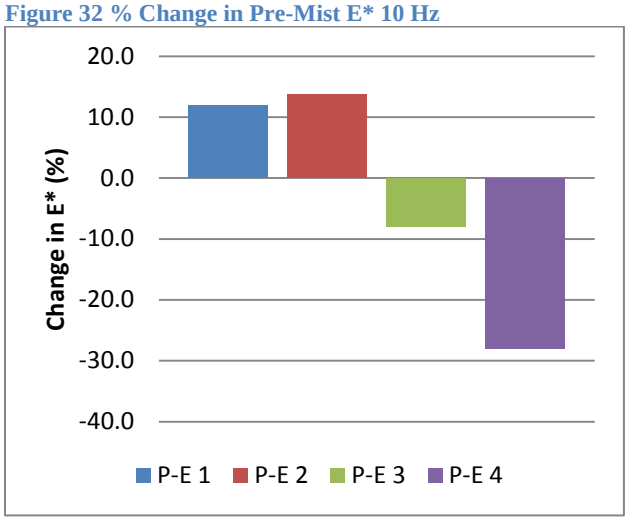

Figure 34 % Change in Pre-Mist E* 10 Hz

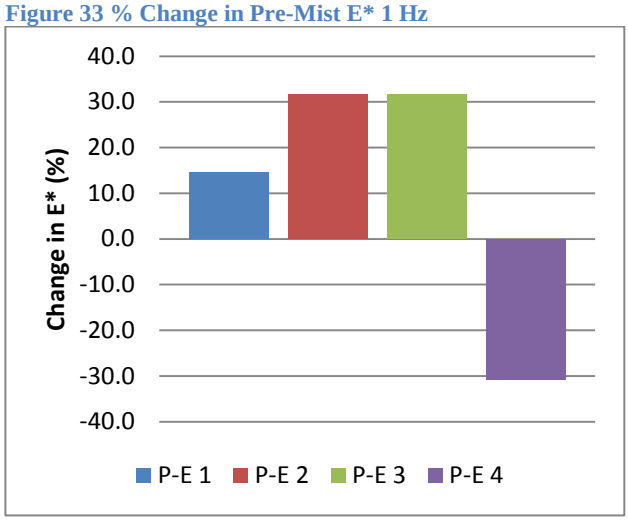

Figure 35 % Change in Pre-Mist E* 1 Hz

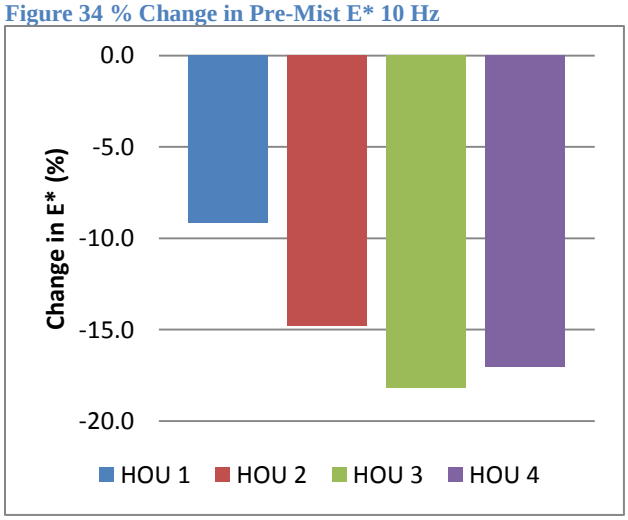

Figure 36 % Change in Pre-Mist E* 10 Hz

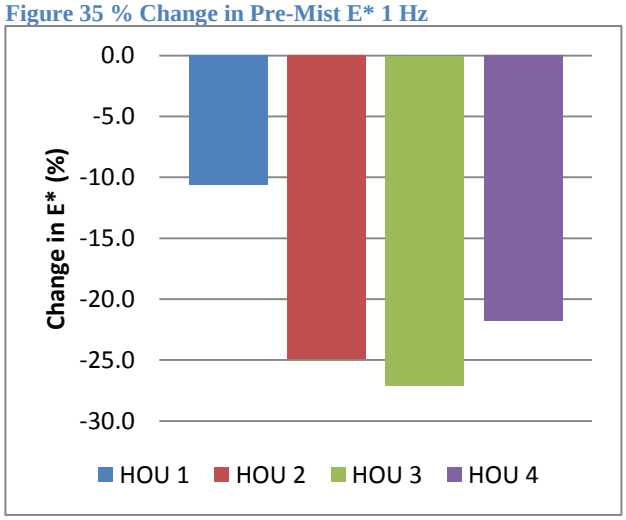

Figure 37 % Change in Pre-Mist E* 1 Hz

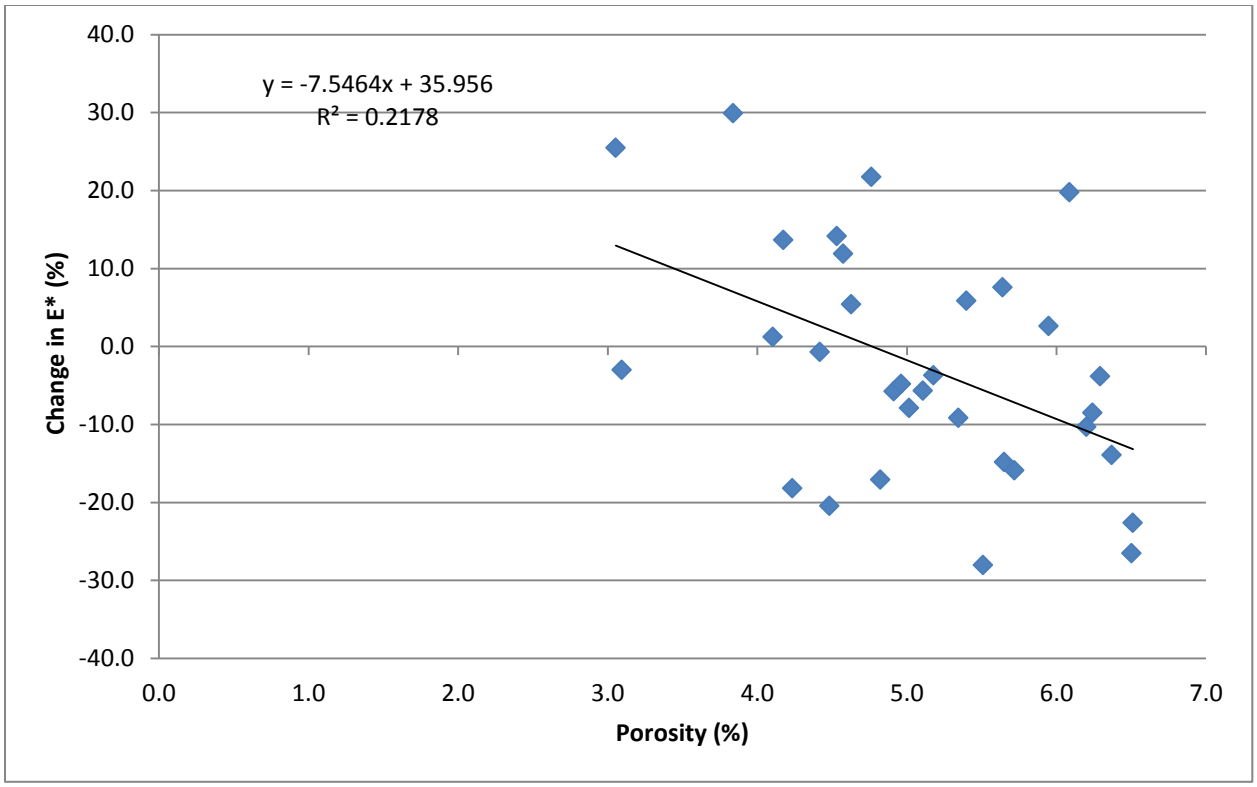

Figure 38: % Change Pre-Mist E* 10 Hz Vs. Porosity

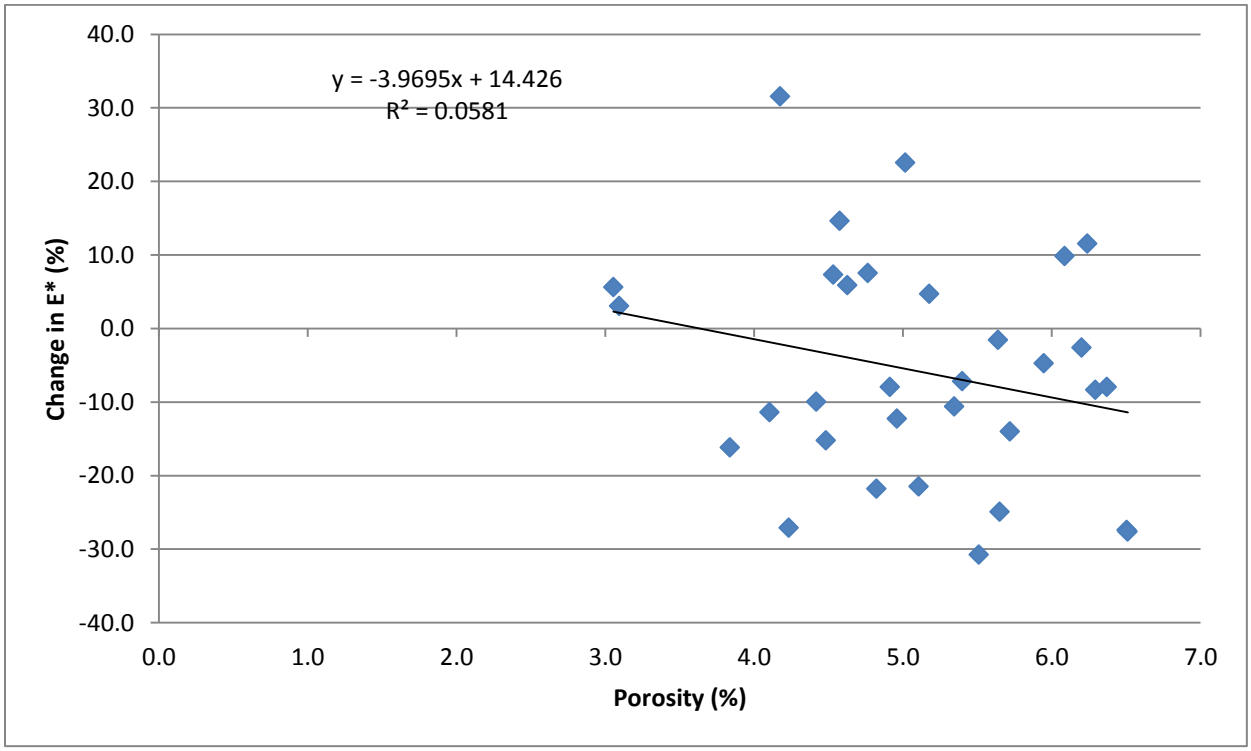

Figure 39 % Change Pre-Mist E* 1 Hz Vs. Porosity

One particular difference in the samples' condition before and after MIST was the amount of saturation presented in the samples. The test samples of Post-MIST E* were tested a day after completion of the MIST conditioning, at which time the samples were essentially under high saturation condition as detected by increased mass of the samples, compared to the dry mass. Saturation content of the samples was calculated and Table 7 in Appendix A presents the calculated data. A scatterplot was plotted against change in E* versus saturation content. Figure 40 and 41 present the plots of percent change in E* versus saturation content. There was no correlation between change in E* for 10 Hz and saturation content. However, a very weak correlation between change in E* for 1 Hz and saturation content could be seen in the graph with the R^2 value of 0.305.

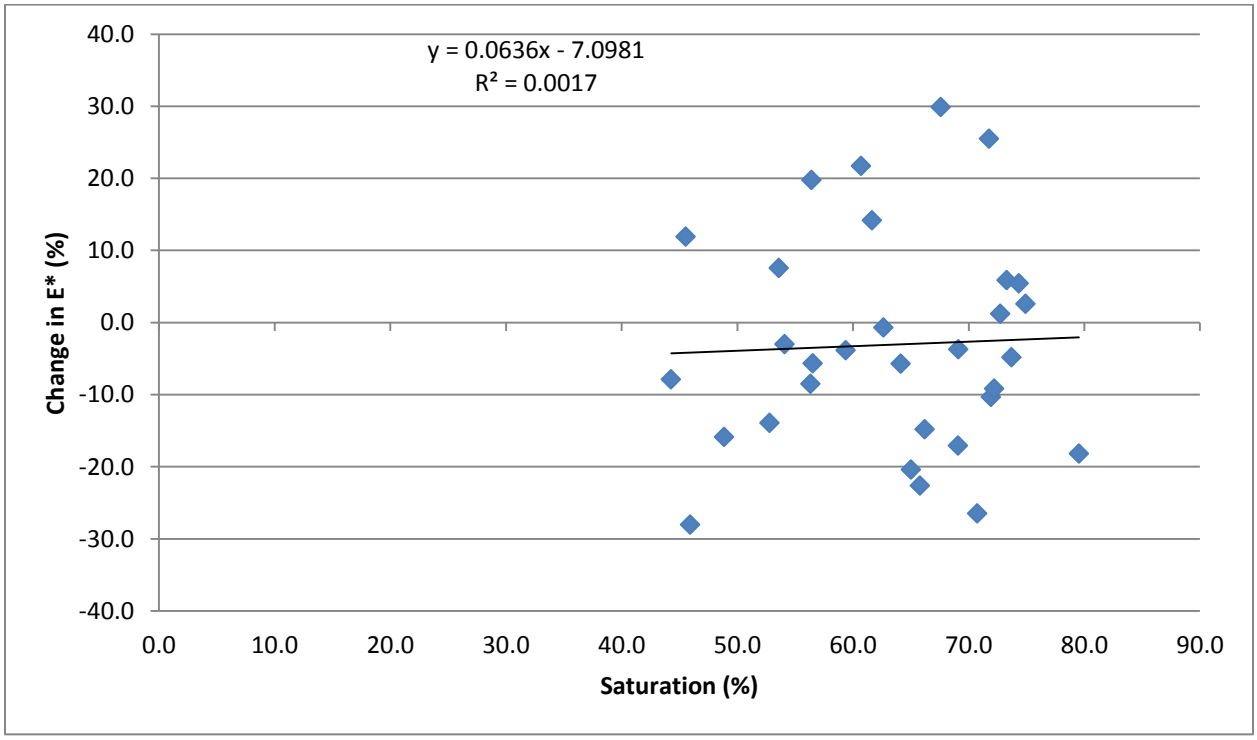

Figure 40 % Change in E* for 10 Hz Vs. Saturation

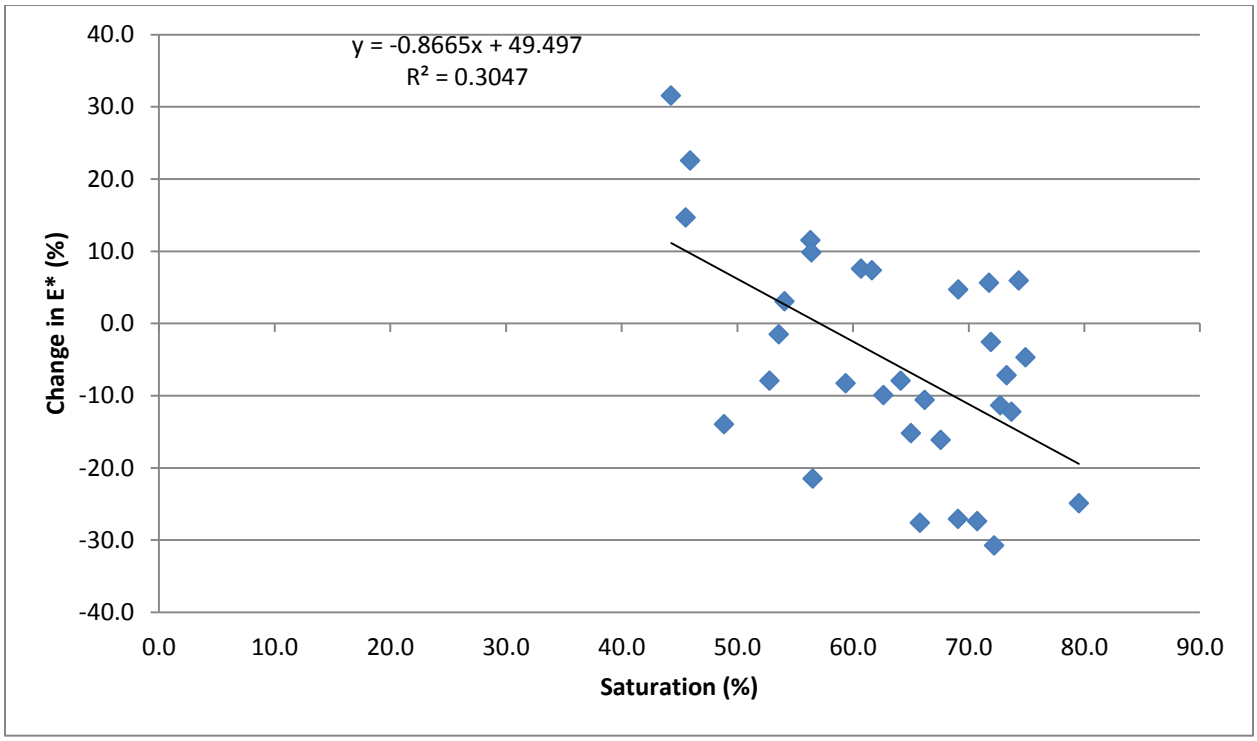

Figure 41 % Change in E* for 1 Hz Vs. Saturation

Plot of Mixes Properties vs. Deterioration of Mixes

Change in E versus Materials and Mix Properties*

The experimental data of the change in E* (1 Hz) was more consistent compared to the experimental data of change in E* (10 Hz). Therefore the analysis of the data was more heavily focused on change in E* of 1 Hz. Furthermore, the decision to focus on 1 Hz experiment data is based on the theoretical consideration that pavements are more susceptible to damages at lower frequencies of loading than at higher frequencies of loading. At lower frequency of loading, the behavior of pavement largely depends on the viscous property of the asphalt.

The change in E*, using mean E* of the sample for different mixes, (1 Hz) was plotted against the mix properties. The properties that were examined were fines to binder ratio (FBE), binder content, aggregate nominal size, reclaimed asphalt pavement content (RAP), aggregate Micro-Deval properties and fine aggregate absorption. There were no significant correlations between the individual mix properties and the change in E*. Figure 42 through 45 present the graphs of the x-y plots between change in E* (1 Hz) and the mix properties. Figure 46 and 47 presents the bar graph of change in E* (1 Hz) of different mixes for their nominal aggregate size

and the Reclaimed asphalt pavement (RAP) content in each mixes. However, if Micro-Deval property and fine aggregate absorption of mix property were to be combined and used as a composite value and plotted against absolute change in E*, a good correlation could be found , as shown in Figure 48. This can be explained by the fact that a combination of weak coarse aggregates (as indicated by the Micro-Deval Test) and a highly absorptive fine aggregate (indicated by absorption) is the worst combination for the potential of moisture damage.

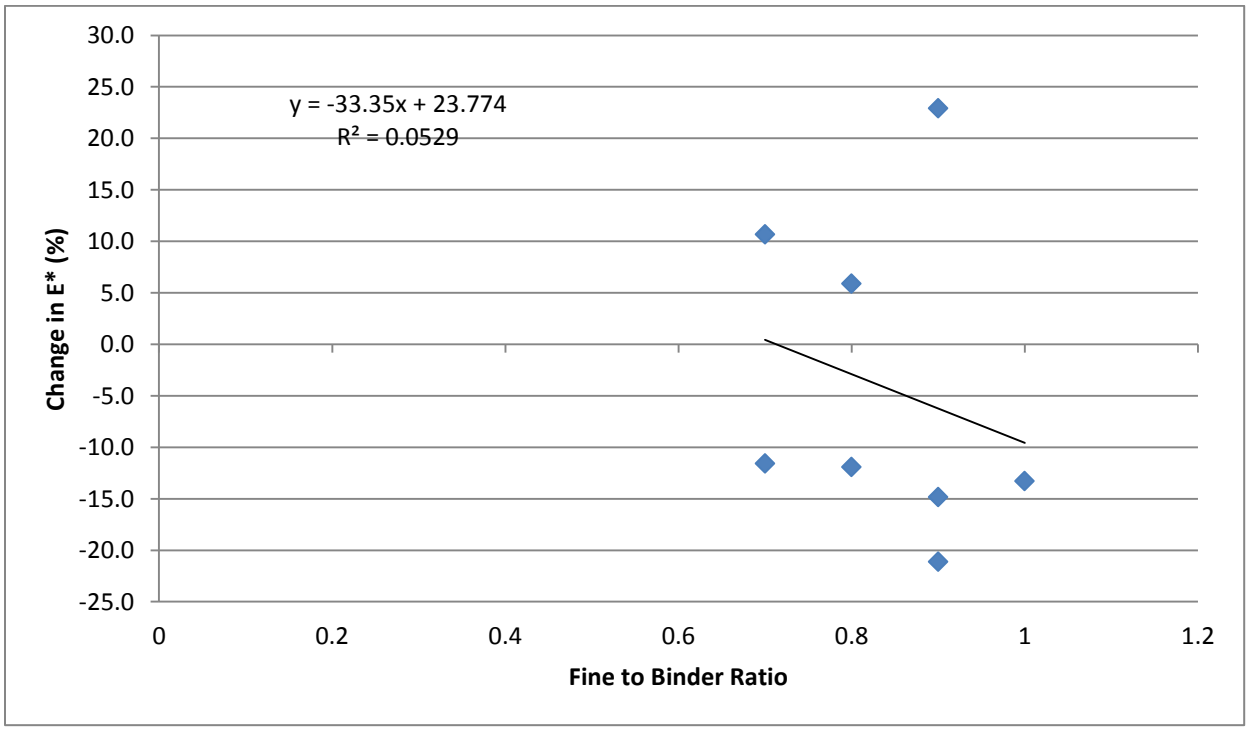

Figure 42 % Change in E* for 1 Hz vs FBE

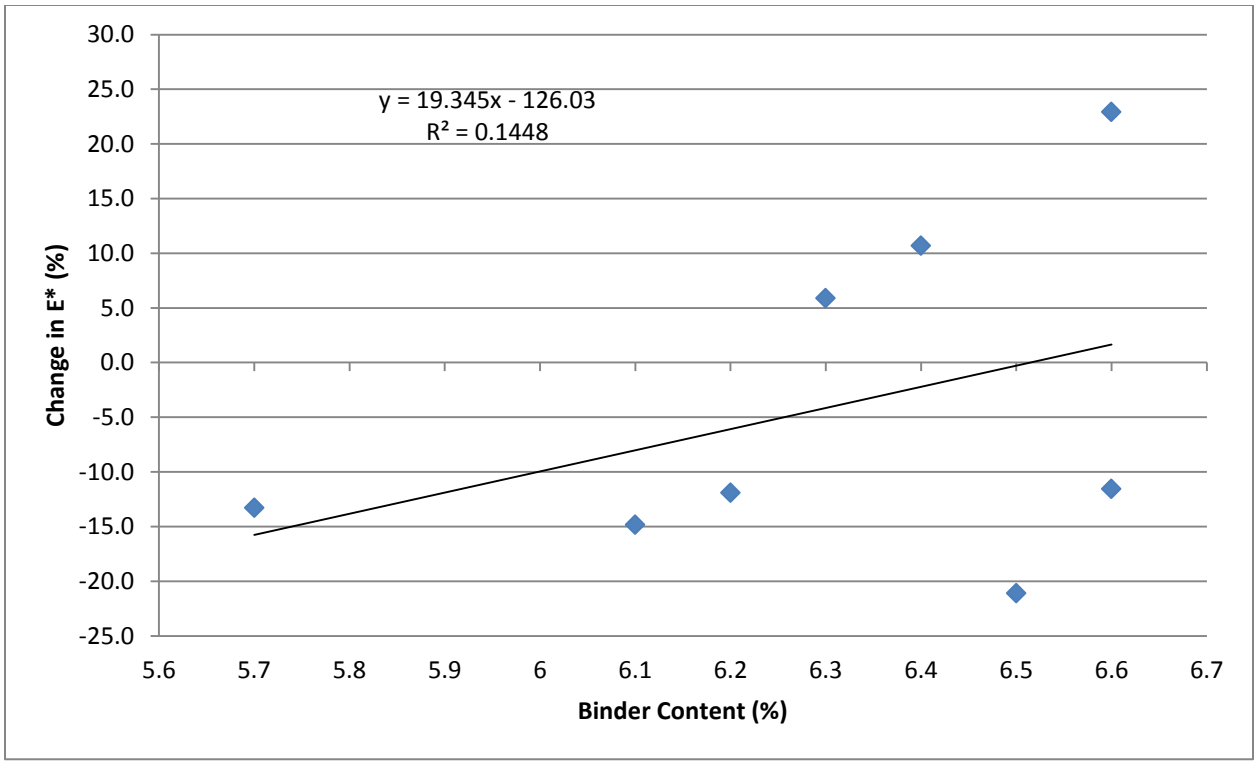

Figure 43 % Change in E* for 1 Hz Vs Binder Content

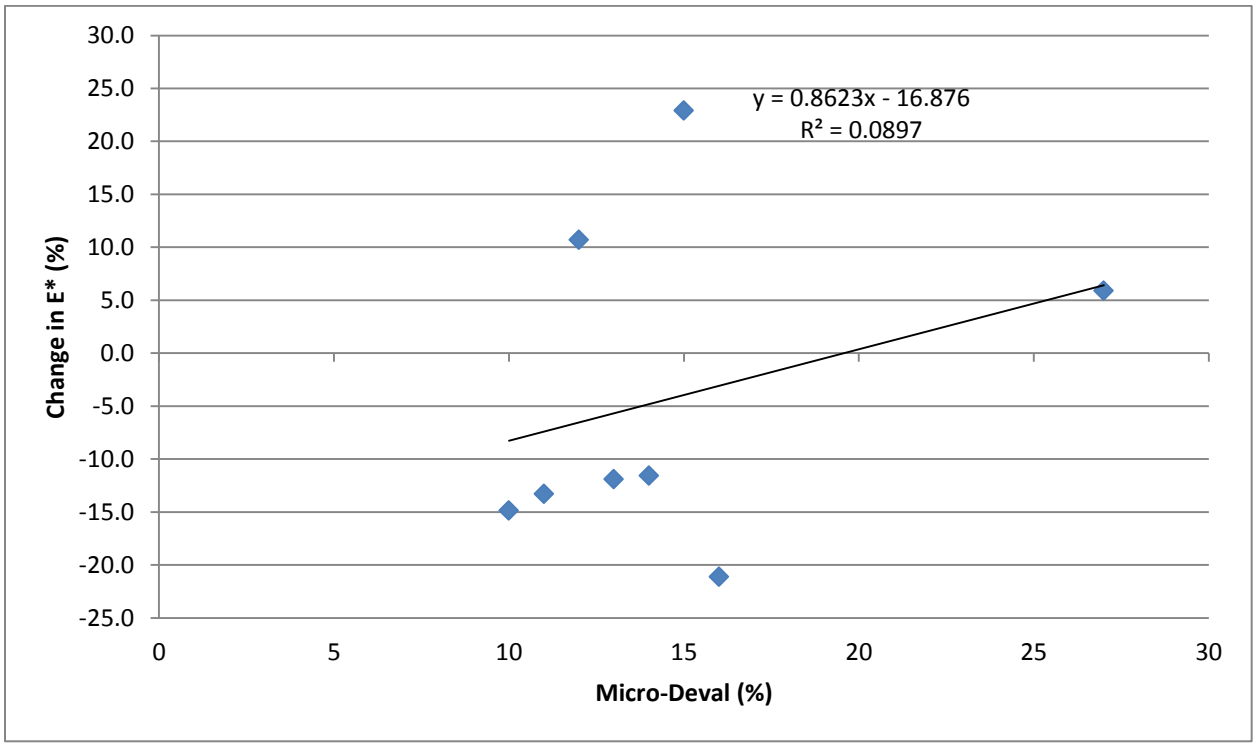

Figure 44 % Change in E* for 1 Hz vs Micro-Deval

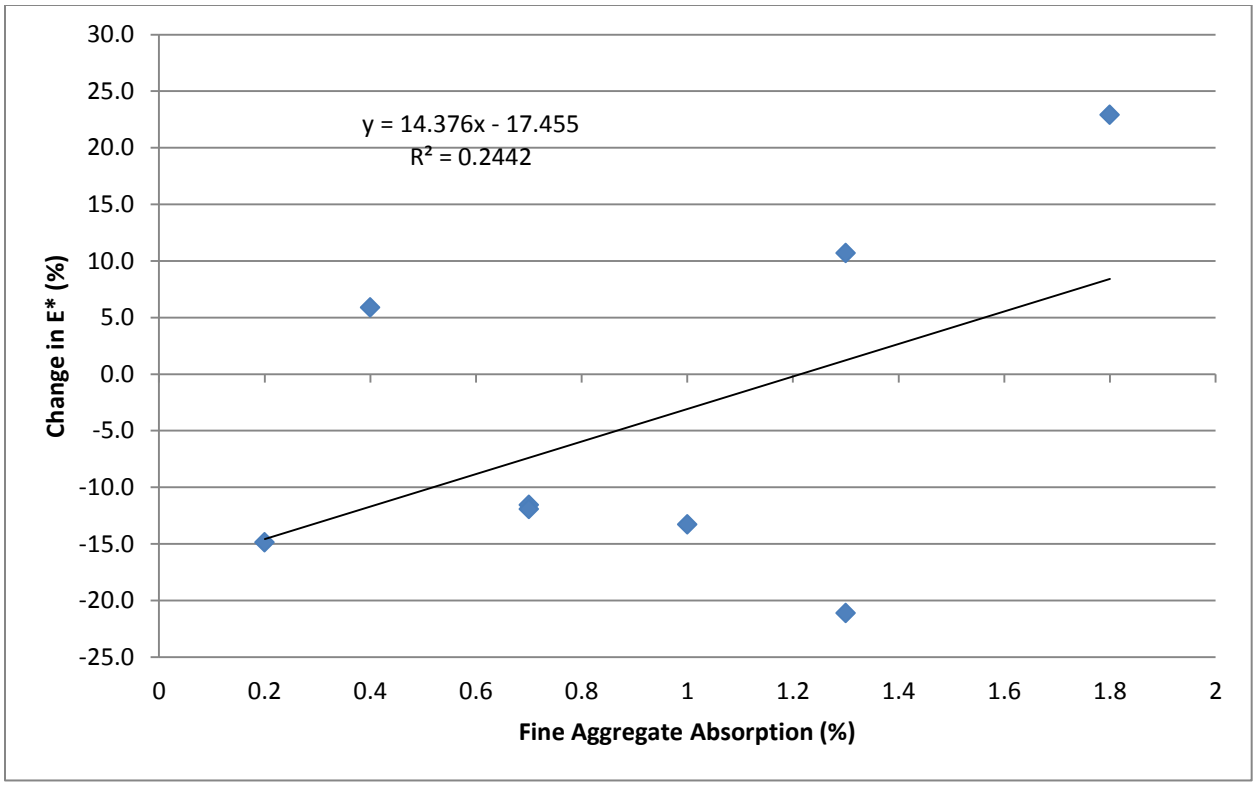

Figure 45 % Change in E* for 1 Hz vs Fine Aggregate Absorption

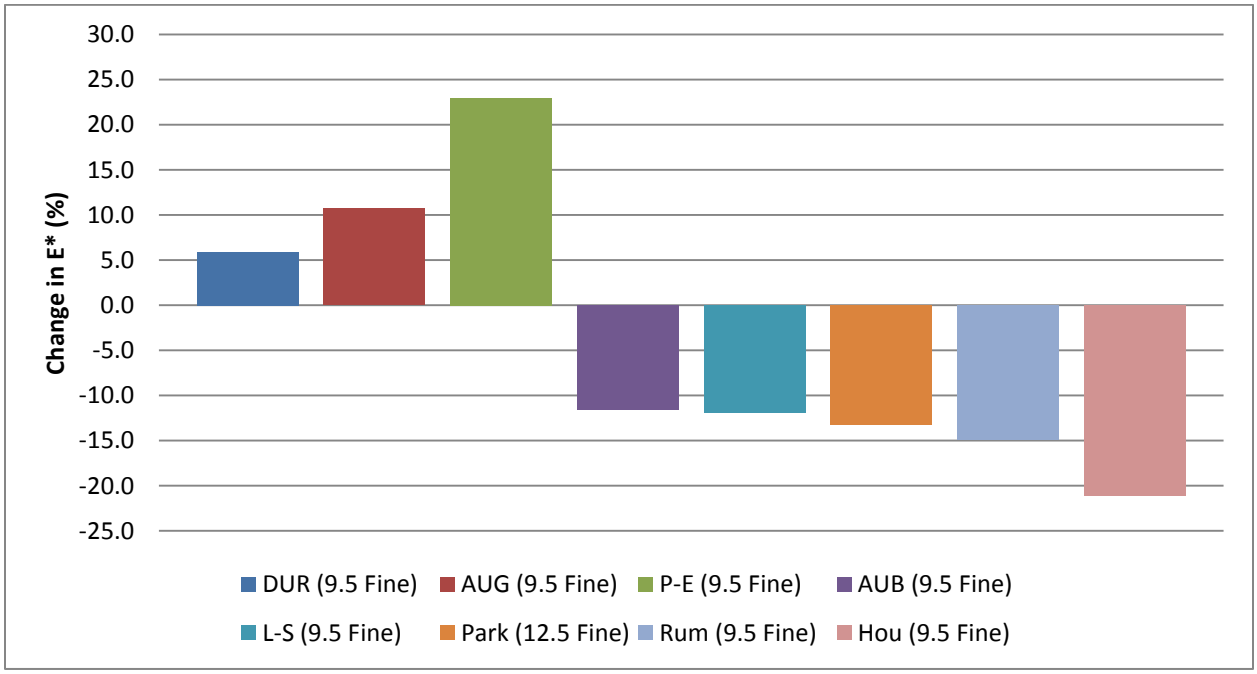

Figure 46 % Change in E* for Mix Aggregate Nominal Size

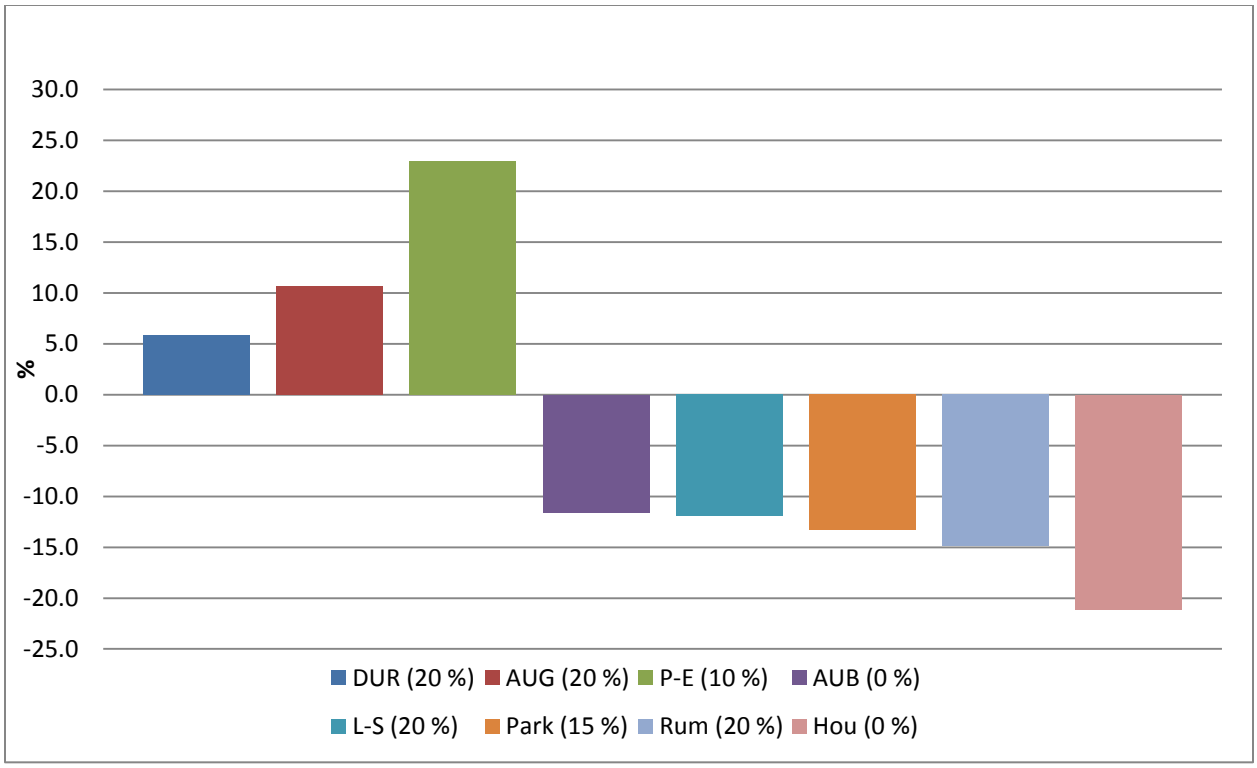

Figure 47 % Change in E* for Mix Rap Content

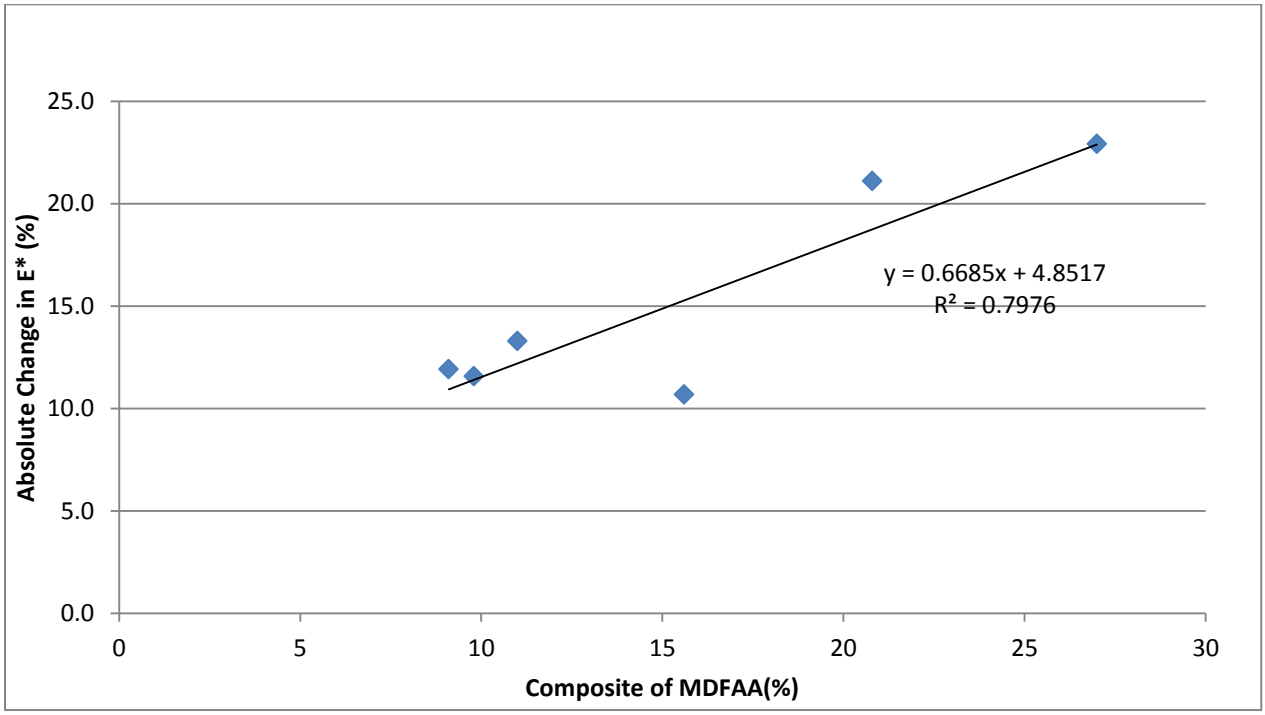

Figure 48 % Absolute Mean Change in E* vs. Micro-Deval*Fine Aggregate Absorption

Note: MDFAA = Micro-Deval value * Fine Aggregate Absorption

Change in Phase angle Vs. Mix Properties

Phase angle represents the lag between stress and strain – and a high value would indicate a material with properties similar to that of a highly viscous material, as opposed to an elastic material. The change in phase angle (1 Hz) between the pre and post MIST samples was also examined and was plotted against the mix properties for the tested mixes (fines to binder ratio (FBE), binder content, aggregate nominal size, reclaimed asphalt pavement content (RAP), aggregate Micro-Deval properties and fine aggregate absorption. No correlation was found in this analysis as well. Figure 49 through 52 present the x-y plot of change in phase angle and mix properties. Figure 53 and 54 present the bar chart of phase angle of different mixes for their nominal aggregate size and RAP content.

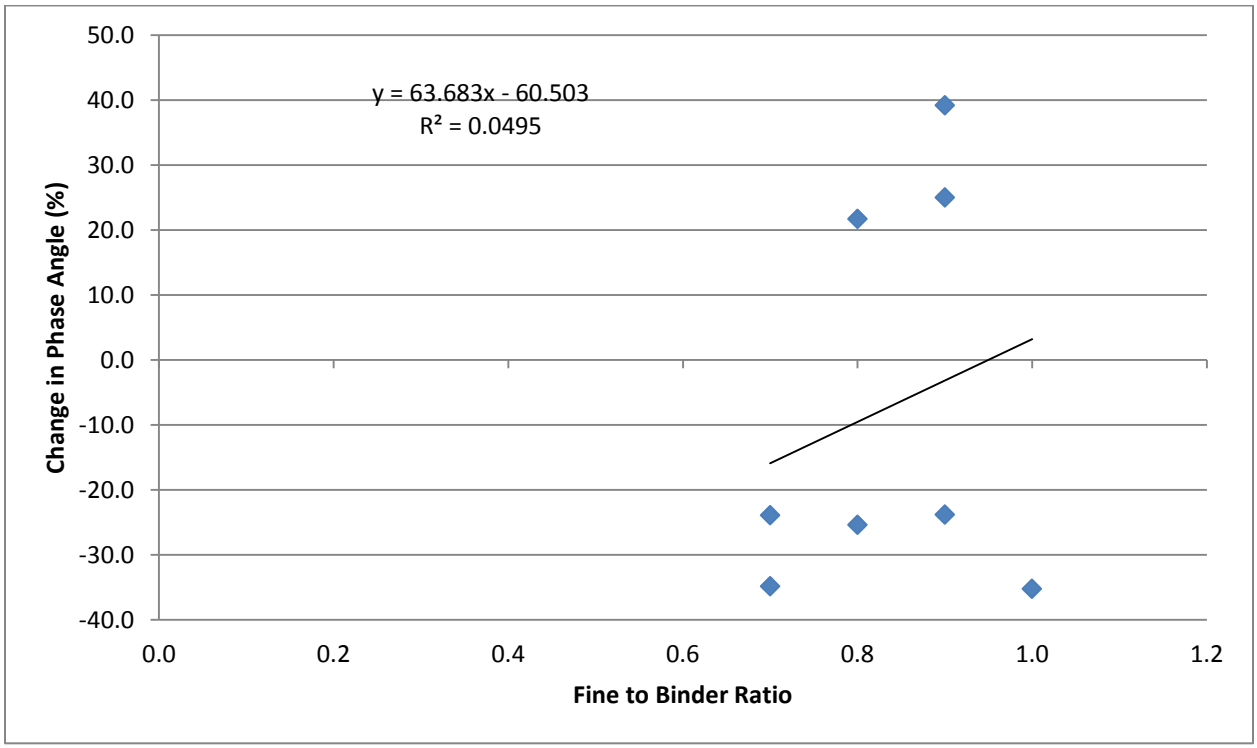

Figure 49 % Change in Phase Angle Vs. FBE

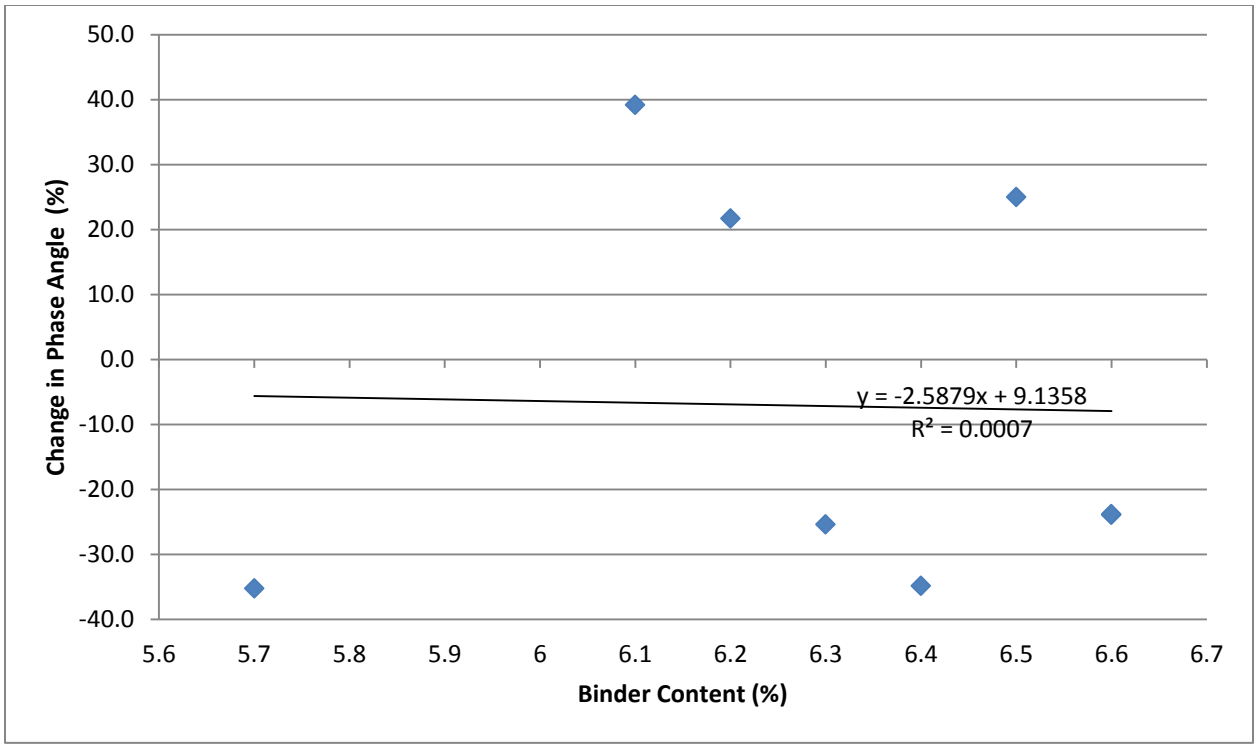

Figure 50 % Phase Angle vs. Binder Content

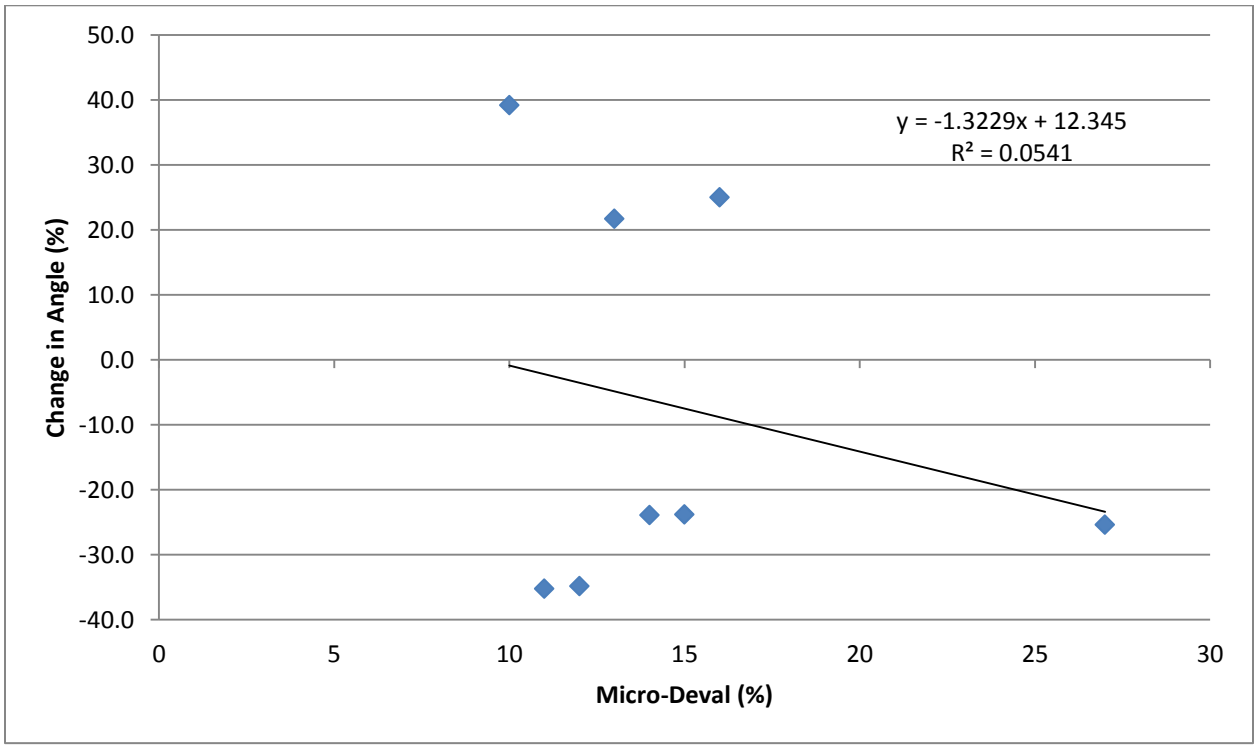

Figure 51 % Change in Phase Angle Vs. Micro-Deval

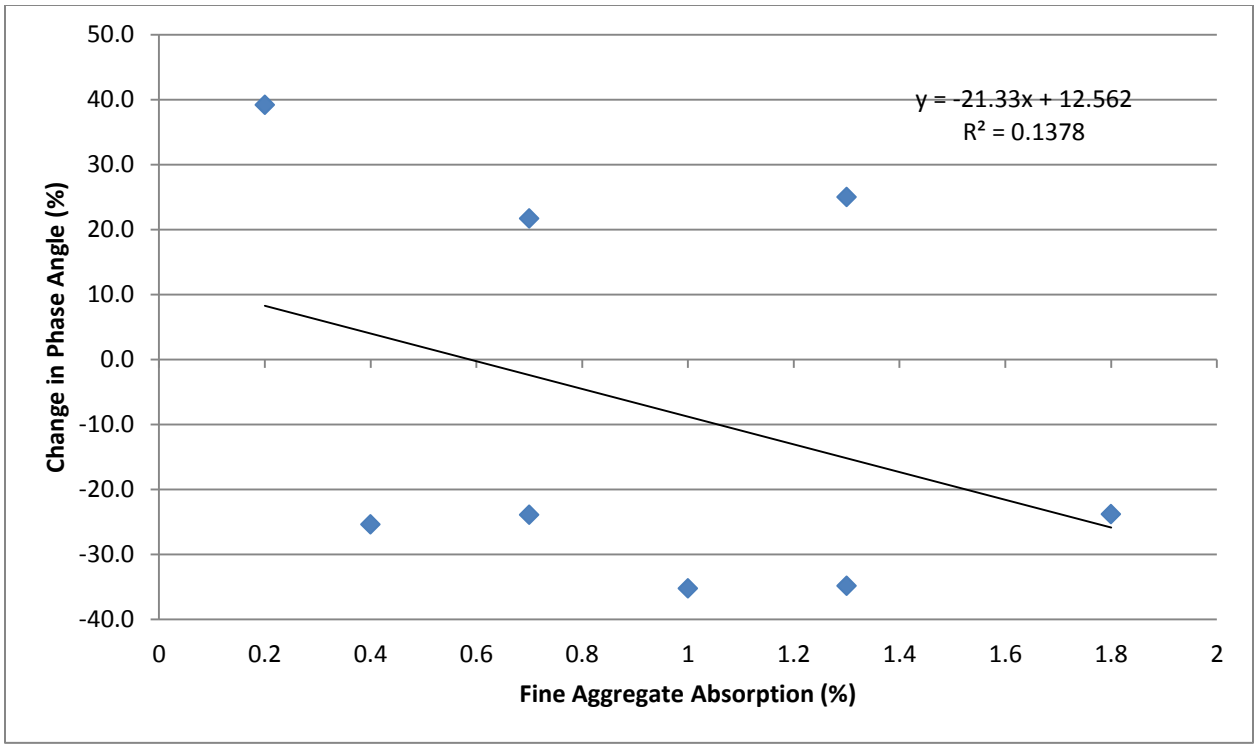

Figure 52 % Change in Phase Angle vs. Fine Aggregate Absorption

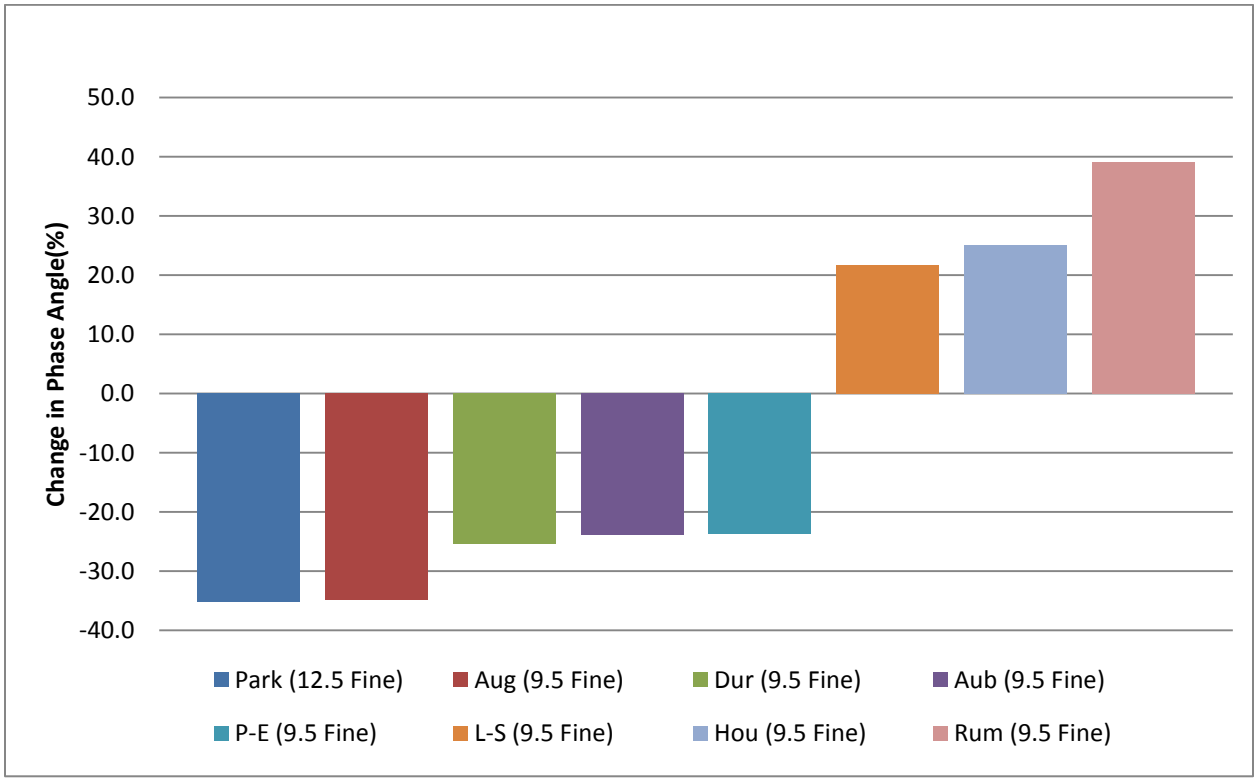

Figure 53 % Change in Phase Angle for the Mix Aggregate Nominal Size

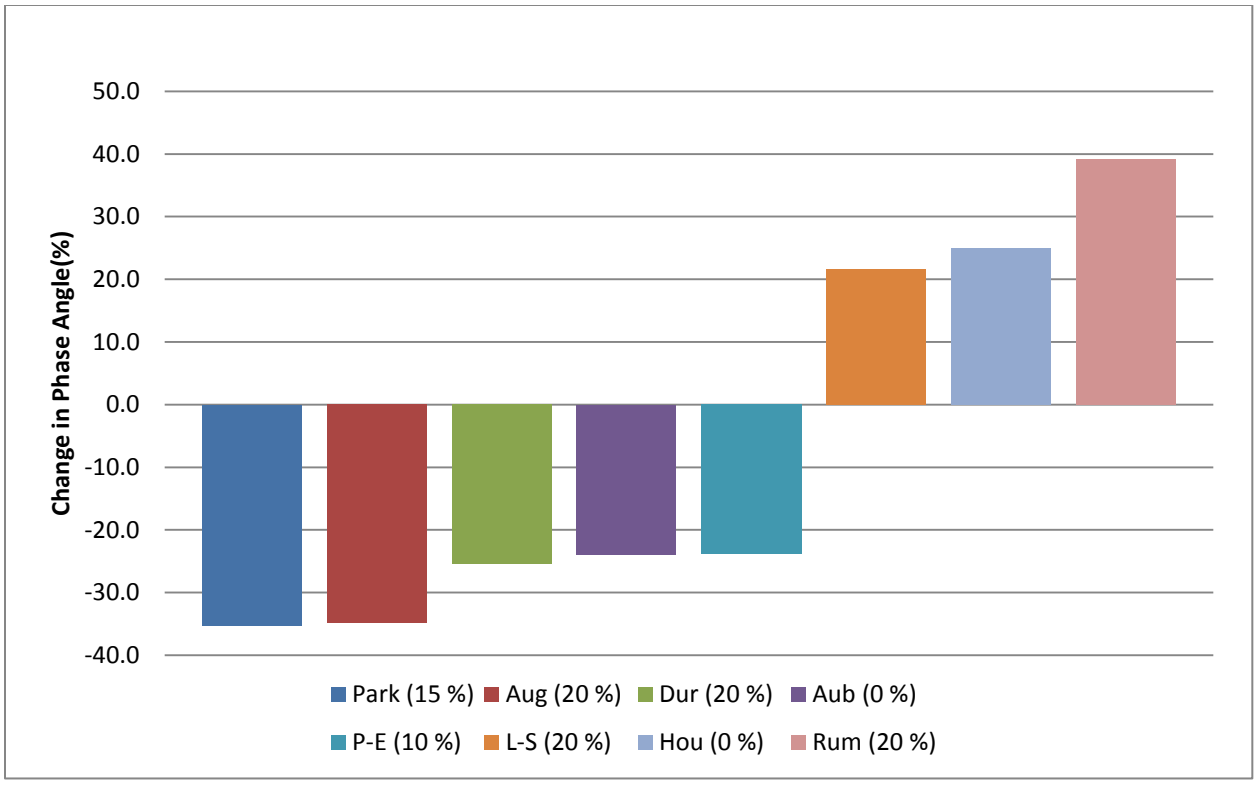

Figure 54 % Phase Angle & RAP Content

Indirect Tensile Test versus Properties

Figure 55 through 58 present x-y plot of the indirect tensile strength against mix various mix properties. Figure 59 and 60 presents the bar chart of indirect tensile strength for various mixes with different nominal aggregate size and RAP content. There were no significant correlations between indirect tensile strength and fine to binder ratio, binder content and aggregate Micro-Deval abrasion properties. However, a significant negative correlation (R^2 = 0.75) was found between indirect tensile strength and fine aggregate absorption (Figure 54). Also indirect tensile strength test indicated that Presque Isle-Easton and Houlton mixes had the lowest indirect tensile strength among the tested mixes. The indirect tensile strength of these two mixes can be found in Table 1 of Appendix A. Moisture induced damage in mixes correlated with aggregate from these two regions has been reported by Maine DOT.

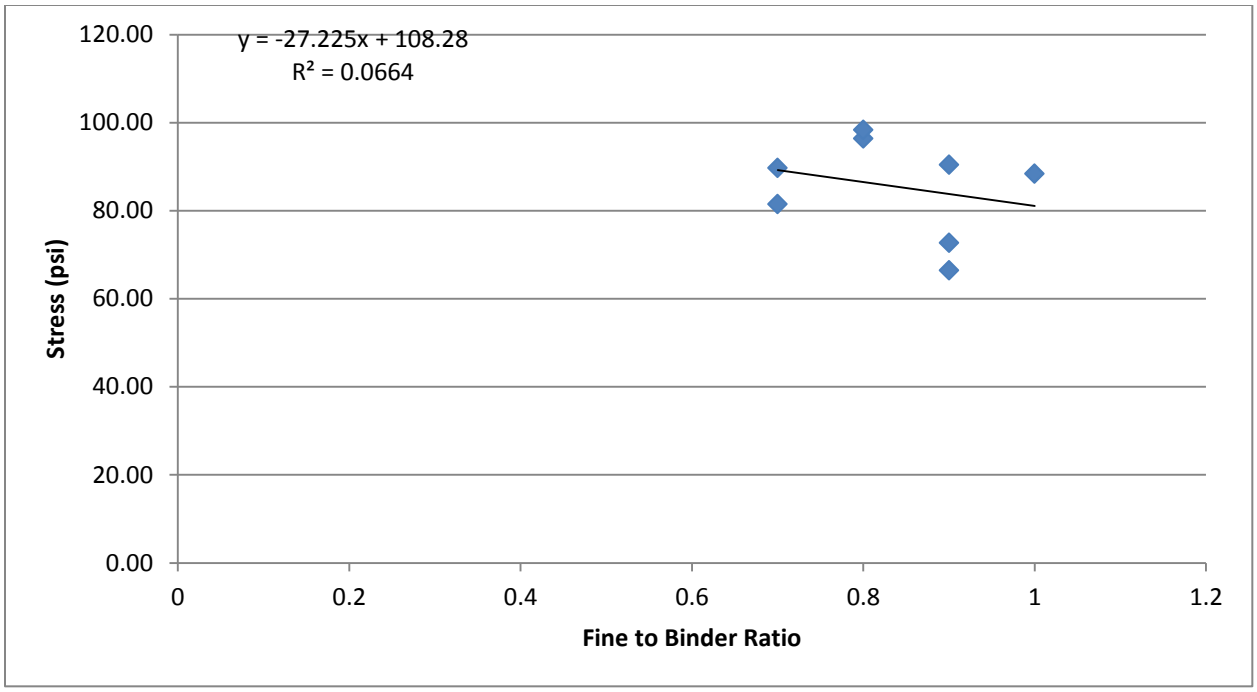

Figure 55 IDT Strenth Vs FBE

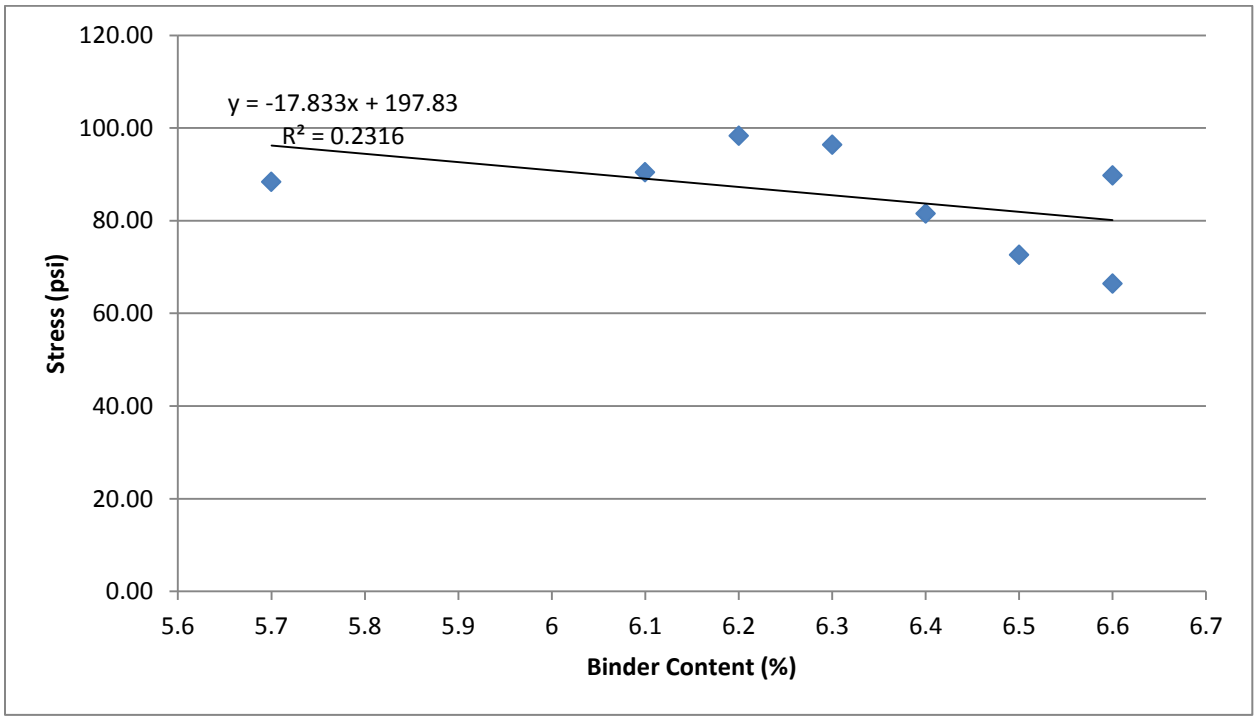

Figure 56 IDT Strength Vs Binder Content %

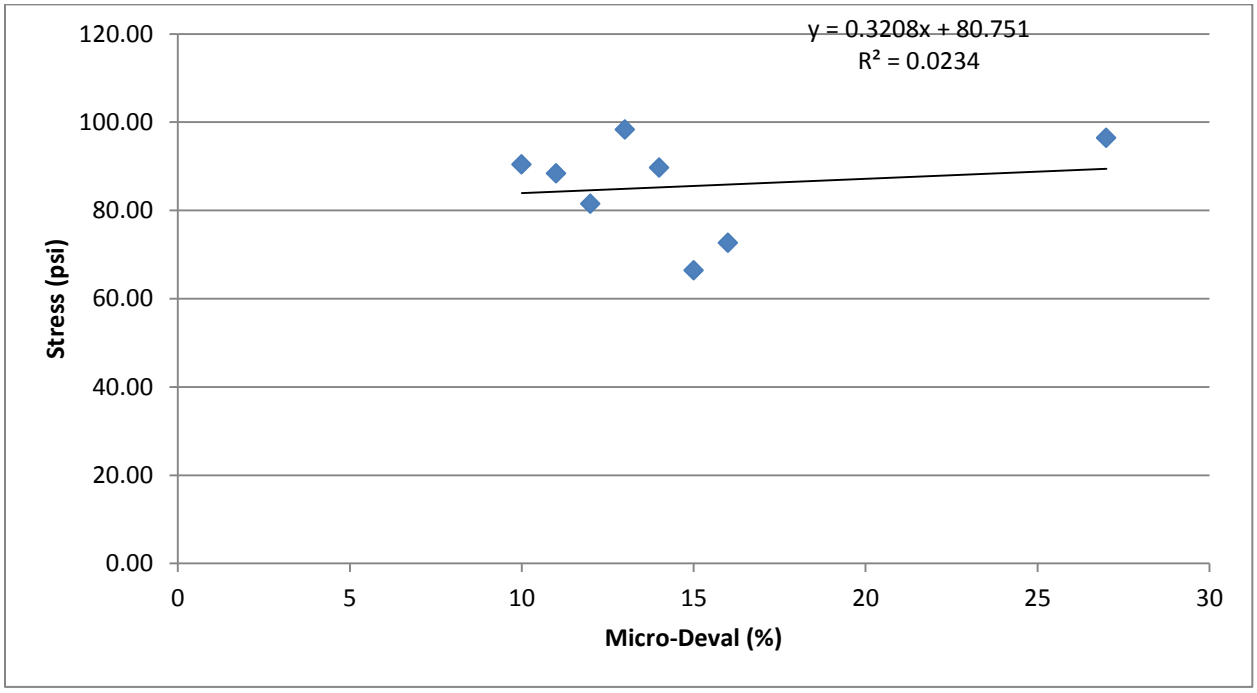

Figure 57 IDT Strength Vs Micro-Deval

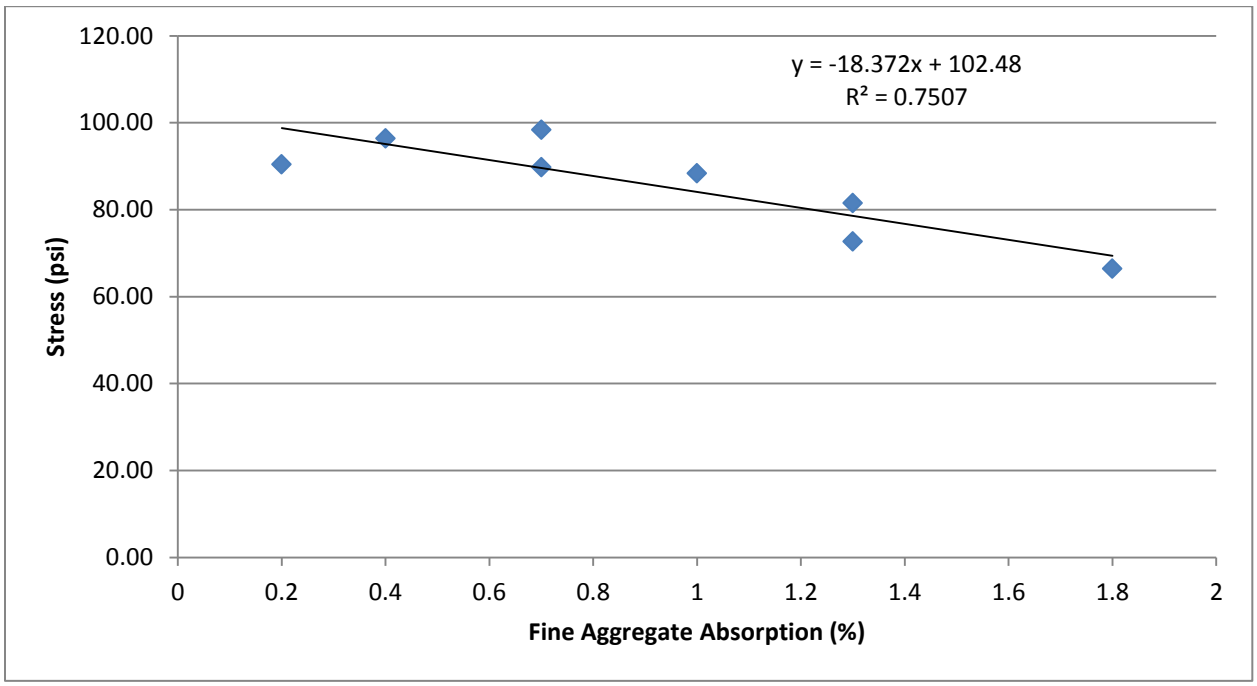

Figure 58 IDT Strength Vs Fine Aggregate Absorption

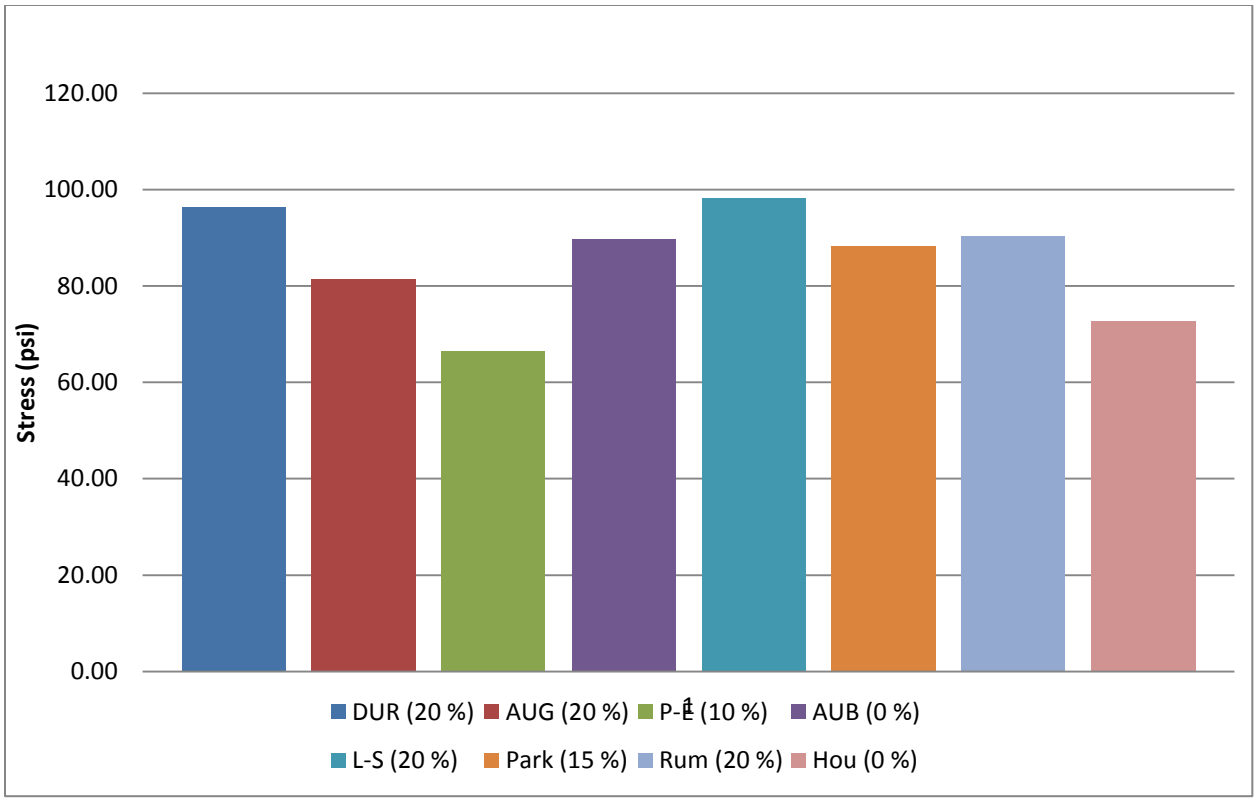

Figure 59 IDT Strenght for different mixes with various Rap Content

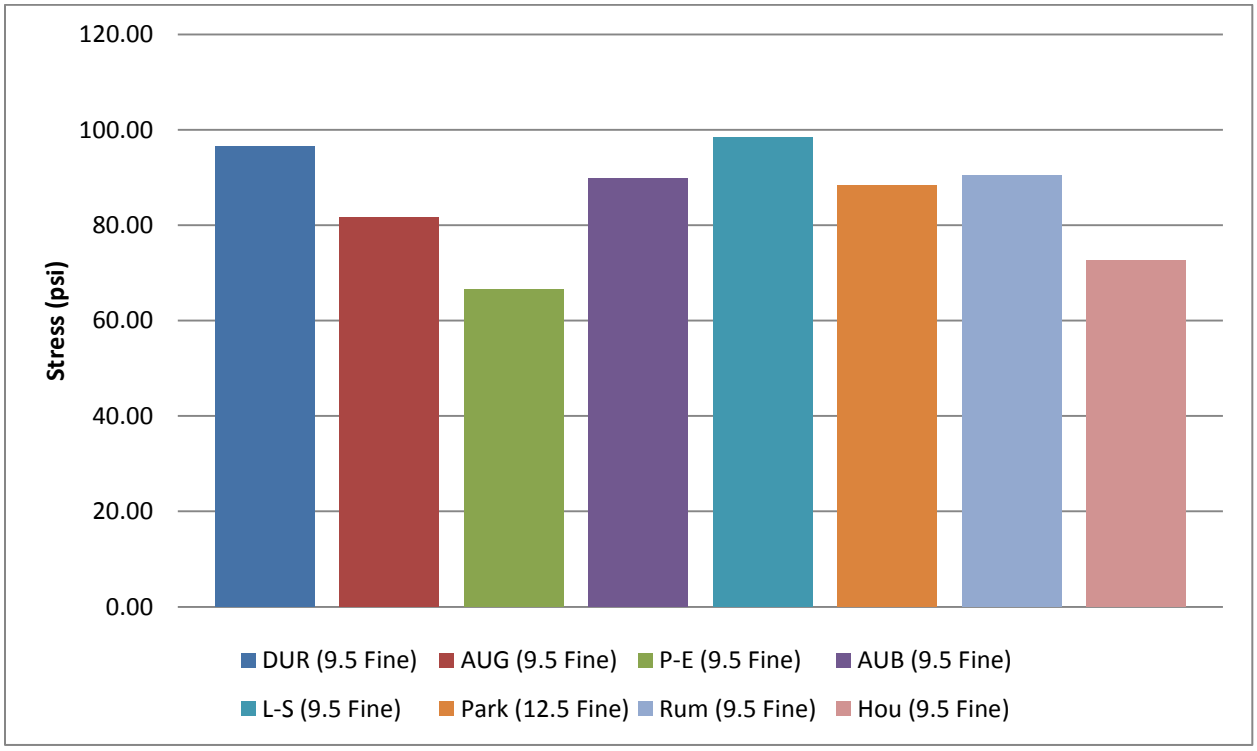

Figure 60 IDT Strength for Different Aggregate Nominal Size

ANOVA Analysis of 1 Hz Experimental Data

Using the mean and standard deviation of the samples' E* for different mixes, a one way ANOVA analysis was conducted to determine if there were significant differences in the mixes which were affected by the moisture induced damages. Out of eight mixes, five of the mixes exhibited negative change in E* and three of the mixes showed positive change in E*, and these two groups were analyzed separately. Table 5 presents the ANOVA analysis of the negative change in E* and Table 6 presents the positive change in E*. No significant differences were found in the mixes that were affected by the moisture-induced damage. However, ANOVA analysis of mixes with positive change in E* indicated that there was at least one mix that differs from the others. The three mixes that exhibited positive change in E* include Durham, Augusta and Presque Isle-Easton mixes.

Layered Elastic Analysis

After conducting correlation analysis and ANOVA analysis of the tested samples, layered elastic analysis was performed to be used in conjunction with performance analysis with fatigue cracking model. Analysis of the reduction in pavement design life is essential because the effects of the moisture-induced damages should be directly linked to the reduction of pavement design life. Layered elastic model is used to determine the stress, strain and deflection of the pavement structure caused by any surface load. The theory of layered elastic model is based on the assumption of a homogenous, isotropic and linearly elastic material [11]. Layered elastic analysis was conducted using a program called WinJULEA [16]. Using this software the strain values were determined for a typical Maine DOT state road (most likely to contain the mixes used in this study) as shown in Figure 61. The tensile strain, ε_t, which is critical for the development of fatigue cracking, was determined at the bottom of the HMA layer. After determining the strain values for a range of different E* values, a regression equation was developed between E* and strain. Figure 62 presents the relationship between E* and tensile strain. The objective was to link the change in E* with a change in fatigue performance through the use of a fatigue model, as explained below.

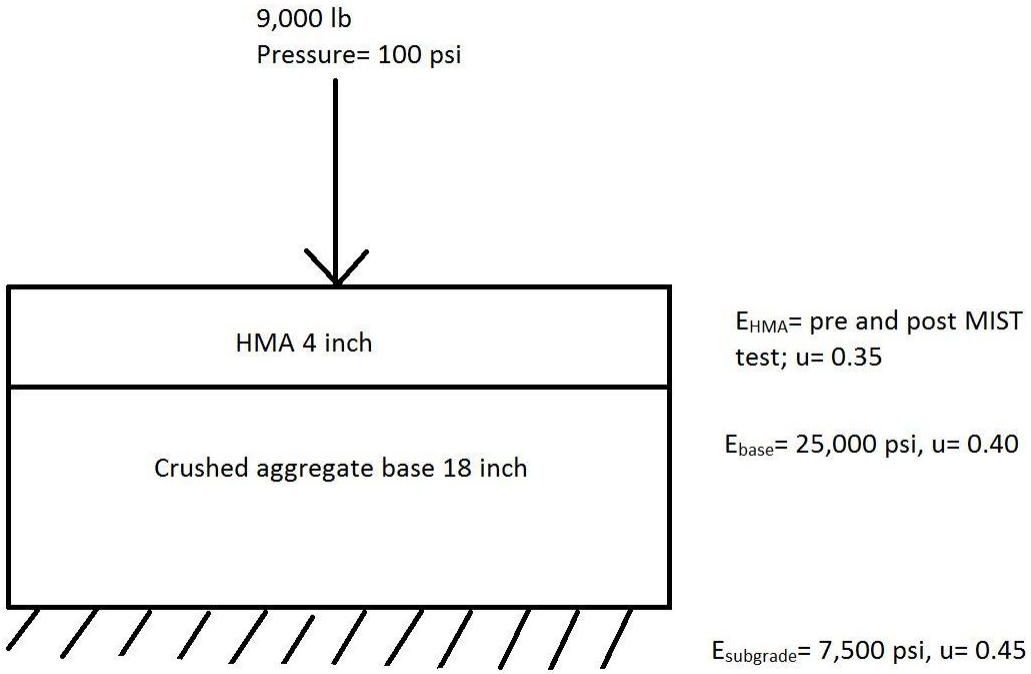

Figure 61 Schematic of Layered Elastic Model

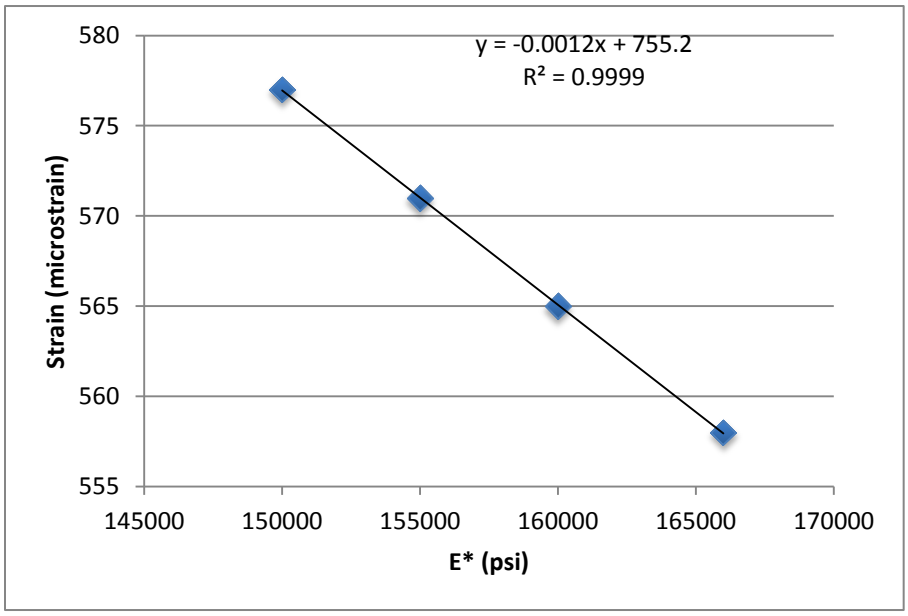

Figure 62 Tensile strain and E* Relationshiop Graph

Monte Carlo Analysis

Monte Carlo simulation was used in the performance analysis model. Monte Carlo simulation is a probability simulation technique that is used to understand the impact of risk associated with any prediction model. In this Monte Carlo simulation of the fatigue cracking model, two variables/inputs are randomly selected for each of the tasks, based on the range of estimates. The number of repetitions to failure by fatigue cracking was calculated based on these randomly selected values. The two variables that controlled the output (number of load repetition to failure) are mean and standard deviation air void and mean and standard deviation of E* of the mixes. An add-in tool for excel, @Risk [17] was used in determining the distribution of mean and standard deviation for the output N_f (number load repetition to fatigue cracking failure). The model was simulated for 5,000 times for each mixes. Pre-MIST air void content was used in simulation of both N_{fpre} and N_{fpost} because the post-MIST air void content for the sample could not be determined accurately as a result of saturation from the MIST conditioning process.

Performance Analysis Using Fatigue Cracking Model

Fatigue cracking in pavement structure is considered as a major distress mechanism in asphalt pavements, on the basis of which the design life (N_f) is determined. Pavement design life is calculated based on fatigue cracking models. Fatigue cracking models are related to the number of load repetitions that a pavement can be subjected to before a failure occurs. There are many types of fatigue cracking models and the models have different parameters in prediction of the pavement design life. The applications of the models are associated with the definition of failure. The type of fatigue cracking model used in this experiment was developed by the Asphalt Institute (AI; 1991) [9]. The formulas and equations associated with AI fatigue cracking model are presented below.

$$N_f = 0.00432C(\varepsilon_t)^{-3.291}(E)^{-0.854}$$

$$C = 10^M$$

$$M = 4.84\left(\frac{V_b}{V_a + V_b} - 0.69\right)$$

Where;

N_f = number of load repetitions to failure, which is defined as fatigue cracking over 20% of the entire pavement area

C= correction factor

ε_t = tensile stain at the bottom of the HMA layer

V_a= air void (%) in the asphalt mix

V_b = asphalt content (%) by volume in the asphalt mix

E =dynamic Modulus of asphalt mix, psi

The shift factor, needed to transform the laboratory fatigue data to field data, for AI equation is 18.4.

Monte Carlo simulation of the fatigue cracking model provided the distribution of N_f. N_f mean and standard deviation of each mixes were determined for pre-MIST and post-MIST mixes. Using the mean and standard deviations of N_f, normal distribution curve were plotted for pre-MIST and post-MIST conditions of the mixes. Out the eight samples, six of the mixes exhibited decrease in number of load repetition to failure in post-MIST (N_f) condition and two of the mixes exhibited increase in N_f. The increase in N_f can be associated with the increase in E* of the mixes in the post- MIST condition. Figure 64 through 71 present the comparison between normal distribution curves of pre and post MIST N_f and Figure 63 presents the graphical representation of the change in mean N_f (Post-Pre). Table 8 in Appendix A presents the changes in distribution of mean N_f due to MIST conditioning. The reduction in N_f was found to range from 1-30% of the total life of the pavement. On the other hand, an increase in N_f was found from 1-5%. Based on the simulated N_f and change in E*, Houlton and Lebanon-Sanford mixes were most sensitive to moisture damages.

Durham mix has the highest Micro-Deval abrasive property and targeted air void (7+/-%) was not achieved due to the breakage of aggregates during compaction. Durham mix also had increase in E* and N_f after MIST conditioning. A possible explanation for this result of Durham mix might be correlated to its Micro-Deval properties. A high Micro-Deval property of the mix might be causing the coarse aggregates to be broken into fine aggregates. These new fine aggregates in the sample might be transported to different location in the sample due to water passing through the sample under confined condition. The transportation of the fine aggregates inside the sample could decrease the air void content and increase the density of the property. The increase in density of the sample property leads to higher stiffness value, E* and higher E* value leads to higher N_f.

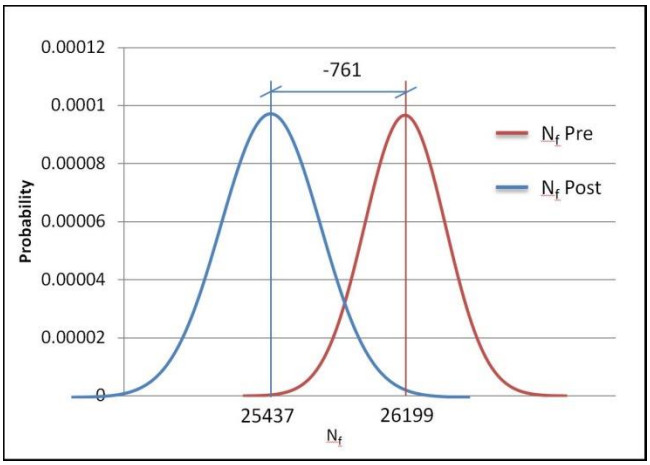

AUB

(a)

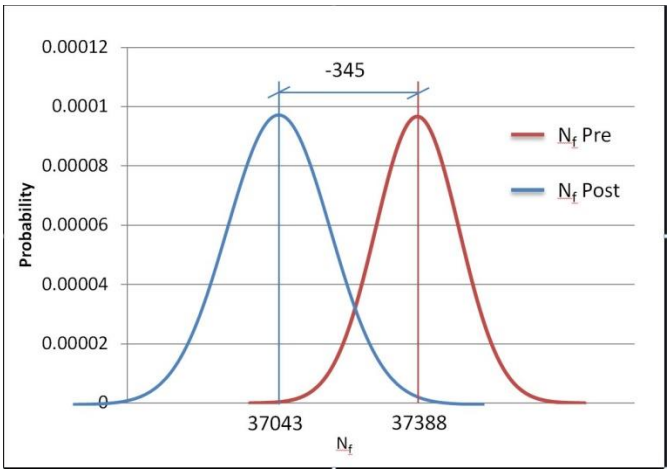

P-E

(b)

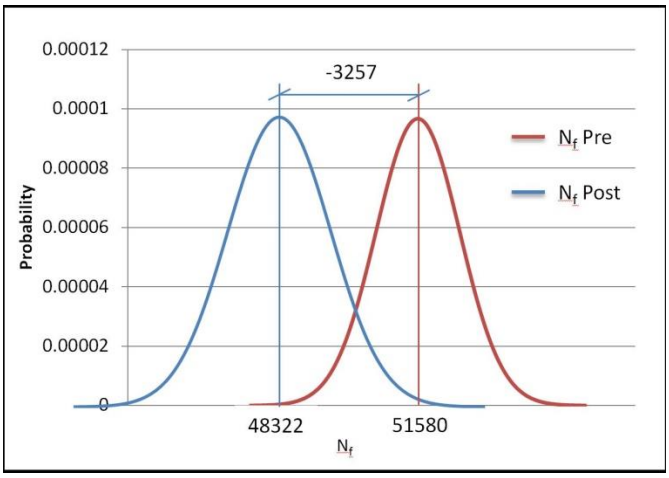

RUM

(c)

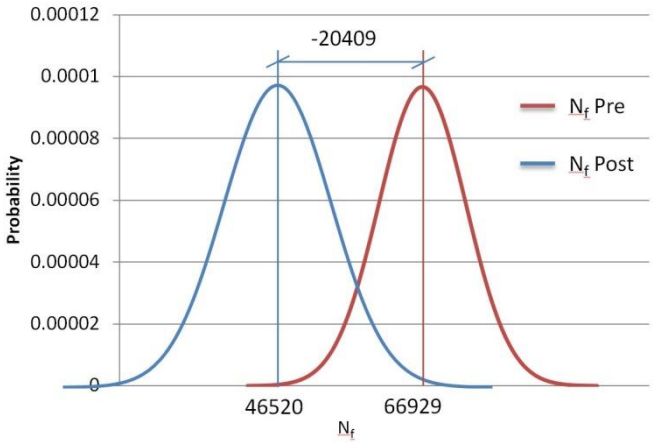

HOU

(d)

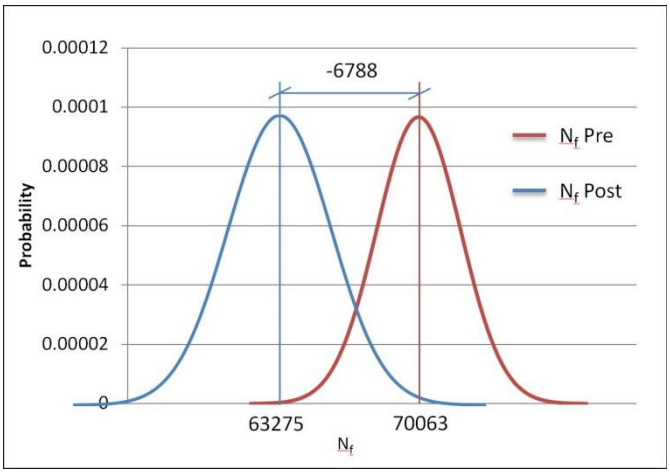

PARK

(e)

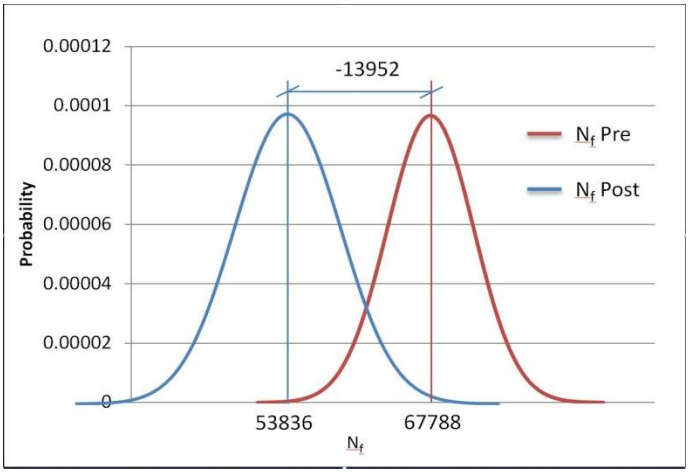

L-S

(f)

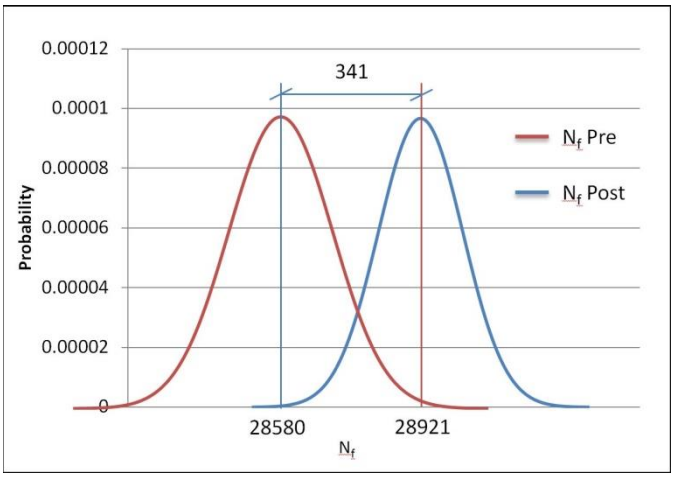

AUG

(g)

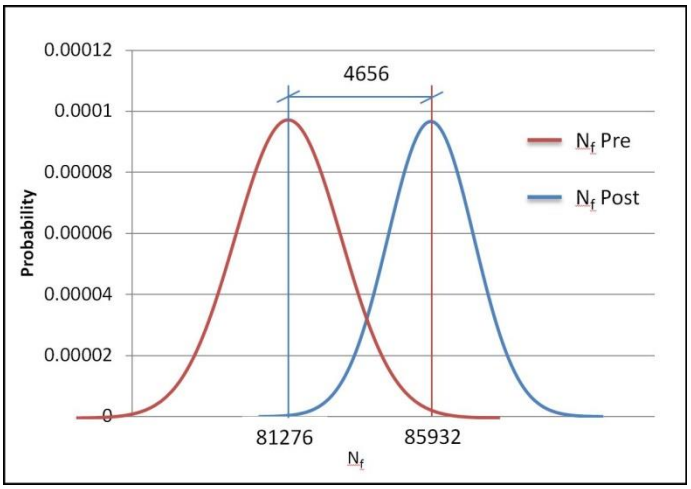

DUR

(g)

Figure 63 (a-h) Graphical representation of Difference in mean of N_{fpost} and N_{fpre} for different mixes

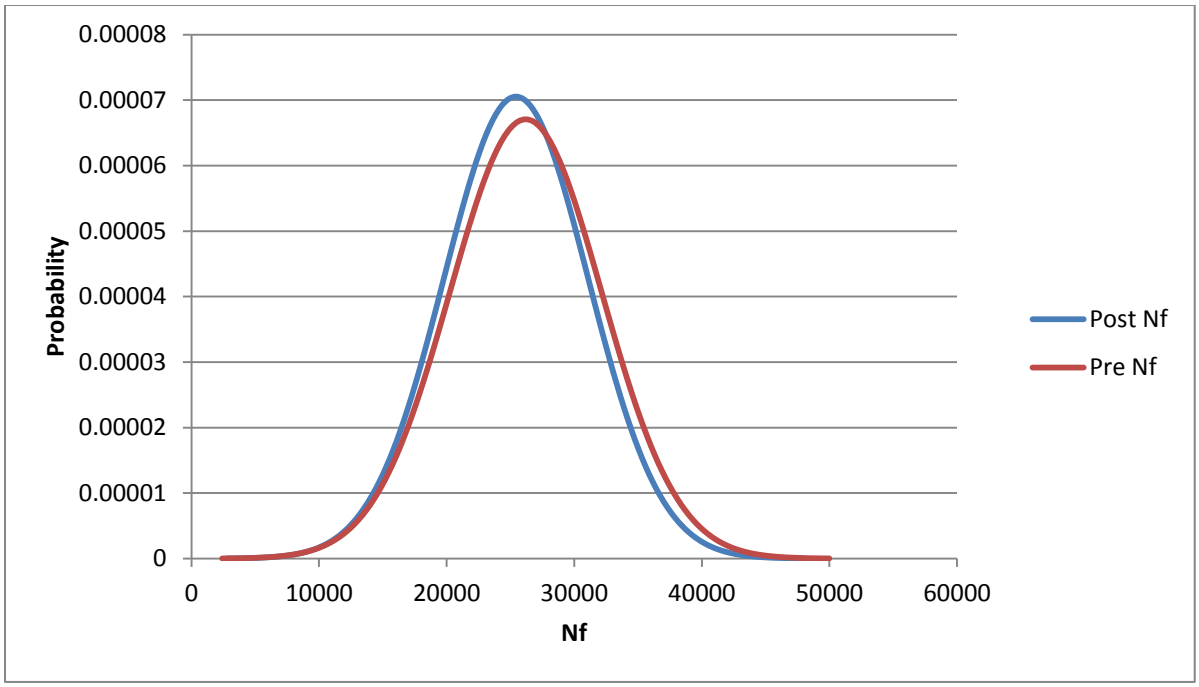

Figure 64 Normal Distribution Curve of Nf for Auburn Mix

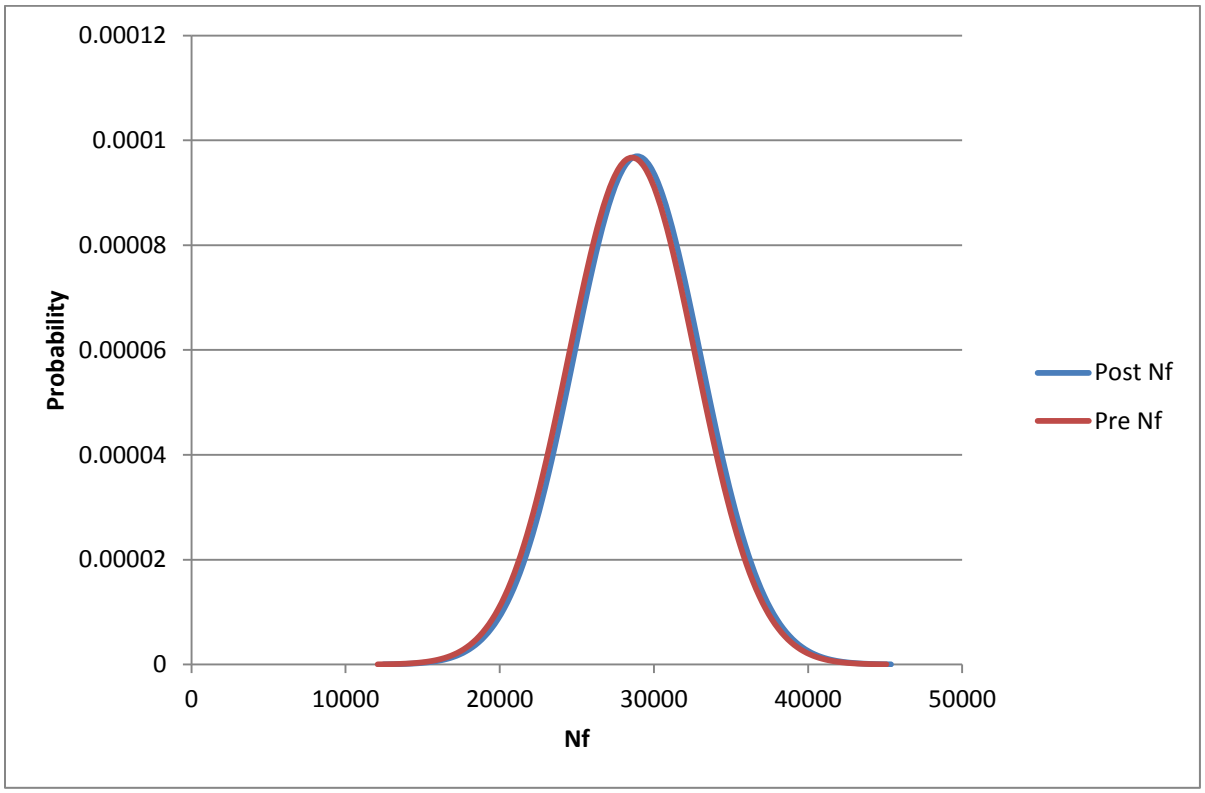

Figure 65 Normal Distribution Curve Nf for Augusta Mix

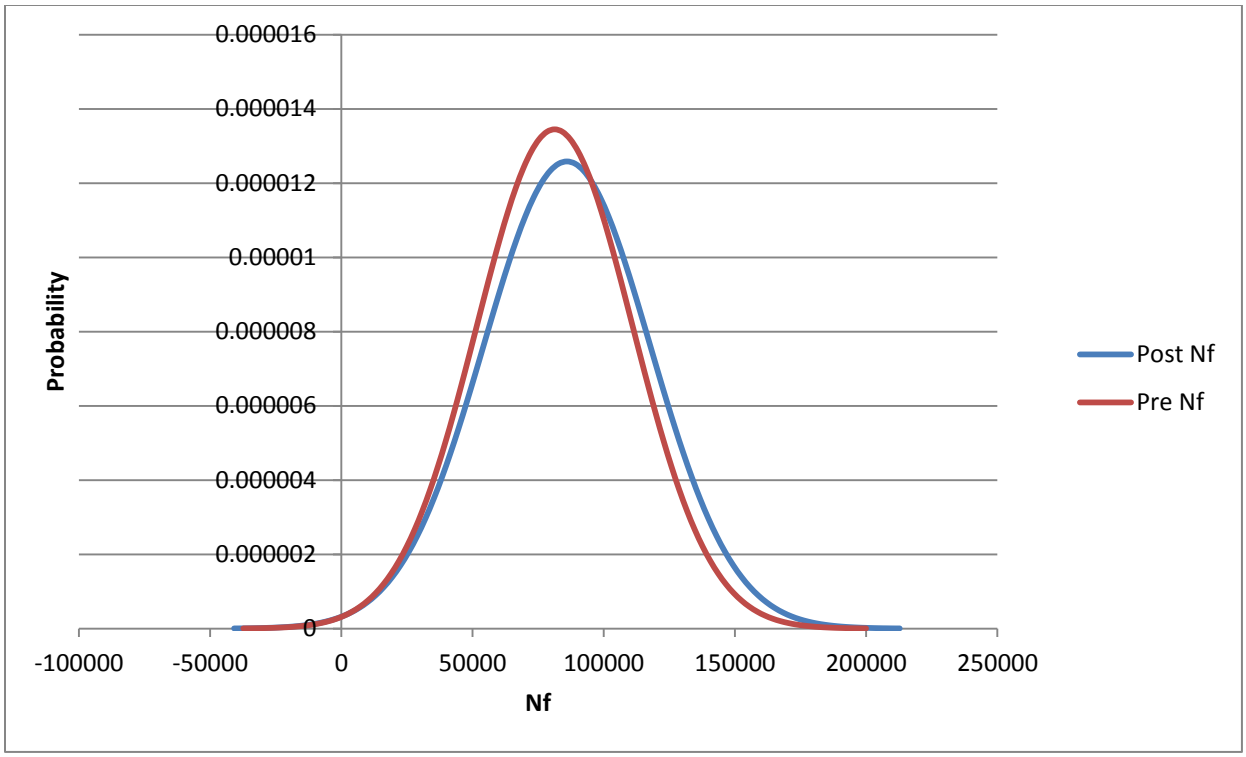

Figure 66 Normal Distribution Curve of Nf of Durham Mix

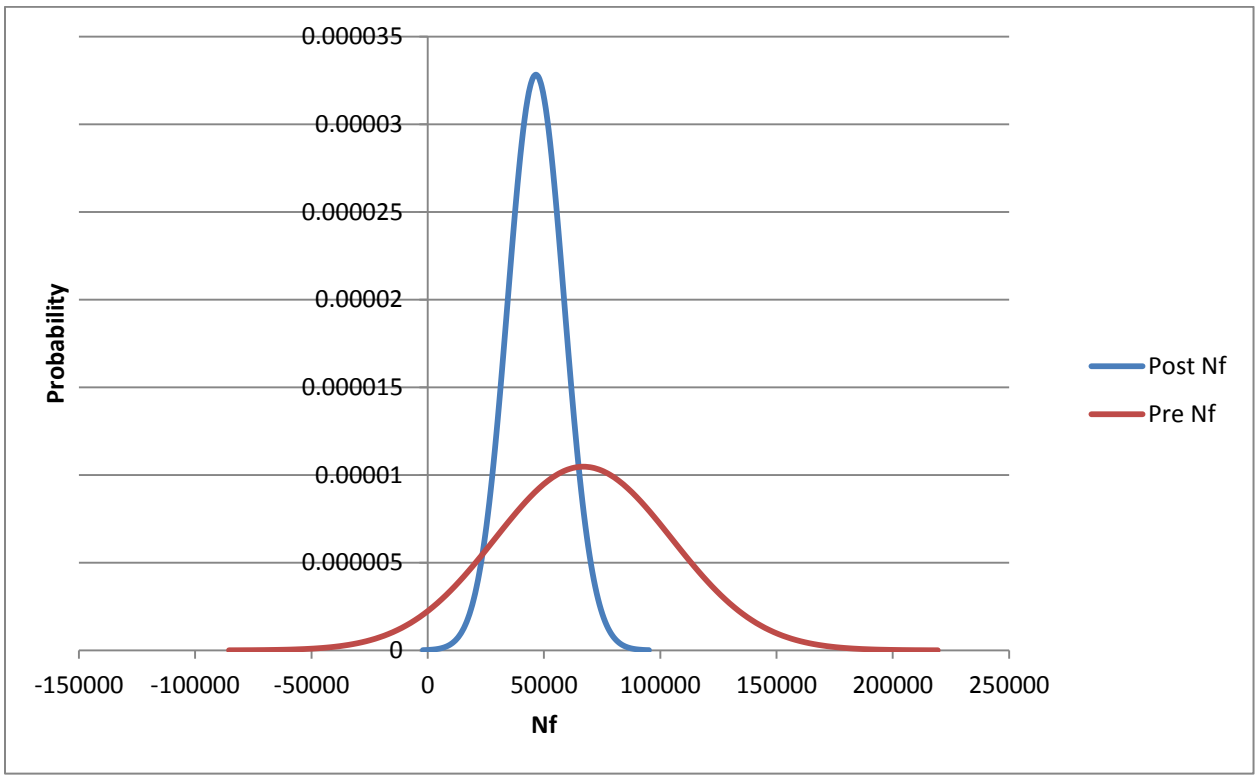

Figure 67 Normal Distribution Curve of Nf of Houlton Mix

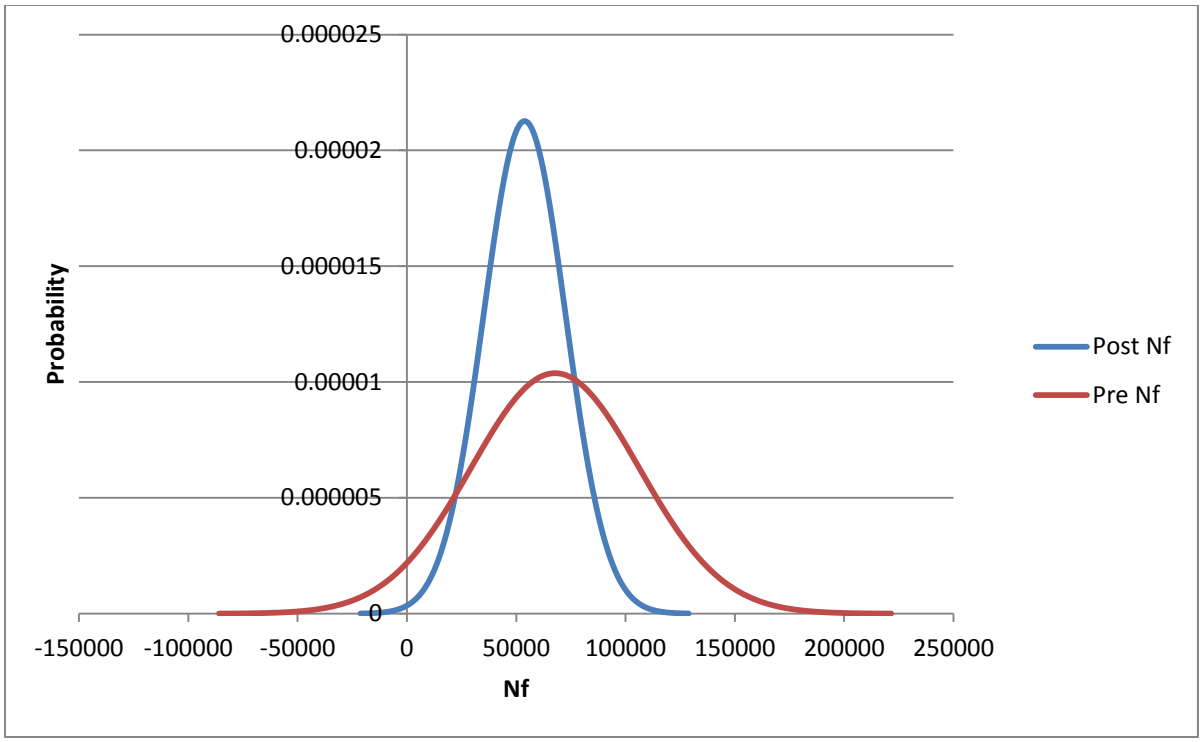

Figure 68 Normal Distribution Curve of Nf for Lebanon-Sanford Mix

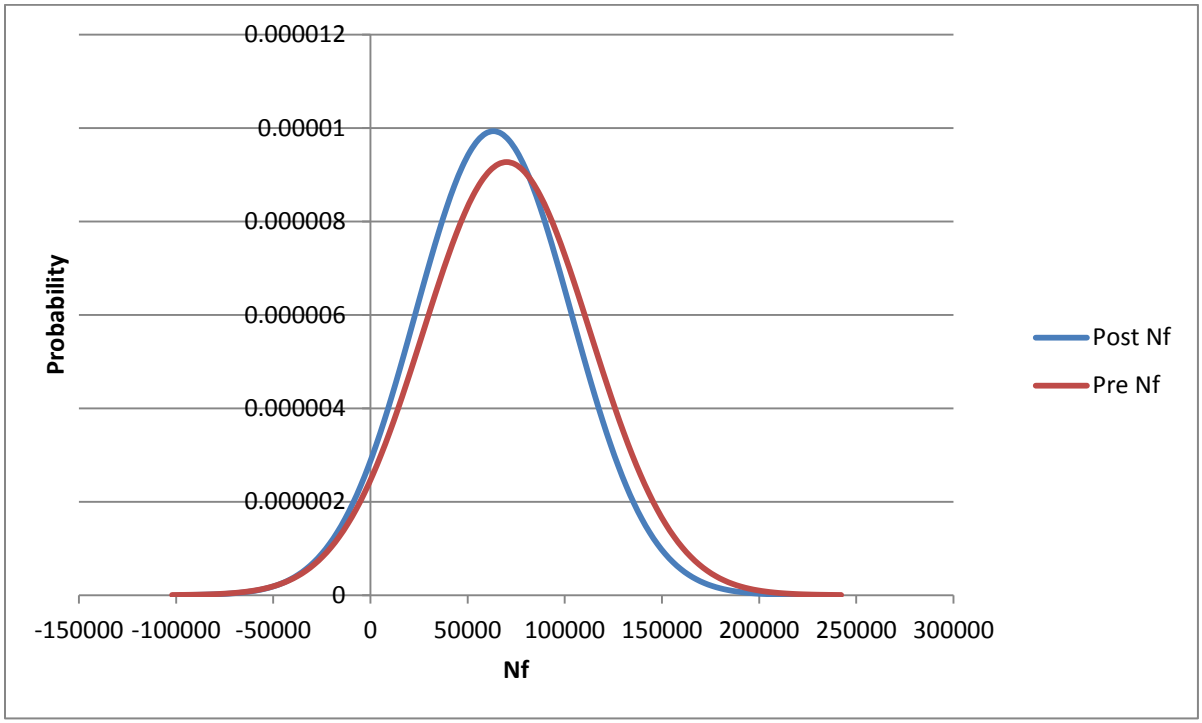

Figure 69 Normal Distribution Curve of Nf for Parkman Mix

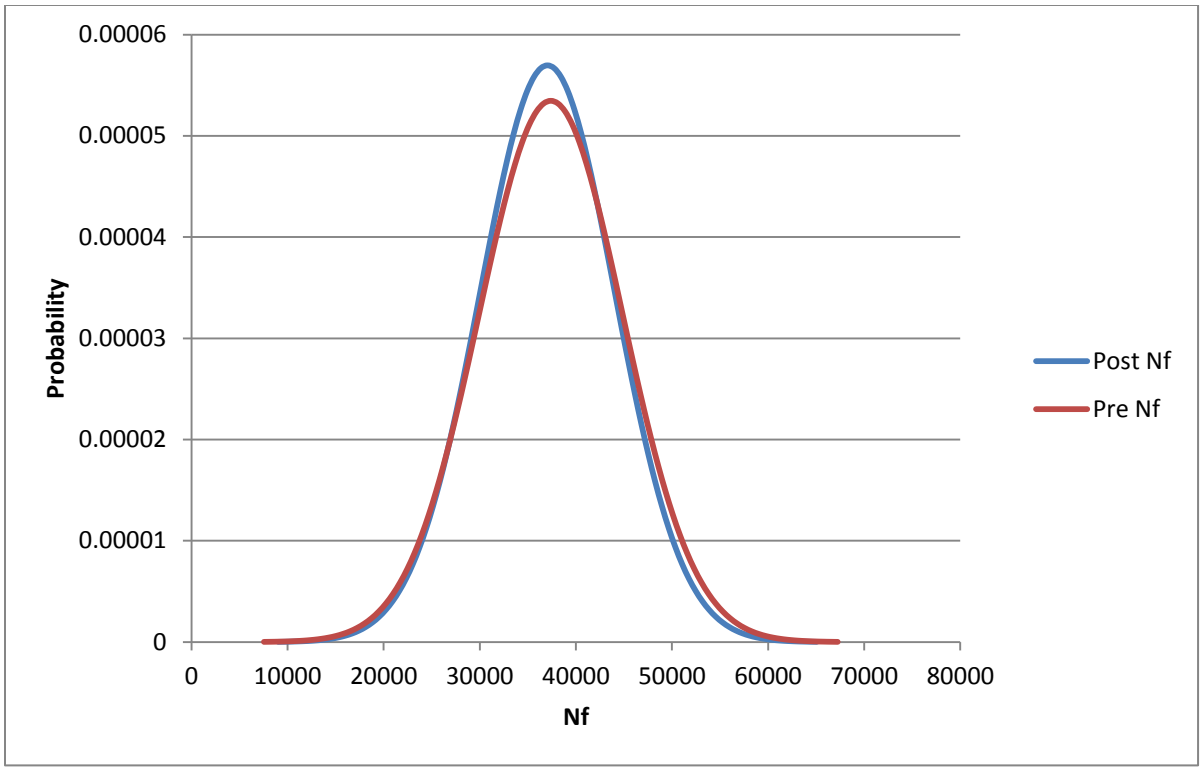

Figure 70 Normal Distribution Curve of Nf Presque Isle-Easton Mix

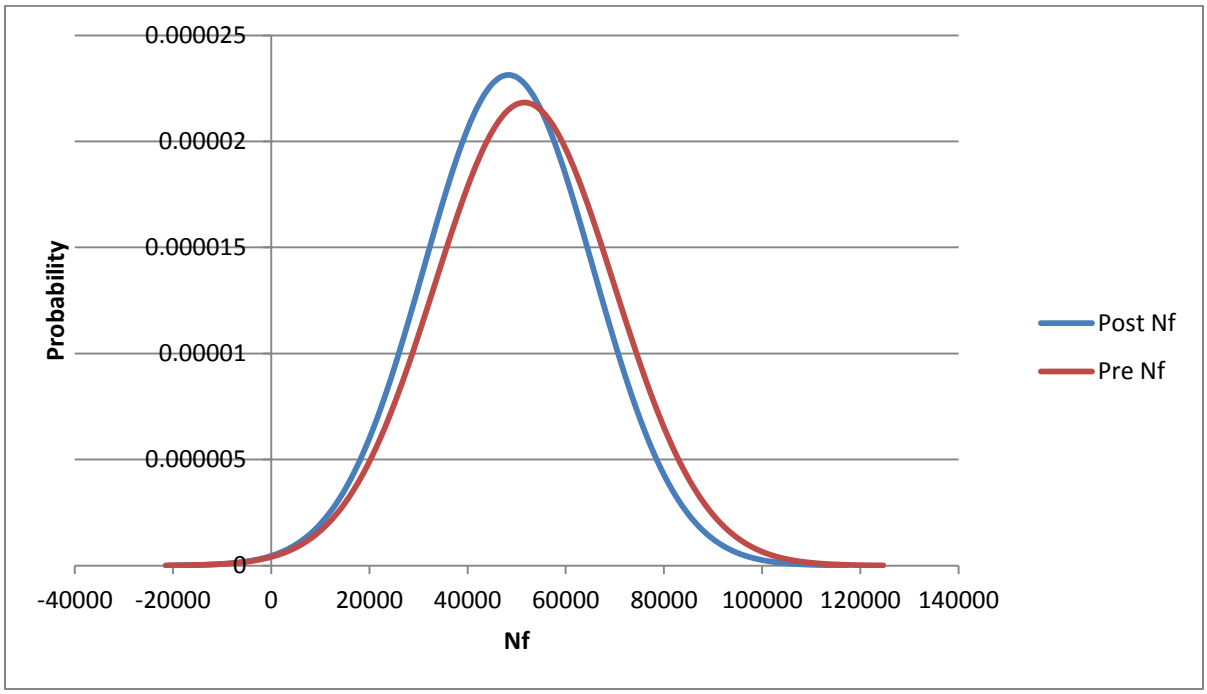

Figure 71 Normal Distribution Curve of Nf for Rumford Mix

Conclusions

An assessment of moisture-induced damages in asphalt pavement was conducted through laboratory conditioning and testing and analysis of the data, along with layered elastic analysis and Monte Carlo simulation. On the basis of the results the following conclusions can be made.

1. Most of mixes showed an impact of MIST conditioning process on the stiffness
2. Most of the mixes also showed a resultant decrease in life of the pavements, which can be as high as 30%
3. A composite value of Micro-Deval property fine aggregate absorption exhibited good correlation with change in E as a result of moisture conditioning in the MIST.
4. MIST conditioning can lead to both increase or decrease in E*. Both types of changes should be considered detrimental for the mix. In cases where aggregates have high breakdown potential, finer aggregates created under confined conditions in the repeated pumping action in the MIST can artificially decrease voids and stiffen up mixes.
5. Indirect tensile strengths of mixes after moisture conditioning through the MIST showed good correlation with fine aggregate absorption
6. Experimental results suggest that the Houlton and Lebanon-Sanford mixes are most sensitive to moisture-induced damages since N_f is reduced significantly after MIST conditioning and E* is decreased for both the loading frequencies (10 and 1 Hz) in all the tested samples.
7. Presque Isle-Easton mix had the lowest indirect tensile strength compared to other mixes

Recommendations

Based on the conclusions from this study the following recommendations are made.

1. Consider the regular use of MIST as a conditioning process for the evaluation of moisture damage potential of mixes
2. Consider results of MIST testing and Monte Carlo simulation with predicted lives to evaluate the potential loss of pavement life for different mixes, and use the results during the design of pavement structures for specific design lives
3. Develop a specification on the basis of a composite factor that includes both Micro-Deval and Fine aggregate absorption to screen poor quality aggregates
4. Utilize indirect tensile strength along with MIST conditioning to identify moisture susceptible mixes
5. Conduct further research to evaluate the breakdown of aggregates after MIST conditioning process
6. Conduct further research to develop a framework for regular use, which will include all of the above 5 recommendations

References

[1] *Guide for Mechanistic-Empirical Design of New and Rehabilitated Pavement Structures*. March 2004, National Cooperative Highway Research Program, Transportation Research Board, National Research Council Champaign, Illinois.

[2] *Moisture Sensitivity of Asphalt Pavements*, February 2003, National Seminar, Transportation Research Board.

[3] Kevin Gaspard, Mark Martinez, Zhongjie Zhang , *Impact of Hurricane Katrina on Roadways in New Orleans Area*, March 2007, LTRC Pavement Research Group.

[4] Khaled Helali, Michael Robson, Randy Nicholson, Wel Bekheet, *Importance of a Pavement Management System in Assessing Pavement Damage from Natural Disasters: A case Study to Assess the Damage from Hurricane Katrina and Rita in Jefferson Parish, Louisiana*, 2008

[5] Juraidah Ahmad, Nur Izzi Md. Yusoff , Mohd Rosli Hainin, Mohd Yusof Abd Rahman, Mustaque, Hossain *Investigation into hot-mix asphalt moisture-induced damage under tropical climatic conditions***,** 2014, Construction and Building Materials

[6] Mallick et al., *Development of a Rational Procedure for Evaluation of Moisture Susceptibility of Asphalt Paving Mixes*, January 2013

[7] ASTM D4013, *Standard Practice for Preparation of Test Specimens Bituminous Mixtures by Means of Gyratory Shear Compactor 2009*, American Society for Testing and Materials.

[8] ASTM D7063/D8063M, *Standard Test Method for Effective Porosity and Effective Air Voids of Compacted Bituminous Paving Mixture Samples 2011*, American Society for Testing and Materials.

[9] AASHTO TP 342-11, *Standard Method of Test for Determining Dynamic Modulus of Hot Mix Asphalt 2011*, American Association of State and Highway Transportation Officials.

[10] Kim et al., *Dynamic Modulus Testing of Asphalt Concrete in Indirect Tension Mode*, November 2003, North Carolina State University, NC

[11] "Flexible Pavement Mechanistic Models" 13 March 2008. http://www.pavementinteractive.org <http://www.pavementinteractive.org/article/flexible-pavement-mechanistic-models/> 16 April 2015

[12] Mallick, R.B. and T. El-Korchi, *Pavement Engineering: Principles and Practice*. 2009: New York: Taylor & Francis Group.

[13] InstroTek, Inc. (n.d.). Retrieved April 18, 2015, from http://instrotek.com/material-testing/laboratory-products/mist/

[14] Matlab (2014a, MathWorks, Massachusetts, Ma)

[15] InstroTek, Inc. (n.d.). Retrieved April 18, 2015, from http://instrotek.com/material-testing/laboratory-products/corelok/

[16] ERDC Developed Software WINJULEA (Window Layered Elastic Analysis)- Airfields & Pavement Branch, pcase.com, Vicksburg, Mississippi

[17] Palisade Corporation 2015 (The DecisionTools Suite), @Risk Analysis, New York

[18] Rajib B., Mallick, Robert Pelland and Frederick Hugo, *Use of Accelerated Loading Equipment for Determination of Long Term Moisture Susceptibility of Hot Mix Asphalt*, IJPE, Volume 6, Number 2, June, 2005.

[19] AASHTO Design Guide for Design Pavement Structure, 1993, American Association of State Highway and Transportation Officials

Appendix A

Table 3 Experimental Data of 8 Different Mixes (A total of 32 samples)

Sample ID	TMD	Avg Diameter (in.)	Avg Thickness (in.)	Pre-MIST Bulk Specific Gravity (g/cm^3)	Pre MIST Percent Air Void (%)	Pre MIST Porosity (%)	POST-MIST Bulk Specific Gravity (g/cm^3)	Post MIST Percent Air Void	Post MIST Porosity (%)	Pre-MIST Dynamic Modulus in IDT for 10 Hz (MPa)	Pre-MIST Dynamic Modulus in IDT for 1 Hz (MPa)	Post-MIST Dynamic Modulus in IDT for 10 Hz (MPa)	Post-MIST Dynamic Modulus in IDT for 1 Hz (MPa)	IDT Test (psi)
AUG #1	2.493	5.916	1.522	2.297	7.9	6.24	2.311	7.3	6.64	2287	651	2093	726	
AUG #2		5.916	1.532	2.304	7.6	6.09	2.317	7.1	6.31	2129	717	2550	787	78.1
AUG #3		5.094	1.53	2.322	6.9	5.64	2.336	6.3	5.73	2377	839	2557	826	92.5
AUG #4		5.895	1.504	2.325	6.7	5.72	2.338	6.2	5.93	3687	1337	3101	1150	74
DUR #1	2.449	5.904	1.452	2.34	4.5	3.09	2.36	3.7	2.88	4404	1823	4271	1879	
DUR #2		5.915	1.52	2.34	4.5	3.05	2.357	3.8	1.31	3407	1384	4275	1462	117.5
DUR #3		5.916	1.52	2.301	6.1	4.76	2.305	5.9	5.34	3419	1475	4161	1587	91.3
DUR #4		5.908	1.522	2.304	5.9	4.53	2.323	5.1	4.14	3831	1473	4373	1582	80.4
PARK # 1	2.504	5.912	1.518	2.354	6	4.48	2.374	5.2	3.88	4351	1687	3462	1431	89.9
PARK # 2		5.912	1.475	2.334	6.8	4.91	2.352	6.1	4.4	5234	2021	4934	1860	89.8
PARK # 3		5.91	1.528	2.296	8.3	6.5	2.299	8.2	7.01	3436	1251	2525	908	85.4
PARK # 4		5.924	1.519	2.296	8.3	6.2	2.324	7.2	5.26	3042	1050	2728	1023	
L-S #1	2.47	5.907	1.532	2.289	7.3	6.29	2.3	6.9	6.7	3068	1343	2950	1231	95.9
L-S #2		5.921	1.536	2.294	7.1	6.37	2.308	6.6	6.44	3198	1357	2753	1250	97.6
L-S #3		5.91	1.528	2.335	5.5	4.42	2.346	5	4.57	3324	1435	3300	1292	101.6
L-S #4		5.914	1.524	2.32	6.1	5.11	2.334	5.5	5.2	5298	2269	4997	1781	

AUB #1	2.486	5.912	1.527	2.313	7	4.1	2.329	6.3	5.12	3431	1300	3472	1152	101.5
AUB #2		5.92	1.53	2.317	6.8	3.84	2.332	6.2	0.73	3196	1301	4151	1090	78.4
AUB #3		5.904	1.527	2.276	8.4	5.4	2.291	7.8	5.26	2420	892	2562	828	89.3
AUB #4		5.912	1.516	2.285	8.1	5.18	2.306	7.3	4.55	3195	1090	3077	1141	
RUM #1	2.428	5.903	1.517	2.28	6.1	4.63	2.395	5.2	3.89	3612	1530	3807	1621	96.3
RUM #2		5.913	1.532	2.269	6.6	4.96	2.387	5.7	4.09	3104	1328	2954	1165	81.2
RUM #3		5.917	1.523	2.227	8.3	6.51	2.401	7.7	6.71	3808	1670	2947	1209	93.8
RUM #4		5.902	1.542	2.24	7.7	5.95	2.391	6.8	5.33	3177	1263	3260	1203	
P-E #1	2.461	5.872	1.536	2.314	6	4.57	2.322	5.6	5.26	2917	995	3264	1141	67
P-E #2		5.895	1.532	2.321	5.7	4.17	2.326	5.5	5.04	2989	1008	3397	1327	66.2
P-E #3		5.886	1.525	2.292	6.9	5.02	2.305	6.3	5.48	3544	932	3264	1142	66.1
P-E #4		5.836	1.533	2.292	6.9	5.51	2.303	6.4	6.09	4965	1452	3572	1006	
HOU #1	2.449	5.883	1.507	2.283	6.8	5.34	2.404	7.6	5.85	4100	1614	3724	1443	72.2
HOU #2		5.906	1.495	2.279	7	5.65	2.473	5.1	6.02	3389	1389	2887	1042	70.1
HOU #3		5.89	1.51	2.306	5.8	4.23	2.43	5.6	4.92	4403	1918	3602	1398	75.7
HOU #4		5.906	1.531	2.299	6.1	4.82	2.441	5.8	5.43	5636	2375	4674	1858	

Table 4 Change in Phase Angle and Different type of Mix Properties comparison table

Mixes	Mean % change in Phase Angle	Mean % Change in 1 Hz	Binder Type (PG)	AC Source	Aggregate Nominal Size (mm)	Rap Conent (%)	Coarse Micro-Deval	Fine Aggregate Absorption (%)	Binder Content (%)	New Binder %	Fines to Binder Ratio (FBE)	Modifier	WMA
Gorham [Durham (RTE 136)]	-25.40	5.9	64	Irving (St. John Canada)	9.5 Fine	20	27	0.4	6.3	5.6	0.8	SBR, 3%	Water, 275-325F
Augusta	-34.82	10.7	64	Irving (St. John Canada)	9.5 Fine	20	12	1.3	6.4	5.4	0.7	SBR, 3%	
PI-Easton	-23.79	22.9	58	Irving (St. John Canada)	9.5 Fine	10	15	1.8	6.6	6.1	0.9	SBR, 3%	
Auburn	-23.93	-11.6	64	United (Warren, PA)	9.5 Fine	0	14	0.7	6.6	0	0.7	SBR, 3%	Sonnewar mix, 0.5%, 240-325F

Lebanon-Sanford	21.67	-11.9	64	Bitumar, Montreal Canada	9.5 Fine	20	13	0.7	6.2	5.4	0.8	SBR, 3%	
Parkman	-35.24	-13.3	58	Irving (St. John Canada)	12.5 Fine	15	11	1	5.7	5	1.0	SBR, 3%	
Rumford	39.17	-14.9	64	Irving (St. John Canada)	9.5 Fine	20	10	0.2	6.1	5.2	0.9	SBR, 3%	
Houlton	25.00	-21.1	58	Irving (St. John Canada)	9.5 Fine	0	16	1.3	6.5	0	0.9	SBR, 3%	

Table 5 ANOVA Analysis of Negative Change in E*

	% Change Pre-MIST Dynamic Modulus in IDT for 1 Hz (MPa)	Ti	Tgrand	SS	Mean Total	Xi	df all	(Xi-Meantotal)^2	Sall^2	Tss	SS error	MS	MS error	F
Parkman	-15.2	53.1	264.5	232.7434	14.69681	15.2	17.0	0.245513	69.196	1176.34	943.5942	58.18586	72.5842	0.8016
	-7.9	4.0	18.0			7.9		45.62701						
	-27.4					27.4		161.4155						
	-2.6					2.6		146.434						
Lebanon-Sanford	-8.3	47.7				8.3		40.64528						
	-7.9	4.0				7.9		45.64						
	-9.9					9.9		22.71772						
	-21.5					21.5		46.15475						
Auburn	-11.4	34.7				11.4		11.06187						
	-16.2	3.0				16.2		2.152797						
	-7.2					7.2		56.44662						
Rumford		44.6												
	-12.2	3.0				12.2		6.051782						
	-27.6					27.6		166.6788						
	-4.7					4.7		99.5361						
Houlton	-10.6	84.4				10.6		16.60593						
	-24.9	4.0				24.9		104.8009						
	-27.1					27.1		153.8155						
	-21.8					21.8		50.30757						

Table 6 ANOVA Analysis of Positive Change in E*

	% Change Pre-MIST Dynamic Modulus in IDT for 1 Hz (MPa)	Sum of Each Mixes	Tgrand	SS	Mean Total	Xi	df all	(Xi-Meantotal)^2	Sall^2	Tss	SS error	MS	MS error	F
Gorham [Durham (RTE 136)]	3.1	23.6	113.7	506.3557	12.63007	3.1	8	91.71506	82.996	663.964	157.6086	253.1779	22.5155	11.245
	5.6	4	9			5.6		49.07214						
	7.5					7.5		25.84185						
	7.3					7.3		27.99796						
Augusta	11.5	21.4				11.5		1.210869						
	9.8	2				9.8		7.770309		9.11019				
										82.9955				
PI-Easton	14.6	68.7				14.6		4.051359						
	31.6	3				31.6		358.1621						
	22.5					22.5		98.14268						

Table 7 Saturation Content of the Samples

Sample ID	Percent Change Pre-MIST Dynamic Modulus in IDT for 10 Hz (MPa)	Percent Change Pre-MIST Dynamic Modulus in IDT for 1 Hz (MPa)	Pre MIST Porosity (%)	Saturation After Mist (Through Porosity)	Saturation After CoreDry (Through Porosity)
AUG #1	-8.5	11.5	6.2	56.3	9.6
AUG #2	19.8	9.8	6.1	56.4	13.1
AUG #3	7.6	-1.5	5.6	53.6	12.2
AUG #4	-15.9	-14.0	5.7	48.9	9.4
DUR #1	-3.0	3.1	3.1	54.1	30.3
DUR #2	25.5	5.6	3.1	71.8	35.9
DUR #3	21.7	7.5	4.8	60.7	10.1
DUR #4	14.2	7.3	4.5	61.7	30.0
PARK # 1	-20.4	-15.2	4.5	65.0	35.3
PARK # 2	-5.7	-7.9	4.9	64.1	33.4
PARK # 3	-26.5	-27.4	6.5	70.8	11.6
PARK # 4	-10.3	-2.6	6.2	71.9	30.8
L-S #1	-3.8	-8.3	6.3	59.4	13.6
L-S #2	-13.9	-7.9	6.4	52.8	14.0
L-S #3	-0.7	-9.9	4.4	62.6	22.1
L-S #4	-5.7	-21.5	5.1	56.5	18.0
AUB #1	1.2	-11.4	4.1	72.7	39.7
AUB #2	29.9	-16.2	3.8	67.6	32.9
AUB #3	5.9	-7.2	5.4	73.3	24.1
AUB #4	-3.7	4.7	5.2	69.1	30.0
RUM #1	5.4	5.9	4.6	74.3	40.3
RUM #2	-4.8	-12.2	5.0	73.7	37.4
RUM #3	-22.6	-27.6	6.5	65.8	6.9
RUM #4	2.6	-4.7	5.9	74.9	23.1
P-E #1	11.9	14.6	4.6	45.6	7.4
P-E #2	13.7	31.6	4.2	-9.4	7.3
P-E #3	-7.9	22.5	5.0	44.3	6.2
P-E #4	-28.0	-30.8	5.5	45.9	5.9
HOU #1	-9.2	-10.6	5.3	72.2	25.1
HOU #2	-14.8	-24.9	5.6	66.2	20.0
HOU #3	-18.2	-27.1	4.2	79.5	22.8
HOU #4	-17.1	-21.8	4.8	69.1	19.9

Table 8 Change in Distribution Mean of Nf

Mixes	Pre Nf	Post Nf	Change in Nf (N_{fpost}-N_{fpre})	Percent Change
AUB	26199	25437	-761	-2.91
AUG	28580	28921	341	1.19
DUR	81276	85932	4655	5.73
HOU	66929	46520	-20409	-30.49
L-S	67788	53836	-13952	-20.58
PARK	70063	63275	-6788	-9.69
P-E	37388	37043	-345	-0.92
RUM	51580	48322	-3257	-6.32

Table 9 $\beta_1, \beta_2, \gamma_1$,and γ_2 values for different gauge length

Specimen Radius (mm)	Gauge Length (mm)	β1	β2	γ1	γ2
76.2	25.4	-0.0095	-0.0031	0.003	0.0092
76.2	38.1	-0.0145	-0.0046	0.0043	0.0134
76.2	50.8	-0.0198	-0.0062	0.0054	0.0172

Appendix B

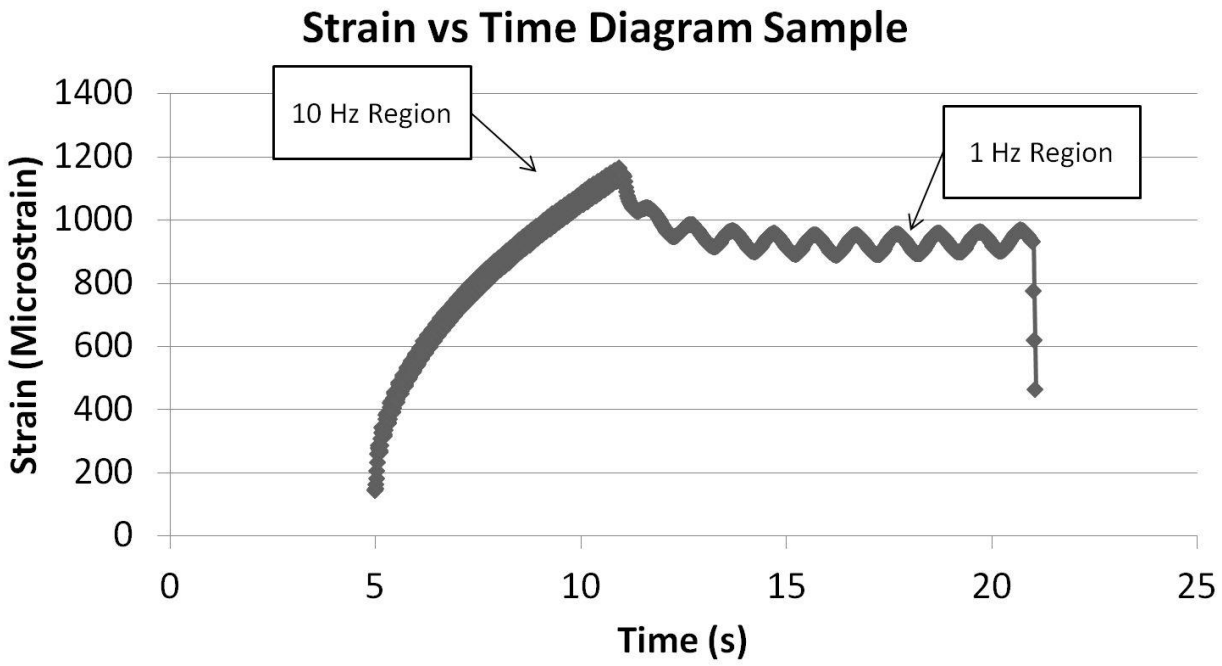

Figure 72 Excepted strain vs time (x-y) plot for any given sample under sinousoidal loading

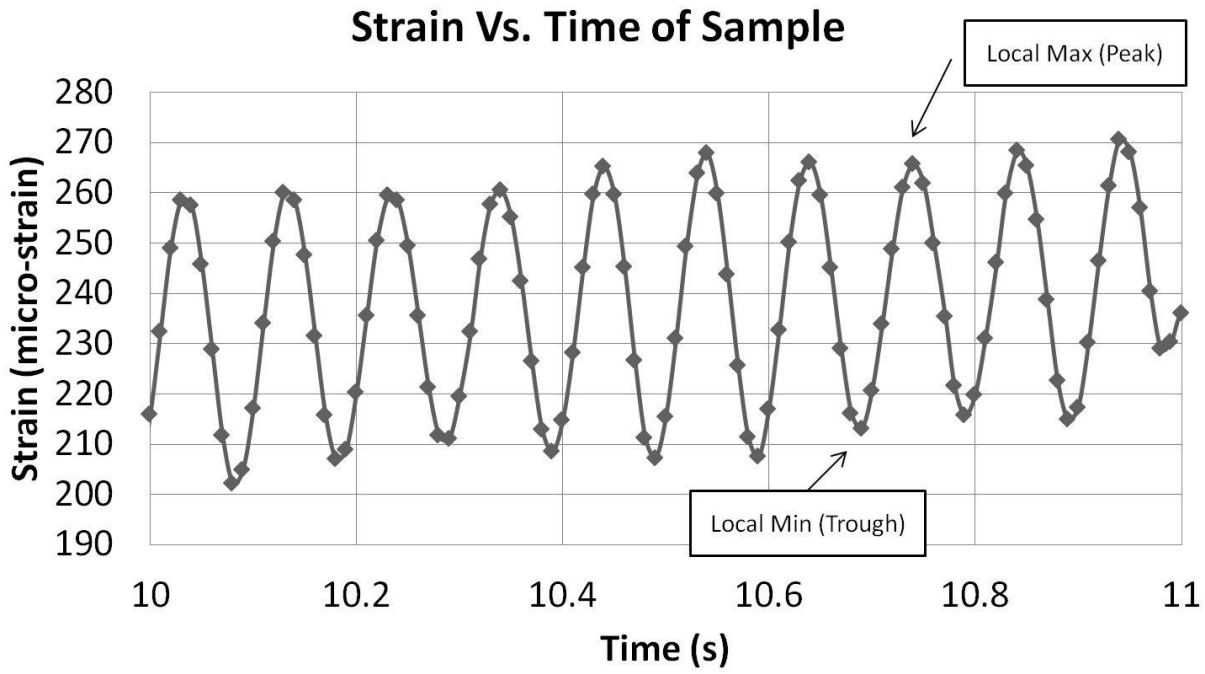

Figure 73 Peak to Peak Strain Region of 10Hz

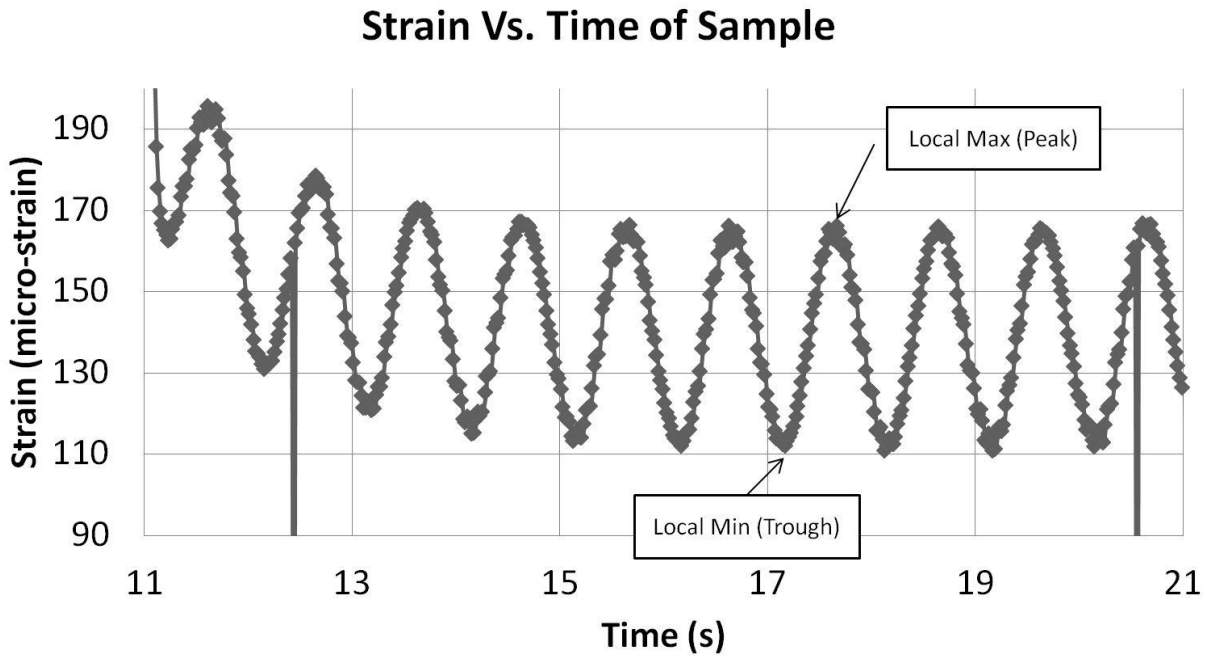

Figure 74 Peak to Peak Strain Region of 1Hz

Appendix C

Matlab Code for Beta & Gamma Coefficients

```
a= .01905;
R= 0.1524/2;
alpha= atan((a/2)/R);
l= .0254;
m= @(y) ((1-y^2/R^2)*sin(2*alpha))/(1-2*y^2/R^2*cos(2*alpha)+y^4/R^4)
n= @(y) atan(((1+y^2/R^2)/(1-y^2/R^2))*tan(alpha))

f= @(x)((1-x^2/R^2)*sin(2*alpha))/(1+2*x^2/R^2*cos(2*alpha)+x^4/R^4);
g= @(x) atan(((1-x^2/R^2)/(1+x^2/R^2))*tan(alpha));

beta1= -integral(n,-l,l,'ArrayValued',true)-integral(m,-l,l,'ArrayValued',true)
beta12= integral(n,-l,l,'ArrayValued',true)-integral(m,-l,l,'ArrayValued',true)

gamma1= integral(f,-l,l,'ArrayValued',true)-integral(g,-l,l,'ArrayValued',true)
gamma2= integral(f,-l,l,'ArrayValued',true)+integral(g,-l,l,'ArrayValued',true)
```

Matlab code for Identifying Peak to Peak Deformation and Maximums Load associated with the deformation

```
clear all;
close all;
clc
format long g
data=xlsread('test1.xlsx');

sampling_rate_10Hz = 100;   %data points in 1 second
sampling_rate_1Hz = 50;     % data points in 1 second
data_type = 10;      % 10 = Horizontal, 11 = Vertical

data_10Hz = data(548:600,:);

for i = 1:5
   max_point_10Hz(i) = max(data_10Hz(10*(i-1)+1:10*i,data_type));
   min_point_10Hz(i) = min(data_10Hz(10*(i-1)+1:10*i,data_type));
end
% for i = 1:5
%     min_point_10Hz(i) = min(data_10Hz(10*(i-1)+1:10*i,data_type));
%     max_point_10Hz(i) = max(data_10Hz(10*(i-1)+1:10*i,data_type));
```

```
% end
for i = 1:length(data_10Hz)
   min_load_10Hz = min(data_10Hz(:,6));
   max_load_10Hz = max(data_10Hz(:,6));
end

for i = 1:5
   for j = 10*(i-1)+1:10*i
      if data_10Hz(j,data_type) == max_point_10Hz(i)
         max_point_10Hz_data(i,:) = data_10Hz(j,:);
      end
      if data_10Hz(j,data_type) == min_point_10Hz(i)
         min_point_10Hz_data(i,:) = data_10Hz(j,:);
      end
   end
end

for i = 1:length(data_10Hz)
   if data_10Hz(i,6) == max_load_10Hz
      max_load_10Hz_data = data_10Hz(i,:);
   end
   if data_10Hz(i,6) == min_load_10Hz
      min_load_10Hz_data = data_10Hz(i,:);
   end
end

% min_point_10Hz_data
% max_point_10Hz_data
figure(1)
plot(data_10Hz(:,8),data_10Hz(:,data_type))
hold on;
scatter(max_point_10Hz_data(:,8),max_point_10Hz_data(:,data_type));
scatter(min_point_10Hz_data(:,8),min_point_10Hz_data(:,data_type));
hold off;

data_1Hz = data(850:1104,:);

for i = 1:5
   max_point_1Hz(i) = max(data_1Hz(50*(i-1)+1:50*i,data_type));
   min_point_1Hz(i) = min(data_1Hz(50*(i-1)+1:50*i,data_type));
end
%
% for i = 1:5
%    min_point_1Hz(i) = min(data_1Hz(50*(i-1)+1:50*i,data_type));
%    max_point_1Hz(i) = max(data_1Hz(50*(i-1)+1:50*i,data_type));
% end
```

```
for i = 1:length(data_1Hz)
   min_load_1Hz = min(data_1Hz(:,6));
   max_load_1Hz = max(data_1Hz(:,6));
end

for i = 1:5
   for j = 50*(i-1)+1:50*i
      if data_1Hz(j,data_type) == max_point_1Hz(i)
         max_point_1Hz_data(i,:) = data_1Hz(j,:);
      end
      if data_1Hz(j,data_type) == min_point_1Hz(i)
         min_point_1Hz_data(i,:) = data_1Hz(j,:);
      end
   end
end
% min_point_1Hz_data
% max_point_1Hz_data

for i = 1:length(data_1Hz)
   if data_1Hz(i,6) == max_load_1Hz
      max_load_1Hz_data = data_1Hz(i,:);
   end
   if data_1Hz(i,6) == min_load_1Hz
      min_load_1Hz_data = data_1Hz(i,:);
   end
end
figure(2)
plot(data_1Hz(:,8),data_1Hz(:,data_type));
hold on;
scatter(max_point_1Hz_data(:,8),max_point_1Hz_data(:,data_type));
scatter(min_point_1Hz_data(:,8),min_point_1Hz_data(:,data_type));
hold off

Horizontal = min_point_10Hz_data(:,10)
Vertical = min_point_10Hz_data(:,11)
Load = min_point_10Hz_data(:,6)
Time_min_10_hor = min_point_10Hz_data(:,8)
A=table(Horizontal, Vertical, Load, Time_min_10_hor);
filename = 'yz1.xlsx';
writetable(A,filename,'Sheet',1,'Range','A1')

Horizontal = max_point_10Hz_data(:,10)
Vertical = max_point_10Hz_data(:,11)
Load = max_point_10Hz_data(:,6)
Time_max_10_hor = max_point_10Hz_data(:,8)
```

```
A=table(Horizontal, Vertical, Load, Time_max_10_hor);
filename = 'yz1.xlsx';
writetable(A,filename,'Sheet',1,'Range','A8')

Horizontal_change_10Hz = [max_point_10Hz_data(:,10)-
min_point_10Hz_data(:,10);mean(max_point_10Hz_data(:,10)-min_point_10Hz_data(:,10))];
A=table(Horizontal_change_10Hz);
writetable(A,filename,'Sheet',1,'Range','M1')

Horizontal = min_point_1Hz_data(:,10)
Vertical = min_point_1Hz_data(:,11)
Load = min_point_1Hz_data(:,6)
Time_min_1_hor = min_point_1Hz_data(:,8)
A=table(Horizontal, Vertical, Load, Time_min_1_hor);
filename = 'yz1.xlsx';
writetable(A,filename,'Sheet',1,'Range','A15')

Horizontal = max_point_1Hz_data(:,10)
Vertical = max_point_1Hz_data(:,11)
Load = max_point_1Hz_data(:,6)
Time_max_1_hor = max_point_1Hz_data(:,8)
A=table(Horizontal, Vertical, Load, Time_max_1_hor);
filename = 'yz1.xlsx';
writetable(A,filename,'Sheet',1,'Range','A22')

Horizontal = [max_load_10Hz_data(:,10);min_load_10Hz_data(:,10)];
Vertical = [max_load_10Hz_data(:,11);min_load_10Hz_data(:,11)];
Load = [max_load_10Hz;min_load_10Hz];
Time_max_10_load = [max_load_10Hz_data(:,8);min_load_10Hz_data(:,8)];
A=table(Horizontal, Vertical, Load, Time_max_10_load);
filename = 'yz1.xlsx';
writetable(A,filename,'Sheet',1,'Range','Q1')

Horizontal = [max_load_1Hz_data(:,10);min_load_1Hz_data(:,10)];
Vertical = [max_load_1Hz_data(:,11);min_load_1Hz_data(:,11)];
Load = [max_load_1Hz;min_load_1Hz];
Time_max_1_load = [max_load_1Hz_data(:,8);min_load_1Hz_data(:,8)];
A=table(Horizontal, Vertical, Load, Time_max_1_load);
filename = 'yz1.xlsx';
writetable(A,filename,'Sheet',1,'Range','Q15')

Horizontal_change_1Hz = [max_point_1Hz_data(:,10)-
min_point_1Hz_data(:,10);mean(max_point_1Hz_data(:,10)-min_point_1Hz_data(:,10))];
A=table(Horizontal_change_1Hz);
writetable(A,filename,'Sheet',1,'Range','M15')
```

```
%%%%%%%%%%%%%%%%%%%%

data_type = 11;      % 10 = Horizontal, 11 = Vertical

data_10Hz = data(548:600,:);

for i = 1:5
   max_point_10Hz(i) = max(data_10Hz(10*(i-1)+1:10*i,data_type));
   min_point_10Hz(i) = min(data_10Hz(10*(i-1)+1:10*i,data_type));
end
for i = 1:5
   min_point_10Hz(i) = min(data_10Hz(10*(i-1)+1:10*i,data_type));
   max_point_10Hz(i) = max(data_10Hz(10*(i-1)+1:10*i,data_type));
end


for i = 1:5
   for j = 10*(i-1)+1:10*i
      if data_10Hz(j,data_type) == max_point_10Hz(i)
         max_point_10Hz_data(i,:) = data_10Hz(j,:);
      end
      if data_10Hz(j,data_type) == min_point_10Hz(i)
         min_point_10Hz_data(i,:) = data_10Hz(j,:);
      end
   end
end
figure(3)
plot(data_10Hz(:,8),data_10Hz(:,data_type))
hold on;
scatter(max_point_10Hz_data(:,8),max_point_10Hz_data(:,data_type));
scatter(min_point_10Hz_data(:,8),min_point_10Hz_data(:,data_type));
hold off



data_1Hz = data(850:1104,:);


for i = 1:5
   max_point_1Hz(i) = max(data_1Hz(50*(i-1)+1:50*i,data_type));
   min_point_1Hz(i) = min(data_1Hz(50*(i-1)+1:50*i,data_type));
end

for i = 1:5
```

```
   min_point_1Hz(i) = min(data_1Hz(50*(i-1)+1:50*i,data_type));
   max_point_1Hz(i) = max(data_1Hz(50*(i-1)+1:50*i,data_type));
end


for i = 1:5
   for j = 50*(i-1)+1:50*i
      if data_1Hz(j,data_type) == max_point_1Hz(i)
         max_point_1Hz_data(i,:) = data_1Hz(j,:);
      end
      if data_1Hz(j,data_type) == min_point_1Hz(i)
         min_point_1Hz_data(i,:) = data_1Hz(j,:);
      end
   end
end
figure(4)
plot(data_1Hz(:,8),data_1Hz(:,data_type))
hold on;
scatter(max_point_1Hz_data(:,8),max_point_1Hz_data(:,data_type));
scatter(min_point_1Hz_data(:,8),min_point_1Hz_data(:,data_type));
hold off

Horizontal = min_point_10Hz_data(:,10)
Vertical = min_point_10Hz_data(:,11)
Load = min_point_10Hz_data(:,6)
Time_min_10_vert = min_point_10Hz_data(:,8)
A=table(Horizontal, Vertical, Load, Time_min_10_vert);
filename = 'yz1.xlsx';
writetable(A,filename,'Sheet',1,'Range','G1')

Horizontal = max_point_10Hz_data(:,10)
Vertical = max_point_10Hz_data(:,11)
Load = max_point_10Hz_data(:,6)
Time_max_10_vert = max_point_10Hz_data(:,8)
A=table(Horizontal, Vertical, Load, Time_max_10_vert);
filename = 'yz1.xlsx';
writetable(A,filename,'Sheet',1,'Range','G8')

Vertical_change_10Hz = [max_point_10Hz_data(:,11)-
min_point_10Hz_data(:,11);mean(max_point_10Hz_data(:,11)-min_point_10Hz_data(:,11))];
A=table(Vertical_change_10Hz);
writetable(A,filename,'Sheet',1,'Range','N1')


Horizontal = min_point_1Hz_data(:,10)
Vertical = min_point_1Hz_data(:,11)
```

```
Load = min_point_1Hz_data(:,6)
Time_min_1_vert = min_point_1Hz_data(:,8)
A=table(Horizontal, Vertical, Load, Time_min_1_vert);
filename = 'yz1.xlsx';
writetable(A,filename,'Sheet',1,'Range','G15')

Horizontal = max_point_1Hz_data(:,10)
Vertical = max_point_1Hz_data(:,11)
Load = max_point_1Hz_data(:,6)
Time_max_1_vert = max_point_1Hz_data(:,8)
A=table(Horizontal, Vertical, Load, Time_max_1_vert);
filename = 'yz1.xlsx';
writetable(A,filename,'Sheet',1,'Range','G22')

Vertical_change_1Hz = [max_point_1Hz_data(:,11)-
min_point_1Hz_data(:,11);mean(max_point_1Hz_data(:,11)-min_point_1Hz_data(:,11))];
A=table(Vertical_change_1Hz);
writetable(A,filename,'Sheet',1,'Range','N15')
```

Appendix D

Location of Aggregate Sources

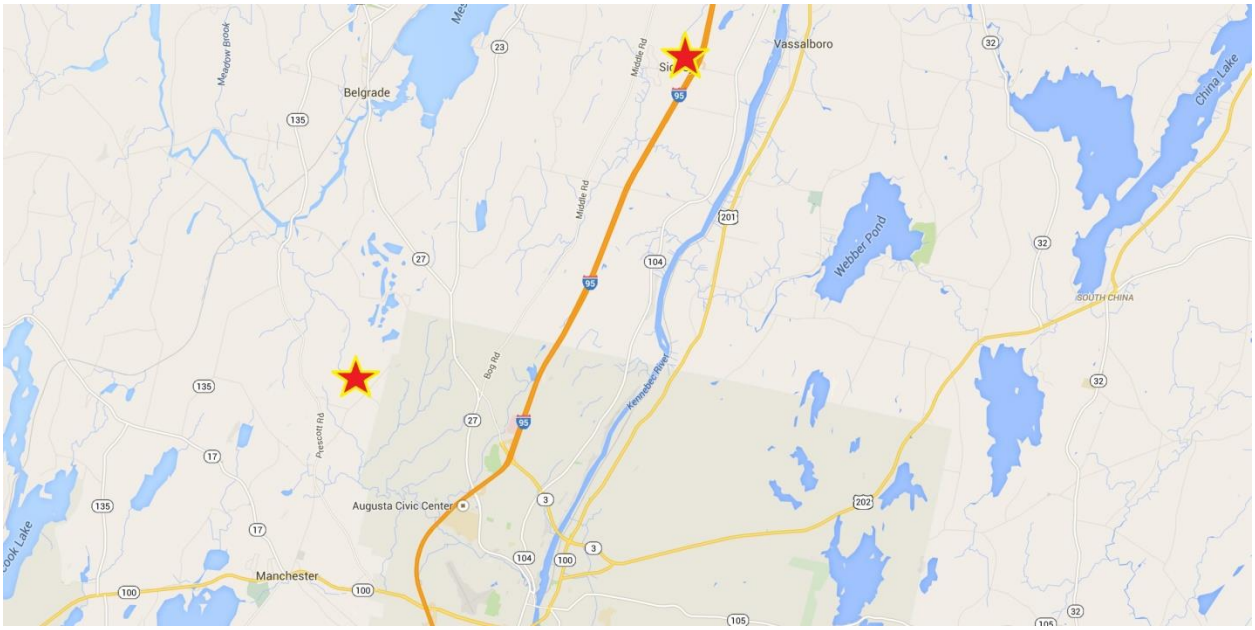

Figure 75 AUG

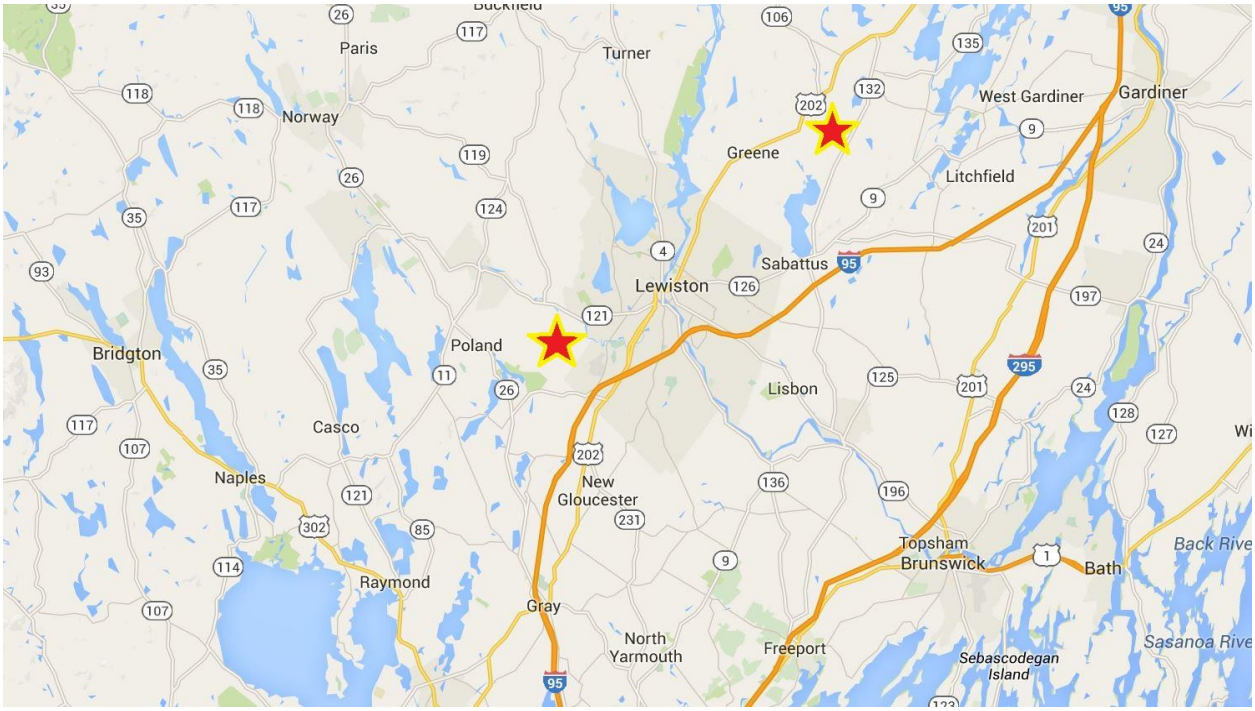

Figure 76 AUB

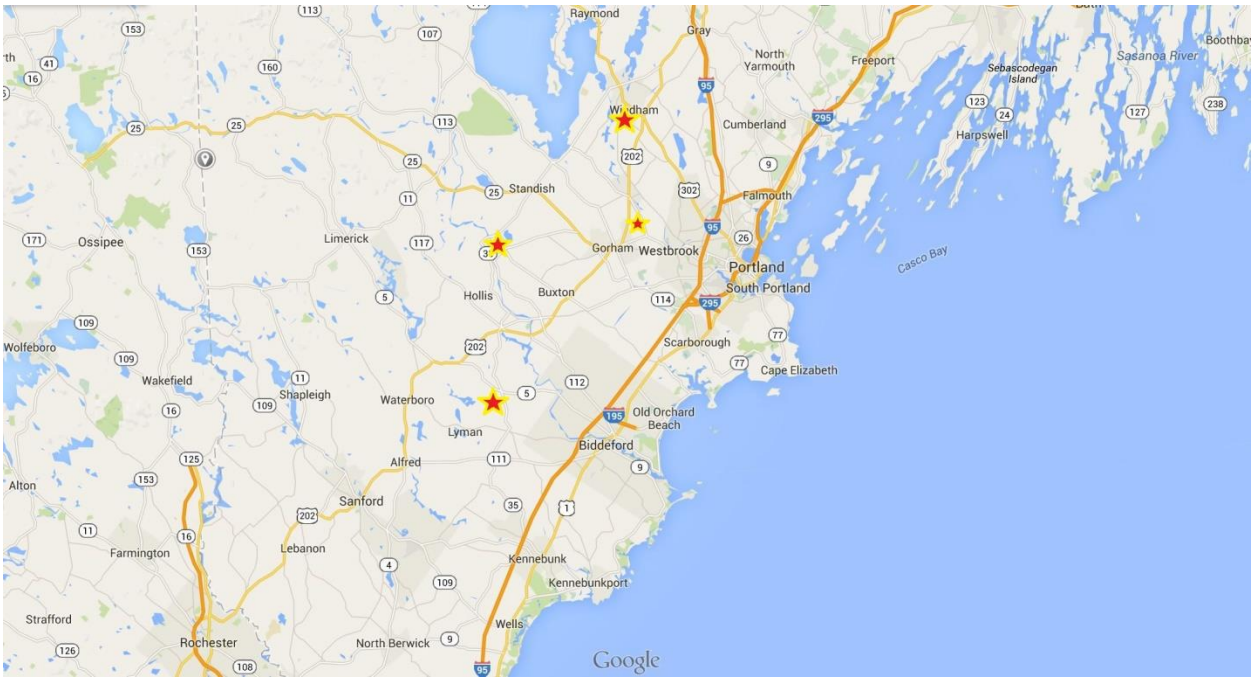

Figure 77 DUR

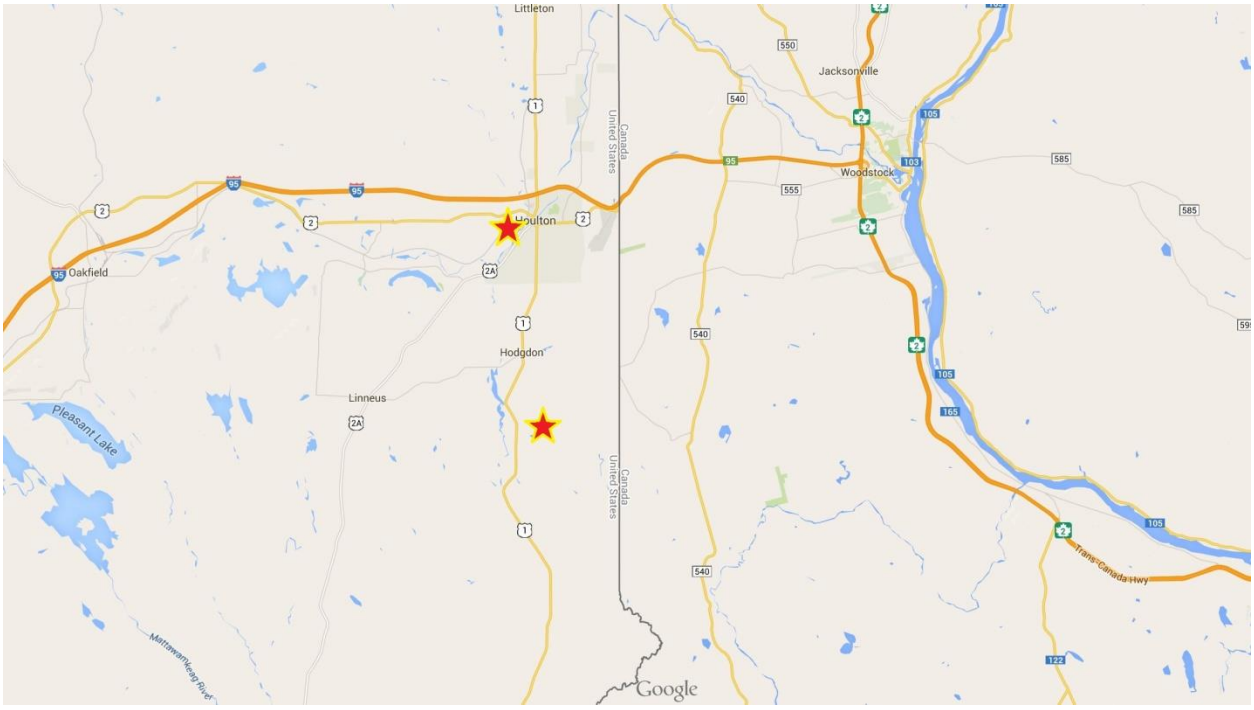

Figure 78 Hou

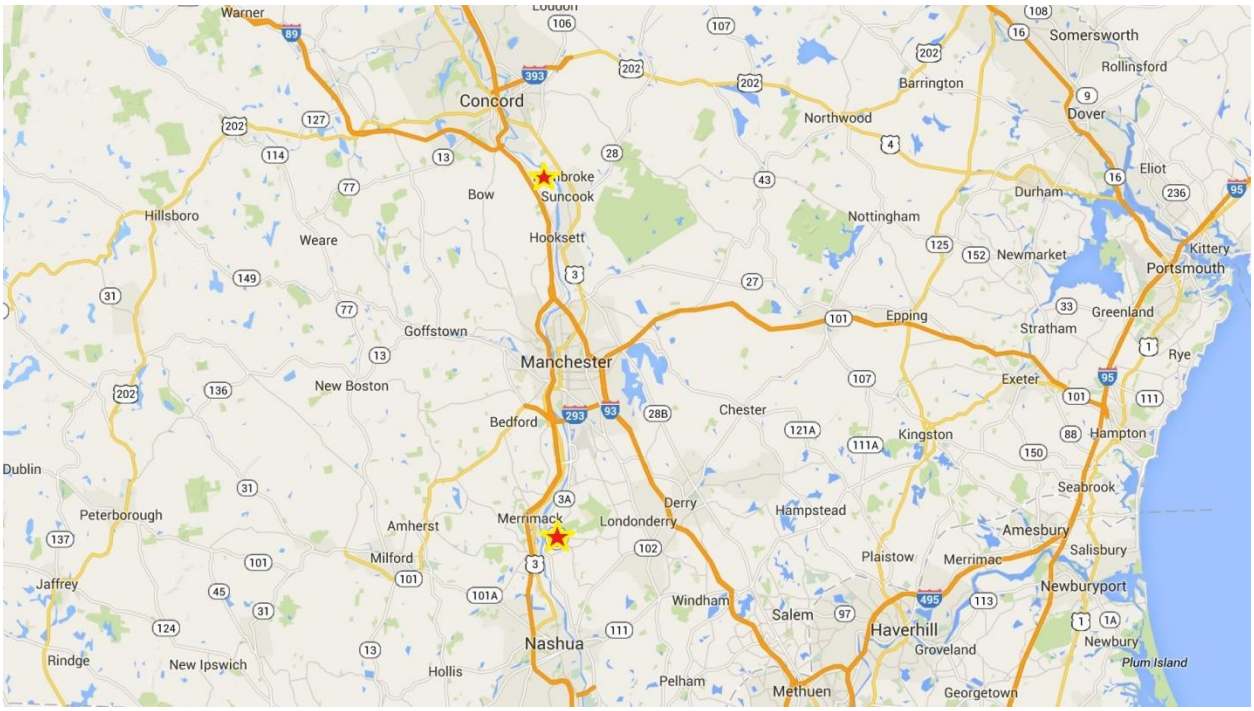

Figure 79 L-S

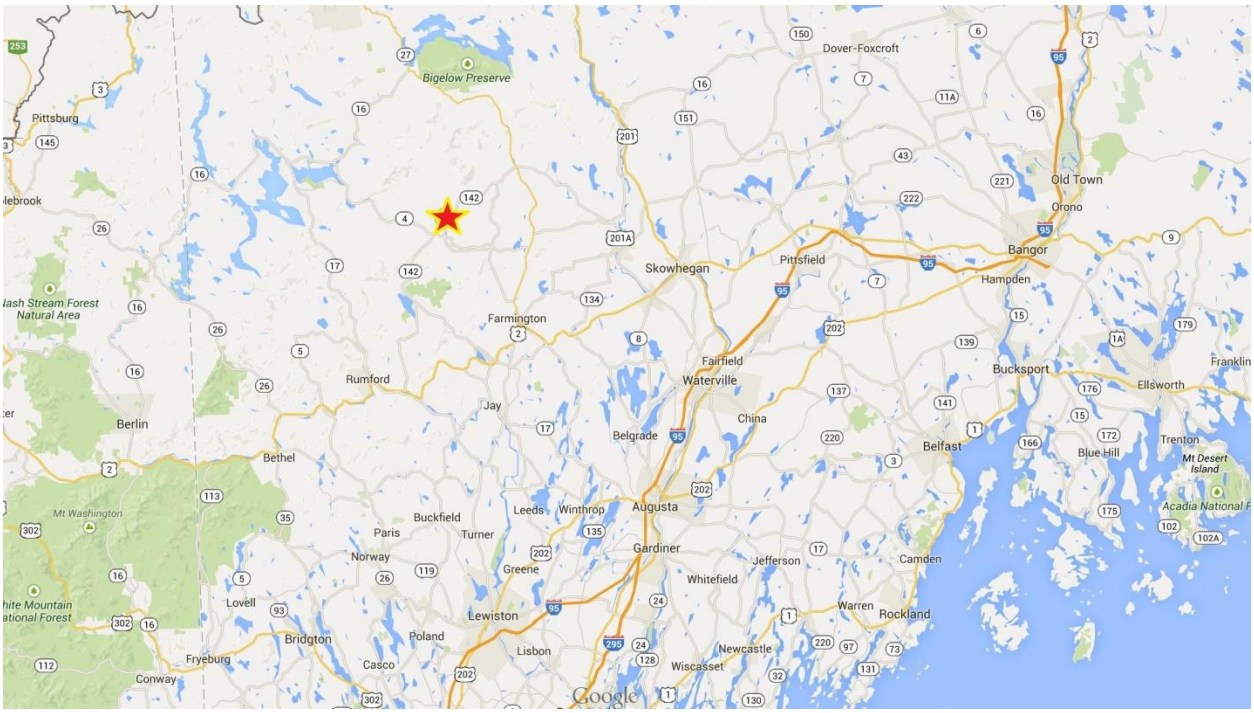

Figure 80 Rum

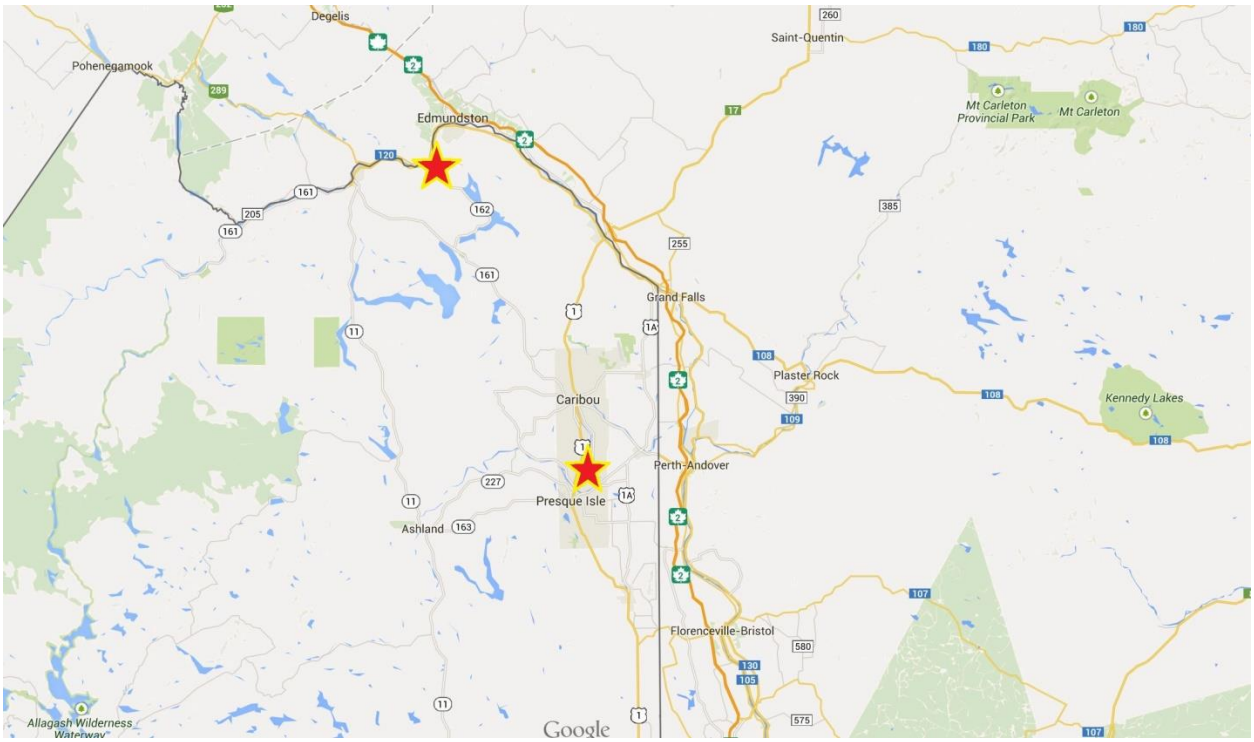

Figure 81 P-E

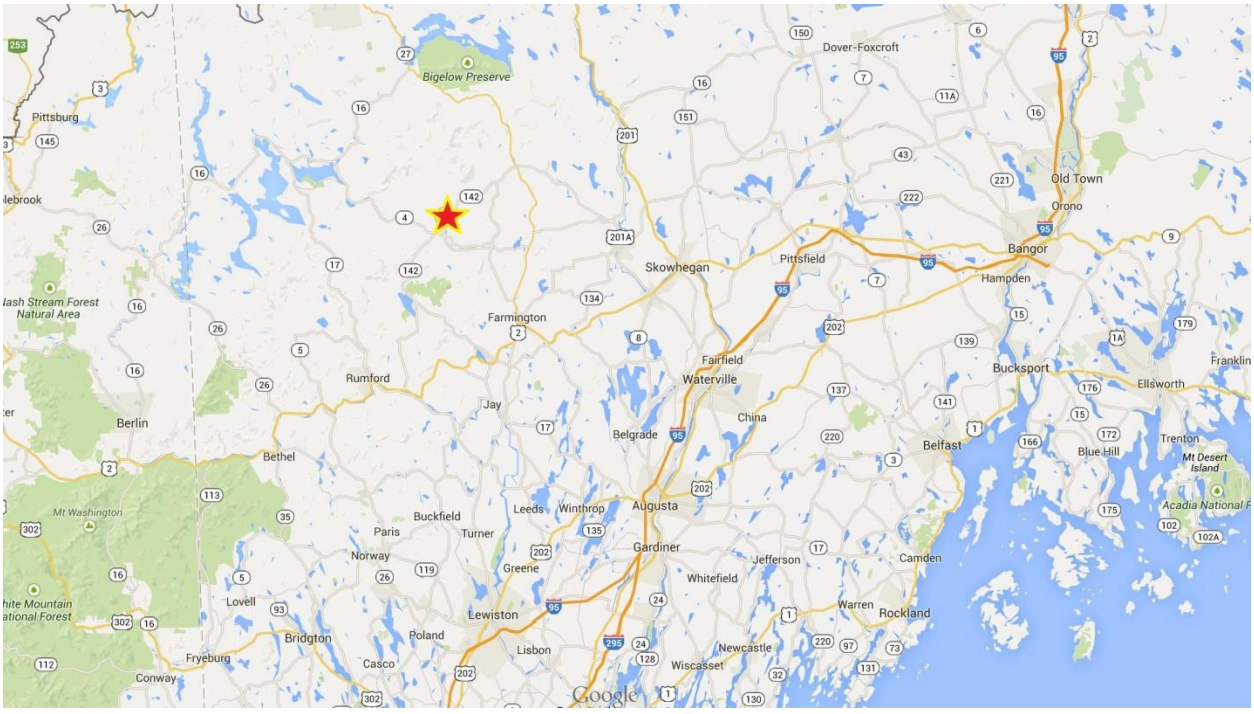

Figure 82 Parkman